Passive Gust Load Alleviation Through Bend-Twist Coupling of Composite Beams on Typical Commercial Airplane Wings

by

Sébastien Gauthier Perron

B.Ing., Mechanical Engineering, Aeronautics Option (Honours)
École Polytechnique de Montréal (2007)

Submitted to the Department of Aeronautics and Astronautics
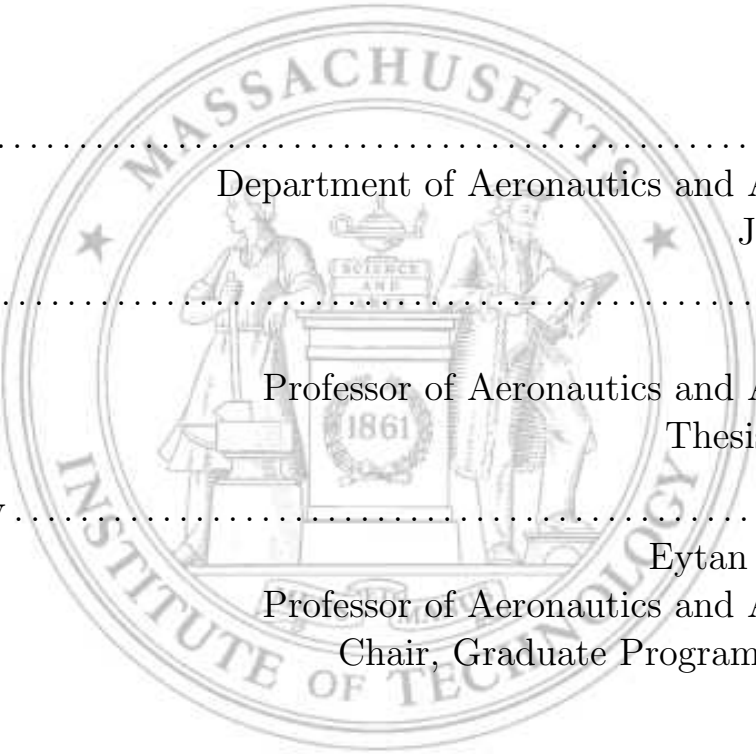in partial fulfillment of the requirements for the degree of

Master of Science in Aeronautics and Astronautics

at the

MASSACHUSETTS INSTITUTE OF TECHNOLOGY

September 2012

Author . . . .
Department of Aeronautics and Astronautics
July 23, 2012

Certified by. . . . .
Mark Drela
Professor of Aeronautics and Astronautics
Thesis Supervisor

Accepted by . . . .
Eytan H. Modiano
Professor of Aeronautics and Astronautics
Chair, Graduate Program Committee

Passive Gust Load Alleviation Through Bend-Twist Coupling of Composite Beams on Typical Commercial Airplane Wings

by

Sébastien Gauthier Perron

Abstract

The effects of bend-twist coupling on typical commercial airplane wings are evaluated. An analytical formulation of the orthotropic box beam bending stiffness matrix is derived by combining Euler-Bernoulli beam theory and classical laminated plate theory. The out-of-plane displacement due to the twist of the cross section is modeled by a bilinear warping function. The analytical model is evaluated and validated against finite element analysis and experimental results. The model can accurately predict the twist and deformation of orthotropic box beams within 15% of the benchmarking data and provides best results for beams of higher aspect ratios and with layup angles below 30 degrees. Airplane level aero-structural simulations are performed in ASWING using models of Boeing's 737 and 777. The composite wings are sized for a static load increase and a set of gusts as prescribed by the FAA. Using unbalanced laminates to generate the structural coupling leads to significant strength penalties if the loading is not parallel to the laminate's fiber directions. The optimal laminate angle for which the weight saving benefits of bend-twist coupling are maximized corresponds to the wing's principal stress direction. Beyond that angle, the wings will exhibit more coupling but the laminate strength penalties are too large to be overcomed by the benefits of bend-twist coupling. The addition of coupling to the wings leads to reductions in peak spanwise bending moments in the order of 20% to 45%. It is demonstrated that the mechanism behind this reduction involves increased wing tip twist which alleviates part of the outboard wing load. This ultimately results in weight savings in the order of 2% to 4%. The findings suggest that the benefits of bend-twist coupling are more important on heavier airplanes such as the 777 due to the effects of the cube-square law.

Thesis Supervisor: Mark Drela
Title: Professor of Aeronautics and Astronautics

Acknowledgments

First and foremost, I would like to thank my thesis advisor, Mark Drela, for accepting to work with me and letting me pick his brain at times. It was an honor to interact with such a great professor and he has been very understanding in answering my (sometimes silly) questions. Thanks to him, I can say that I am now a better engineer, researcher and scientist.

Second, I would like to thank my wonderful girlfriend, Maryse, who is always ready to cheer me on in my life endeavors, be it academically or in my craziest athletic goals. This adventure really started with her during a summer vacation in Boston 3 years ago, when we were just tourists visiting the MIT campus and I decided to pick up an application form. Ever since, she never stopped believing in me, even when I was doubting about myself at times. She encouraged me to pursue my dreams even though she knew I would be away for a while. Through the many ups and downs of grad student life, she always had the right words to bring the best out of me and therefore I am grateful for her unconditional support. I must also thank Aramis for the cuteness and for taking care of Maryse while I was gone.

Next, I would like to thank my entire family back in Quebec, your love and support was invaluable throughout my life and especially during the last few years. To my parents Anne, Yvan and Danny, who I always considered as a my second dad, there are no words to describe how thankful I am for everything you have done for me. If I am where I am today, it is partly because of you. A special thank you goes to Alex, Felix, Sylvain, Esther, Jay, Lili, Jo, Giny, Guy and Mado: your constant support was always appreciated and so many times you brought smiles to my face! *Merci*!

Next, I want to thank the MIT cycling team for the amazing experience they provided me during my stay in Boston. The countless road rides, the two training camps and the race weekends will forever be some of my best memories from those two years. This team is filled with so many extraordinary people, who are both accomplished athletes and scientists. Thanks to you all, I am now an expert in bike mechanics, aerodynamics and legs shaving. Thank you also for helping me redefine

the meanings of the words pain and suffering.

I would also like to thank everyone else I met in Cambridge: friends, class mates, team mates, lab mates and all those other mates, thank you for contributing to making my stay at MIT so enjoyable and special.

Finally, I would like to acknowledge Bombardier Aerospace for the financial support and for believing I was a worthwhile investment.

Life is like riding a bicycle. To keep your balance, you must keep moving.

-Albert Einstein

Contents

List of Figures

List of Tables

Chapter 1

Introduction

1.1 Motivation

In the early days of aviation, the design goals for commercial airplanes were mainly focusing on maximizing range, a design requirement that was driven by the desire to open up new transcontinental and transoceanic air routes. Nowadays, aircraft manufacturers need to give much more importance to efficiency, as airline companies are trying to keep their business sustainable with the constraint of rising jet fuel cost. More stringent environmental regulations have also become unavoidable given the ever-increasing volume of airline traffic across the world. With such a boost in traffic volume over the last decades, extensive knowledge about flight safety was acquired and safety regulations became more demanding and complex. Learning from past design mistakes, new aircraft now have to comply with FAA certification requirements such as multiple load paths, fail safe design and damage tolerance. Those more demanding safety regulations and the improved training of the flight crews both contributed, among other factors, to improve the safety records of commercial aviation. For example, 2007 was the safest year in the history of aviation since 1963 [28]. However, these new design requirements were implemented at the cost of increased structural weight and thus to the detriment of efficiency. To help meet the conflicting objectives of increasing safety while improving efficiency, the last decades have seen huge technical progress in aerodynamics, propulsion and structures.

Until recently, the primary structural material used in commercial aviation was Aluminum. For years, structural weight savings were achieved as a result of increased knowledge of Aluminum properties and its failure modes as well as by improving analysis techniques of isotropic materials. As a result, there now exists extensive properties and analysis techniques databases such as the MMPDS (formerly known as the Milittary Handbook 5) covering the most common types of isotropic alloys [12]. These databases are used as standard references in most modern aerospace companies and are accepted by the certification agencies. The development of faster computers and finite element analysis software were also instrumental in achieving more optimal designs of new airplanes and in improving their structural efficiency. New techniques such as multidisciplinary optimization were also instrumental in understanding the multiple drivers and disciplines influencing the fuel efficiency of commercial airplanes [11].

As substantial weight savings opportunities on Aluminum structures were getting harder to find, aircraft manufacturers started to look into new generations of materials such as composites for new ways to get lighter and more efficient airplanes. The most common type of composite material used in the aeronautics industry today is made of carbon fibers embedded in a thermosetting epoxy resin matrix. This type of composite was initially attractive to aircraft manufacturers because of its very high specific stiffness and strength to weight ratios, it also had an improved fatigue life, better corrosion resistance and enabled part count reduction. All these characteristics were very appealing to the manufacturers looking for new weight saving opportunities. Because of those intrinsic properties, composite materials have first been considered in the 1960s for military projects such as McDonnell-Douglas's F-18. With its first flight in 1978, the F-18 was one of the first airplanes to make extensive usage of composite materials for primary structural elements such as the wing, the vertical fins and the horizontal stabilizer [18]. On the commercial aviation side, it took another 20 years for carbon fiber to make its way into this large market. The Boeing 777, whose first flight was in 1994, only had about 12% of composite structural elements by mass [7]. Initially, composite parts were mostly limited to secondary structural parts such

as aerodynamic fairings, engine cowlings and floor panels. After waiting another 15 years, the latest generation of commercial airplanes such as the Boeing 787 or the Airbus A350 finally started to make extensive use of advanced materials with up to 50% of their structure by mass being made of carbon fiber reinforced plastics [8].
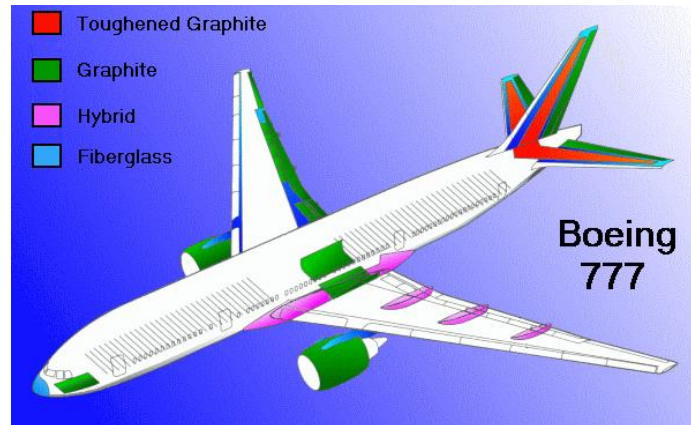
(a) Boeing 777 [18].
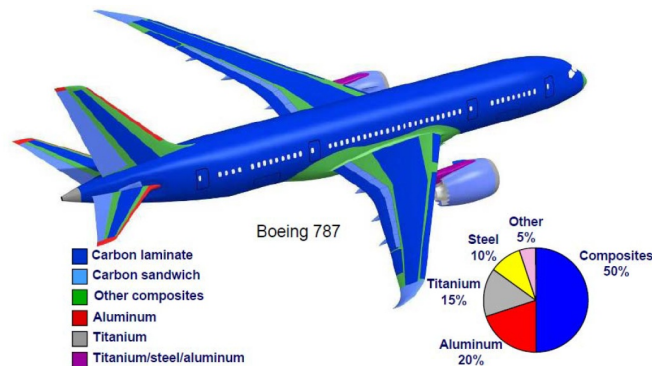
(b) Boeing 787 [21].

Figure 1-1: Composite material usage on 2 different generations of commercial airplanes.

The long wait before composites started to appear in commercial applications can be explained by several factors. First of all, due to their orthotropic nature, as opposed to Aluminum which is an isotropic material, carbon fiber plies have different structural responses depending on their loading direction. This particular behavior not only makes the analysis more complex but also makes it very difficult to develop closed-form solutions to the state equations. Secondly, carbon laminates exhibit complex failure modes such as interlaminar failures which do not exist in conventional

materials. Because of these out-of-plane failure modes and their brittle behavior, classic maximum distortion energy failure criteria such as the Von Mises theorem could not be applied to composite structures. Carbon fiber also exhibit poor impact resistance compared to Aluminum and therefore extensive damage resistance studies need to be completed when working with them [3]. Finally, carbon parts are much more sensitive to their environment than their metallic counterparts. The strength and elastic properties of composite materials can be significantly degraded by high temperatures and high humidity conditions. These effects are aggravated when the temperature gets closer to the glass transition point of the epoxy resin. Therefore, due to the lack of appropriate analysis methodologies and lack of extensive knowledge of the technology, engineers had to use large safety factors in order to compensate for these knowledge gaps. For these reasons, the full potential of composite parts has never been achieved by the aerospace industry.

Because of the orthotropic nature of the lamina, different structural responses can be obtained not only from changing the loading direction but also from ply orientations and from the stacking sequence of the laminate. For example, a laminate (a stack of lamina) can be stiffer in one specific direction, a behavior which is impossible to reproduce with isotropic materials such as Aluminum and Titanium. This feature is very important as engineers can design the parts to be stiffer in the principal loading directions, making for more efficient designs. Moreover, the stacking sequence and the orientation of the different layers will determine if a laminate has any structural coupling.

For sake of clarity, a few definitions will be given in the following lines. A symmetric laminate is defined as one for which the stacking sequence of plies above its midplane is the mirror image of the plies below its midplane. A balanced laminate is defined as a laminate in which all lamina at angles other than 0 or 90 degrees occur in plus or minus pairs, that is for each $+\theta$ ply, there is an associated $-\theta$ ply. The significance here is that an unbalanced laminate will exhibit shear deformation when subjected to in-plane tension/compression loads, while an asymmetric laminate will experience bending deformation when subject to those same in-plane loads.

These types of plate couplings are known as extension-shear coupling and extension-bending coupling respectively. They are characteristics of composite parts which are impossible to reproduce with isotropic materials.

Today, the well accepted rule of thumb for the majority of aeronautics composite parts design guidelines is to make the laminates as close as possible to being symmetric and balanced since it eliminates all forms of elastic couplings and it simplifies the analysis. Although the different types of couplings are well predicted for composite plates by the classical laminated plate theory (CLPT), this theory can't be directly applied to composite beams, especially if structural couplings are involved. The issue is that composites materials are now widely used in applications which can be associated to beam structures. An example of such applications is an airplane wing which can be modeled as a cantilevered beam. The wing is a complex assembly which can be represented as a hollow beam by smearing the internal structure such as the stringers into the beam's walls for quick design evaluation purposes. In order to evaluate the potential of new wing designs, engineers had to build complex finite element models, a task which was often very time consuming. Since the time required to build these models was seldom available in a very schedule driven industry, many important structural tradeoff studies were left aside. For this reason, specific composite beam theories have been developped.

1.2 Background

The development of anisotropic beam theories was triggered by needs in the field of rotary-wing aeroelasticity to study and improve the aeroelastic stability of helicopters [15]. To do so, models of the main rotor blades with accurate structural behavior were required. More specifically, by looking into enabling structural couplings on the main rotor blades, engineers sought to improve the flutter response of helicopters by using bend-twist coupling and also to improve the main rotor's performance by using extension-twist coupling [22]. Even though there has been a lot of research efforts put into composite blades modeling up to recently [2], Friedmann notes that despite

the work from the scientific community, the helicopter industry is still not taking advantage of the potential of structural coupling. It seems that the increased fatigue life of carbon compared to aluminum was the main motivation for the industry to use carbon fiber blades [15]. Outside the rotorcraft industry, the idea to potentially use structural couplings on airplane wings stemmed from the development of Grumman's X-29, a forward swept wing airplane. Due to its particular configuration, this experimental airplane had aeroelastic divergence problems. Librescu and others tried to apply the recently developed anisotropic thin-walled beam theories from the helicopter industry in order to improve the aeroelastic properties of the X-29 by using composite wings and structural coupling [20].

Since then, a number of different anisotropic beam theories emerged. One of the key conclusions most of those theories agree upon is that out-of-plane torsional warping of the cross section influences significantly the coupling behavior of the beam [26, 30]. Without a proper warping representation, the calculated coupling coefficients quickly diverge from the benchmarking data. The importance of wall thickness and transverse shear was also studied [19]. Jung demonstrated that the wall thickness does not have a significant effect until the thickness to depth ratio of the beam reaches 20%. Because of the low transverse shear stiffness of composite plates, the transverse shear deformation also plays an important role in the mechanics of composite beams. However, this effect is inversely proportional to the beam's slenderness. The influence of transverse shear deformation also depends on the layup angle used in the beam.

As noted by Volovoi in his review paper [33], there is no lack of composite beam theories but there is clearly a lack of experimental data to benchmark and evaluate the different theories. Whenever a comparison with experimental data is made, it always comes back to the same benchmark problem: a beam with a cross section of aspect ratio equal to 1.8 tested by Chandra [5]. The main issue with relying on a single test case is that the statistical properties of the results (i.e.: error, standard deviation) are unknown. Moreover, the beam aspect ratio tested by Chandra is too small to be representative of typical airplane wings. Although the different theories seem to perform equally for this problem, it does not mean that they would perform

equally well for beams of higher aspect ratio when warping becomes even more critical. As a consequence, new model evaluations have no choice but to rely on finite element analysis, but once again, the finite element models must be validated against something.

A good review of the state of the art theories of anisotropic beam modeling is presented in [15]. The author classifies the different theories into 3 distinct groups. The first category groups the theories based on variational asymptotic methods such as those described in [4, 25]. The second group combines one dimensional beam theory with 2D finite element analysis of the beam's cross section to evaluate the warping effects [17, 31]. Although they have been shown to perform relatively well, these types of models are not convenient to use in an analytical context as they require a different finite element model for each beam geometry. Finally the third category includes the theories using thin-walled assumptions and appropriate warping functions [5, 6, 27, 30]. This type of analysis is the most convenient one for use in an analytical context as the bending stiffness matrix terms can be evaluated simply based on the geometry of the beam and on the material properties. However, care should be taken when selecting the modeling assumptions. For example, Rehfield [27] presented an overly simplistic analytical model which relied on only one parameter to characterize coupling and did not consider warping, thus it poorly matched the experimental data. Furthermore, some additional work has also been performed in order to develop new types of one dimensional anisotropic beam elements to be used in finite element analysis [23, 29]. Just like the second group of models, this is not very practical to rapidly evaluate the bending stiffness of multiple beam geometries without having to rely on a finite element analysis package.

To build on these existing theories, the intent of this thesis is to identify the gust alleviating potential of bend-twist coupling on typical airplane wings. The first step involves the evaluation of the effects of elastic coupling on laminate strength. Then, knowing the strength of the laminates with and without coupling, the wings would be dimensioned against standard loading scenarios. The static load alleviation potential of coupled composite wings evaluated by a full aero-structural airplane

model is a research area which has not been explored extensively yet, at least in the open literature.

1.3   Outline

This thesis is organized as follows. First, the governing equations of orthotropic box beams bending are derived in chapter 2. A series of structural and geometric assumptions are taken in order to formulate an analytical solution to the orthotropic beam bending equations. The bend-twist coupling term of the stiffness matrix is computed by taking into account the out of plane warping function of the cross section. In chapter 3, the quality of the analytical equations is evaluated by benchmarking the model against finite element analysis and experimental data. The validation set covers beams of various aspect ratios and laminate angles. Next, chapter 4 presents the aero-structural sizing methodology which is used to evaluate the effect of bend-twist coupling on the wings. The models, the loading conditions, the composite material properties and the chosen composite failure criteria are introduced. The iterative sizing process and the wing twist evaluation are also assessed. The numerical results are presented in chapter 5, where the effects of bend-twist coupling on the airplane's root bending moment and wing weight are evaluated. Finally, chapter 6 provides a summary of the findings along with suggestions for future work in this field.

For reference, appendix A provides the listings of the Fortran and Matlab codes which have been developed for this thesis. Appendix B presents additional results charts which have not been used in the main text.

Chapter 2

Beam Governing Equations

This chapter presents the derivation of the governing equations required to determine the full bending stiffness matrix of a composite box beam. These equations will be a function of the dimensions of the beam, the ply properties and the layup of the walls. The ultimate goal of this chapter is to relate the bending moments to the beam curvatures through the bending stiffness matrix. The first step of this process is to present the simplifying assumptions, the beam geometry and the coordinate systems. Then, the isotropic beam bending equations will be reviewed. Next, the equations of classical laminated plate theory (CLPT) required for this problem will be presented. Finally, the theory will be extended to orthotropic box beams and the equations for bending stiffness, torsion rigidity and for the bend-twist coupling coefficient will be derived.

2.1   Geometry and Coordinate System

Modern aircraft wings are extremely complex engineering products, consisting of thousands of parts mechanically fastened together. The main load-carrying structure of a wing, the wingbox, is usually composed of four major members: the top skin, the bottom skin, the forward spar and the rear spar. In addition, typical wings also include internal structural elements such as stringers and ribs which provide the additional torsional rigidity and stability without which the wing would not be able

to carry the flight loads. Consequently, creating high fidelity structural models of a complete wingbox to predict its internal stresses and its deformation is a tedious and time consuming task. In order to save time, engineers often try to develop and use simple analytical models which are able to predict the wing deformations accurately in a computationally efficient way. To be structurally correct, the simplified wing beam model has to possess the same equivalent axial and bending stiffness as the original wingbox in order to properly predict wing deflections and stresses. Ideally, the wing tip deflection of the simplified model should match the deflection of the real wing, for any given applied load.
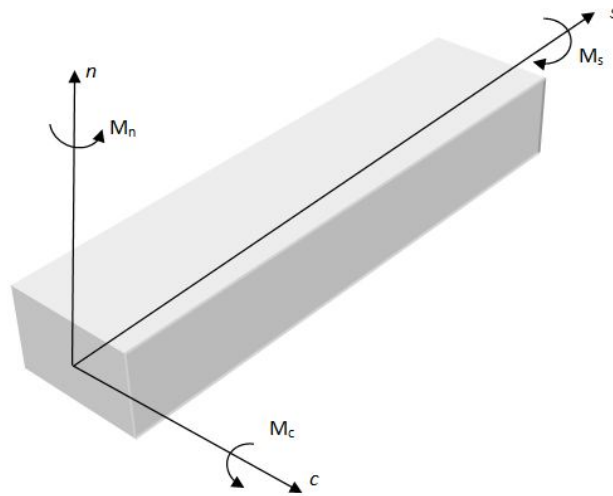
Figure 2-1: Beam inertial coordinate system c,s,n and associated positive moments.

In this study, the wing will be represented by a simple cantilevered hollow rectangular beam (box beam) clamped at the center of the aircraft. The wing's bending moments, deflections and strains are defined in a local coordinate system c, s, n attached to the beam, shown in figure 2-1. The c axis is the chord direction of the wing, the s axis corresponds to the span direction while n corresponds to the normal direction. The wing's aerodynamic and inertial loads will be distributed in the span direction along the beam.

A cross-section of a typical box beam is illustrated in figure 2-2 along with the geometric variables required to describe the beam dimensions. Those variables are

the width (W), the height (H) and the wall thickness t_w.
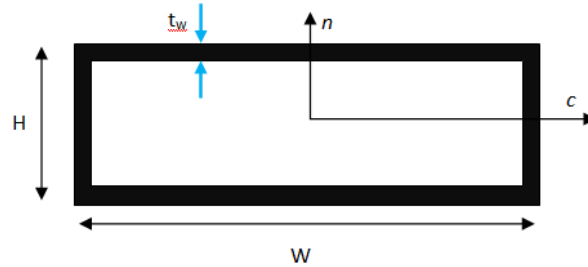
Figure 2-2: Beam cross section showing the geometric variables and coordinate system location.

2.2 Assumptions

As part of the simplification process, some engineering assumptions must be made to reduce the complexity of the problem. Those assumptions are listed below.

- The beam's cross section is symmetric about the c and s axis so that the shear center and tension axis coincide with the beam's axis of symmetry.
- The coordinate system origin coincides with the beam's centroid.
- The beam has a uniform wall thickness t_w around the cross section.
- All beam walls are made of symmetric laminates to avoid bending-extension coupling ($[B] = 0$).
- The vertical walls are made of balanced laminates.
- Thin wall assumption : $t_w \ll W$
- The beam's slenderness should be larger than 20, otherwise warping effects become much more important. $Slenderness = \frac{L}{W} \geq 20$
- The cross section aspect ratio should be larger than 1.8: $AR = \frac{W}{H} \geq 1.8$
- The beam bending loads are carried only by top and bottom plates.

2.3 Isotropic Beam Bending Equations

This section presents the governing equations of isotropic beam bending based on the standard Euler-Bernoulli beam theory [32]. The full beam stiffness matrix $[C]$ is generally composed of 21 independent elements and is symmetric.

$$[C] = \begin{bmatrix} C_{11} & C_{12} & C_{13} & C_{14} & C_{15} & C_{16} \\ - & C_{22} & C_{23} & C_{24} & C_{25} & C_{26} \\ - & - & C_{33} & C_{34} & C_{35} & C_{36} \\ - & - & - & C_{44} & C_{45} & C_{46} \\ - & - & - & - & C_{55} & C_{56} \\ - & - & - & - & - & C_{66} \end{bmatrix} \tag{2.1}$$

The complete matrix won't be required for this particular problem since typically airplane wings are sized by bending loads. Although there is always some amount of in-plane loading, it is not significant compared to the bending moments, therefore only the bending stiffness coefficients will be considered in the equation derivations. The bending terms correspond to the lower right quadrant of the full stiffness matrix and the beam bending stiffness matrix will be referred to as $[\bar{C}]$.

$$[\bar{C}] = \begin{bmatrix} C_{44} & C_{45} & C_{46} \\ - & C_{55} & C_{56} \\ - & - & C_{66} \end{bmatrix} = \begin{bmatrix} EI_{cc} & EI_{cs} & EI_{cn} \\ - & GJ & EI_{sn} \\ - & - & EI_{nn} \end{bmatrix} \tag{2.2}$$

The bending stiffness matrix relates the bending moments in the beam's c, s, n coordinate system to the beam curvatures κ. The moment about the s axis is in fact the torsion moment of the beam (or torque), therefore instead of the curvature κ, it is related to the twist angle derivative ϕ'.

$$\begin{bmatrix} M_c \\ M_s \\ M_n \end{bmatrix} = \begin{bmatrix} EI_{cc} & EI_{cs} & EI_{cn} \\ - & GJ & EI_{sn} \\ - & - & EI_{nn} \end{bmatrix} \begin{bmatrix} \kappa_c \\ \phi' \\ \kappa_n \end{bmatrix} \tag{2.3}$$

Here, EI_{cc} is the spanwise bending stiffness, GJ is the torsional rigidity and EI_{nn} is the chordwise bending stiffness of the beam. The off-diagonal terms are the coupling coefficients. The main focus of this chapter is to develop analytical equations to evaluate EI_{cs}, the bend-twist coupling coefficient of the beam. The other off-diagonal terms can be set to zero based on the assumptions that the c,n axes are aligned with the principal bending axes due to section symmetry and that the beam's vertical walls are symmetric and balanced. The resulting bending stiffness matrix is then:

$$[\bar{E}] = \begin{bmatrix} EI_{cc} & EI_{cs} & 0 \\ - & GJ & 0 \\ - & - & EI_{nn} \end{bmatrix} \tag{2.4}$$

By definition, the second moment of inertia of an area is given by:

$$I_{cc} = \int_A n^2 \mathrm{d}A \tag{2.5}$$

$$I_{nn} = \int_A c^2 \mathrm{d}A \tag{2.6}$$

The usual bending stiffness equations are then obtained by combining the inertia and stiffness terms:

$$EI_{cc} = \int_A En^2 \mathrm{d}A \tag{2.7}$$

$$EI_{nn} = \int_A Ec^2 \mathrm{d}A \tag{2.8}$$

For isotropic materials, all off-diagonal terms of the $[\bar{C}]$ matrix will be zero, and therefore structural couplings can't be achieved for those types of beams. Taking E out of the integrals and using the box beam's coordinate system, the final isotropic bending stiffness equations are obtained:

$$\boxed{EI_{cc} = E \iint n^2 \mathrm{d}c\mathrm{d}n} \tag{2.9}$$

$$EI_{nn} = E \iint c^2 \mathrm{d}c\mathrm{d}n \tag{2.10}$$

For beams made of orthotropic materials, the stiffness is not constant through the thickness of the beam and therefore E can't be taken out of the integral like in equations 2.9 and 2.10, which makes the problem more complex. In order to solve the orthotropic beam bending equations, knowledge of the basic principles of the classical laminated plate theory is required.

2.4   Classical Laminated Plate Theory

Since CLPT is able to accurately predict the stress-strain relationship for composite plates [18], the first step of this analysis is to consider each walls of the beam as individual plates carrying only in-plane loads. As the box beam is subject to a bending moment, the top and bottom plates of the beam will experience in-plane tension and compression forces. It will be assumed that shear loads due to torque are distributed on all four walls of the beam while the bending loads are carried only by the top and bottom plates. The following constitutive relation links the strains to the stress of a particular ply in the material coordinate system (Axis 1 is the fiber direction while axis 2 is the transverse direction). It should be noted that in the material axis, there is no coupling other than the one due to Poisson's effects.

$$\begin{bmatrix} \sigma_1 \\ \sigma_2 \\ \tau_{12} \end{bmatrix} = \begin{bmatrix} Q_{11} & Q_{12} & 0 \\ Q_{12} & Q_{22} & 0 \\ 0 & 0 & Q_{66} \end{bmatrix} \begin{bmatrix} \varepsilon_1 \\ \varepsilon_2 \\ \gamma_{12} \end{bmatrix} \tag{2.11}$$

The stress and strains in the material coordinate system can be very useful to predict failure of the material, however, at this stage of the process, they need to be expressed in the beam's own coordinate system c, s, n. This is achieved by performing a set of transformations using the standard rotation matrix $[T]$. An additional step is required to switch between engineering and tensor strains which

is performed by using Reuter's matrix $[R]$. The resulting stiffness matrix will be referred to as the transformed ply stiffness matrix $[\bar{Q}^{(k)}]$ where k is the kth ply of the laminate. Each ply within one of the beam's walls can be described by this matrix. Just like the conventional 6x6 stiffness matrix $[C]$, the ply stiffness matrix $[Q^{(k)}]$ and the transformed ply stiffness matrix $[\bar{Q}^{(k)}]$ are symmetric.

$$
\begin{bmatrix} \sigma_s^{(k)} \\ \sigma_c^{(k)} \\ \tau_{sc}^{(k)} \end{bmatrix} = [T]^{-1}[Q^{(k)}][R][T][R]^{-1} \begin{bmatrix} \varepsilon_c \\ \varepsilon_s \\ \gamma_{sc} \end{bmatrix} \tag{2.12}
$$

The stress-strain relation in the beam coordinate system for ply k can then be expressed as:

$$
\begin{bmatrix} \sigma_s^{(k)} \\ \sigma_c^{(k)} \\ \tau_{sc}^{(k)} \end{bmatrix} = \begin{bmatrix} \bar{Q}_{11}^{(k)} & \bar{Q}_{12}^{(k)} & \bar{Q}_{16}^{(k)} \\ - & \bar{Q}_{22}^{(k)} & \bar{Q}_{26}^{(k)} \\ - & - & \bar{Q}_{66}^{(k)} \end{bmatrix} \begin{bmatrix} \varepsilon_c \\ \varepsilon_s \\ \gamma_{sc} \end{bmatrix} \tag{2.13}
$$

It should be noted that $[\bar{Q}^{(k)}]$ is a function of the ply elastic moduli and ply angle θ. If $\theta = 0$ or 90, then there is no extension-shear coupling within that ply and $\bar{Q}_{16}$ = $\bar{Q}_{26}$ =0. Also, if the wall thickness t_w is small enough relative to the beam's height H, the strains will be uniform through the laminate following the strain compatibility principle. This explains why the strains are not a function of k in equation 2.13.

The total load per unit width applied on a laminate can be obtained by integrating the stresses over the thickness of the plate. For example, the running load in the s axis would be given by:

$$
N_s = \int_{-t_w/2}^{t_w/2} \sigma_s \, \mathrm{d}n \tag{2.14}
$$

Although the strain is constant through the thickness, the stress σ_s is different for each ply orientation since it depends on the ply's stiffness in the loading axis. To evaluate integral 2.14 for N_s, the stresses can therefore be integrated over the thickness of one ply, and then summed over all the plies of the laminate:

$$
N_s = \sum_{k=1}^{N} \int_0^{t_{ply}^{(k)}} \sigma_s^{(k)} \, \mathrm{d}n \tag{2.15}
$$

31

Finally, equation 2.13 can be converted to a constitutive relation between load and strain by multiplying both sides of the equation by the thickness of each ply and then summing over all the plies of the laminates. The resulting extensional stiffness matrix is known as the laminate [A] matrix and relates the running load (load per unit width) of the laminate to the laminate extensional strains.

$$
\begin{bmatrix} N_s \\ N_c \\ N_{sc} \end{bmatrix} = \begin{bmatrix} A_{11} & A_{12} & A_{16} \\ - & A_{22} & A_{26} \\ - & - & A_{66} \end{bmatrix} \begin{bmatrix} \epsilon_c \\ \epsilon_s \\ \gamma_{sc} \end{bmatrix}
\tag{2.16}
$$

The matrix coefficients are defined as:

$$
A_{ij} = \sum_{k=1}^{N} \bar{Q}_{ij}^{(k)} t_{ply}^{(k)}
\tag{2.17}
$$

Now that the main orthotropic plates equations have been introduced, the orthotropic beam bending stiffnesses can be derived.

2.5 Orthotropic Box Beam Bending Stiffnesses

The following derivation is mainly inspired by the work of [5] and [30]. Both papers proposed similar approaches to analytically evaluate the bend-twist coupling coefficient of composite box beams by using a bilinear warping function. The former focused on the bending stiffness matrix while the latter derived the full beam stiffness matrix and also included the effects of transverse shear.

2.5.1 Reduction to Plane Stress State

For beam structures loaded mainly in one dimensional bending like wings, the transverse (chordwise) in-plane load resultant N_c can be assumed to be zero since it is much smaller than the spanwise load. Following this assumption, equation 2.16 can be simplified further. The new reduced stiffness matrix of ply k will be identified as

$\bar{Q}'^{(k)}$.

$$\bar{Q}_{11}'^{(k)} = \bar{Q}_{11}^{(k)} - \frac{\bar{Q}_{12}^{(k)2}}{\bar{Q}_{22}^{(k)}} \tag{2.18}$$

$$\bar{Q}_{16}'^{(k)} = \bar{Q}_{16}^{(k)} - \frac{\bar{Q}_{12}^{(k)}\bar{Q}_{26}^{(k)}}{\bar{Q}_{22}^{(k)}} \tag{2.19}$$

$$\bar{Q}_{66}'^{(k)} = \bar{Q}_{66}^{(k)} - \frac{\bar{Q}_{26}^2}{\bar{Q}_{22}^{(k)}} \tag{2.20}$$

$$\bar{Q}'^{(k)} = \begin{bmatrix} \bar{Q}_{11}'^{(k)} & \bar{Q}_{16}'^{(k)} \\ \bar{Q}_{16}'^{(k)} & \bar{Q}_{66}'^{(k)} \end{bmatrix} \tag{2.21}$$

Then, the reduced constitutive relation is obtained, with $\sigma_c^{(k)} = 0$:

$$\begin{bmatrix} \sigma_s^{(k)} \\ \tau_{sc}^{(k)} \end{bmatrix} = [\bar{Q}'^{(k)}] \begin{bmatrix} \varepsilon_c \\ \gamma_{sc} \end{bmatrix} \tag{2.22}$$

In a similar fashion, the [A] matrix in equation 2.16 can be reduced to a 2x2 symmetric matrix by setting $N_c = 0$.

$$A' = \begin{bmatrix} A_{11}' & A_{16}' \\ A_{16}' & A_{66}' \end{bmatrix} \tag{2.23}$$

$$\begin{bmatrix} N_s \\ N_{sc} \end{bmatrix} = [A'] \begin{bmatrix} \epsilon_c \\ \gamma_{sc} \end{bmatrix} \tag{2.24}$$

Finally, an equivalent plate shear stiffness can be calculated by assuming a zero net in-plane load for the vertical and horizontal walls.

$$G_v = \frac{1}{t_v} \left(A_{66_v}' - \frac{(A_{16_v}')^2}{A_{11_v}'} \right) \tag{2.25}$$

$$G_h = \frac{1}{t_h} \left(A_{66_h}' - \frac{(A_{16_h}')^2}{A_{11_h}'} \right) \tag{2.26}$$

2.5.2 Warping Function

A two dimensional warping function will be used, where λ is the out-of-plane displacement of the section due to cross section warping. The next steps are inspired mainly by the work of Smith and Chopra [30]. The following bilinear warping function is chosen:

$$\lambda(c, n) = \beta c n \tag{2.27}$$

with β and α defined by:

$$\beta = -\frac{1 - \alpha}{1 + \alpha} \tag{2.28}$$

$$\alpha = \left(\frac{W}{H}\right) \left(\frac{t_v}{t_h}\right) \left(\frac{G_v}{G_h}\right) \tag{2.29}$$

The wall thickness ratio in Equation 2.29 is always equal to one because of the initial assumption on uniform wall thickness around the beam. Therefore, this equation simplifies to:

$$\alpha = \left(\frac{W}{H}\right) \left(\frac{G_v}{G_h}\right) \tag{2.30}$$

The out-of-plane displacement of the section in the s direction due to cross-section warping is proportional to the twist rate and can then be expressed as:

$$U_{warping} = -\lambda \phi'(x) \tag{2.31}$$

2.5.3 Beam Strains Including Warping Effects

Cross section warping will obviously have an influence on the beam's strains. In fact, due to the nature of the warping function chosen, its influence on the strain is linearly proportional to the distance from the center of the beam. It can either increase or reduce the totals strain depending on which corner of the section is investigated. The total axial strain in the beam walls is given by:

$$\varepsilon_{ss} = u' - c\kappa_c - n\kappa_n - \lambda \phi'' \tag{2.32}$$

The first term of equation 2.32 is the strain due to axial loading, the next two terms are the bending strains while the last one is the warping strain. As far as the shear strains are concerned, the classical strain and twist rate relationship must also be modified to account for the effect of warping. The following variable substitution will be used:

$$\hat{c} = c - \frac{\partial \lambda}{\partial n} = c(1 - \beta) = c\frac{2}{1 + \alpha} \tag{2.33}$$

$$\hat{n} = n + \frac{\partial \lambda}{\partial c} = n(1 + \beta) = n\frac{2\alpha}{1 + \alpha} \tag{2.34}$$

By using these new variables, the shear strain in the vertical beam walls is then defined as:

$$\varepsilon_{sn} = \hat{c}\phi' \tag{2.35}$$

and in the horizontal walls:

$$\varepsilon_{sc} = \hat{n}\phi' \tag{2.36}$$

2.5.4 Stiffness Matrix Terms

The derivation of the bending stiffness terms is relatively straightforward since no warping is involved in those loading modes. Surface integrals are performed over both the horizontal walls (h) and the vertical walls (v) of the beam since both of them contribute to the total stiffness.

$$EI_{cc} = \sum_{k=1}^{N} \int_{A:h} \bar{Q}_{11}'^{(k)} n^2 \mathrm{d}A + \sum_{k=1}^{N} \int_{A:v} \bar{Q}_{11}'^{(k)} n^2 \mathrm{d}A \tag{2.37}$$

The reduced stiffness $\bar{Q}_{11}'^{(k)}$ is constant through a ply and it can be taken out of the integral, which results in the final orthotropic beam bending stiffness equation:

$$\boxed{EI_{cc} = \sum_{k=1}^{N} \bar{Q}_{11}'^{(k)} \iint_h n^2 \mathrm{d}c\mathrm{d}n + \sum_{k=1}^{N} \bar{Q}_{11}'^{(k)} \iint_v n^2 \mathrm{d}c\mathrm{d}n} \tag{2.38}$$

The same process can be applied for the chordwise bending stiffness EI_{nn} except this time the inertia is computed about the n axis.

$$EI_{nn} = \sum_{k=1}^{N} \bar{Q}_{11}^{\prime(k)} \iint_h c^2 \mathrm{d}c\mathrm{d}n + \sum_{k=1}^{N} \bar{Q}_{11}^{\prime(k)} \iint_v c^2 \mathrm{d}c\mathrm{d}n \qquad (2.39)$$

For the torsion rigidity, the transformed section variables must be used in order to account for the effect of warping on the total section stiffness.

$$GJ = \sum_{k=1}^{N} \bar{Q}_{66}^{\prime(k)} \int_{A:h} \hat{n}^2 \mathrm{d}A + \sum_{k=1}^{N} \bar{Q}_{66}^{\prime(k)} \int_{A:v} \hat{c}^2 \mathrm{d}A \qquad (2.40)$$

which results in the following equation when the variables are transformed back into their original form by applying relation 2.33 and 2.34:

$$GJ = (1+\beta)^2 \sum_{k=1}^{N} \bar{Q}_{66}^{\prime(k)} \iint_h n^2 \mathrm{d}c\mathrm{d}n + (1-\beta)^2 \sum_{k=1}^{N} \bar{Q}_{66}^{\prime(k)} \iint_v c^2 \mathrm{d}c\mathrm{d}n \qquad (2.41)$$

The bend-twist coupling coefficient is integrated on the horizontal walls of the beam only since the initial assumption is that the vertical walls are balanced laminates and therefore exhibit no extension-shear coupling (i.e. $\sum_{k=1}^{N} \bar{Q}_{16_v}^{\prime(k)} = 0$)

$$EI_{cs} = \sum_{k=1}^{N} \bar{Q}_{16}^{\prime(k)} \int_{A:h} \hat{n}n \mathrm{d}A \qquad (2.42)$$

After the variable substitution, the final equation for the bend-twist coupling term is obtained:

$$EI_{cs} = (1+\beta) \sum_{k=1}^{N} \bar{Q}_{16}^{\prime(k)} \iint_h n^2 \mathrm{d}c\mathrm{d}n \qquad (2.43)$$

Appendix A.1 presents the code listing of the Matlab script created to calculate the bending stiffness matrix of composite box beams based on the equations presented in this chapter.

2.6   Physical Interpretation

Based on equation 2.43, it is obvious that bend-twist coupling of the beam depends on the $\bar{Q}'_{16}$ element of the reduced stiffness matrix. Physically, to obtain a non-zero $\bar{Q}'_{16}$ coefficient, the laminate must be unbalanced. The greater the unbalance, the greater this coefficient will be. Within a single laminate, the unbalance results in extension-shear coupling, however it can translate either into bend-twist coupling or extension-twist coupling at the beam level. To result in bend-twist coupling, the unbalanced laminates which make the top and bottom plates of the beam must be configured in a symmetric arrangement. If they were arranged in an anti-symmetric configuration, the $\bar{Q}'_{16}$ terms of the top and bottom plates would cancel each other out as they would be of opposite signs. This type of configuration would result in extension-twist coupling, but this is out of the scope of this thesis as it does not provide any benefit for airplane wings. Figure 2-3 illustrates the possible layup configurations and the resulting coupling effects on the beam.

Symmetric Layup Beam
- **Bending-Torsion Coupling**
- **Extension-Shear Coupling**

Anti-Symmetric Layup Beam
- **Extension-Torsion Coupling**
- **Bending-Shear Coupling**
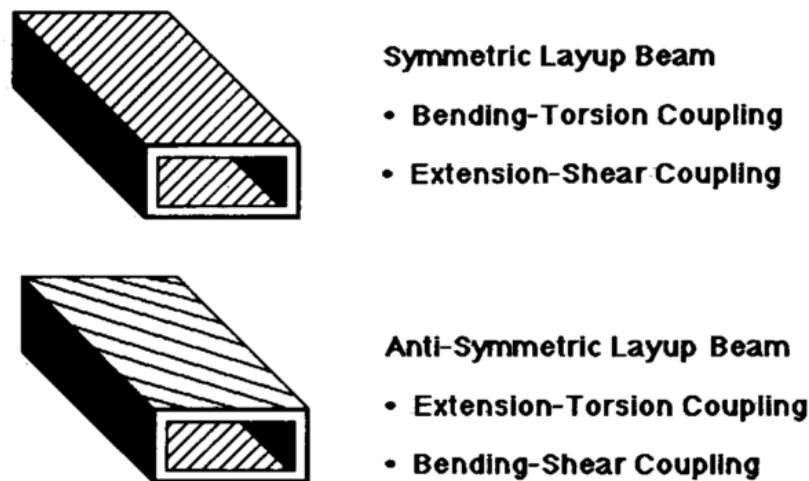
Figure 2-3: Different composite layups on box beams and the resulting coupling [30].

Chapter 3

Analytical Model Validation

This chapter focuses on validating the orthotropic beam bending equations developed in chapter 2 by comparing different scenarios against finite element analysis (FEA) and some experimental data. The impact of the layup angle on the beam's bending stiffness and coupling term is also evaluated.

3.1   Model Descriptions

This first section describes the different beams that will be simulated by the analytical model and the FEA for benchmarking purposes. The material properties, the different layups used as well as information about the various beam geometries are provided.

3.1.1   Material Properties

Table 3.1 presents the material properties that have been used in the simulations and the analytical model. Only the elastic properties are required since no failure analysis are performed at this point. All properties are in the material coordinate system (Axis 1 is the fiber direction and axis 2 is the matrix direction).

Property	Value
E_{11}	20.59×10^6 psi
E_{22}	1.42×10^6 psi
G_{12}	0.89×10^6 psi
ν_{12}	0.42
t_{ply}	0.005"

Table 3.1: Lamina elastic properties for AS4/3501-6 [5].

3.1.2 Layups

Since the model response and quality might depend on the layup angles, the box beams were simulated at four different angles: $\theta = 0, 15, 30$ and 45 degrees. It is not necessary to simulate anything between 45 and 90 degrees since the peak coupling occurs under $\theta = 45$ degrees and the laminate elastic properties should be symmetric about the 45 degree layup angle. The walls of the beams are made of 6 unidirectional plies, resulting in a total wall thickness $t_w = 0.03"$. Table 3.2 has detailed information about the four different layups simulated.

Layup	Horizontal Walls	Verticall Walls
1	$[0]_6$	$[0]_6$
2	$[15]_6$	$[\pm 15]_3$
3	$[30]_6$	$[\pm 30]_3$
4	$[40]_6$	$[\pm 45]_3$

Table 3.2: The various layups used for the analytical model validation.

3.1.3 Beam Geometries

Finally, table 3.3 provides detailed information about the beam geometries that have been simulated. It should be noted that configuration 1 is based on the work of Chandra [5] and was used as a baseline in order to be able to compare with their experimental work. The other two configurations with larger aspect ratios are simulated since they are more representative of an actual wing geometry. The beam length is increased in order to keep the slenderness ($\frac{L}{W}$) of the beam constant even if the width was modified. Warping of the cross section is more important in less slender beams,

so keeping the slenderness constant ensures the relative warping effects are the same for all beams.

Beam	1	2	3
W	0.953	2.12	3.18
H	0.53	0.53	0.53
L	29	64	96
AR	1.8	4	6
$\frac{L}{W}$	30	30	30

Table 3.3: The various beams geometries used for the analytical model validation.

3.2   Analytical Calculations

Based on the equations derived previously, the applied moments can be estimated from the stiffness matrix and the curvature matrix of the beam, the constitutive relation is restated in 3.1 for convenience.

$$
\begin{bmatrix} M_c \\ M_s \\ M_n \end{bmatrix} = \begin{bmatrix} EI_{cc} & EI_{cs} & 0 \\ EI_{cs} & GJ & 0 \\ 0 & 0 & EI_{nn} \end{bmatrix} \begin{bmatrix} \kappa_c \\ \phi' \\ \kappa_n \end{bmatrix} \tag{3.1}
$$

In the benchmarking scenarios, a unit moment is applied and the beam curvatures are the unknowns. Consequently, the bending stiffness matrix $[\bar{E}]$ must be inverted, resulting in equation 3.2. The calculated curvatures and twist slopes can then be compared to the ones obtained from the FEM or experimental data to evaluate the accuracy of the model.

$$
\begin{bmatrix} E^{-1} \end{bmatrix} \begin{bmatrix} M_c \\ M_s \\ M_n \end{bmatrix} = \begin{bmatrix} \kappa_c \\ \phi' \\ \kappa_n \end{bmatrix} \tag{3.2}
$$

3.3 Finite Element Analysis

This section presents the box beam's finite element model as well as the analysis results that were obtained from it. The main goal behind these analyses was to ensure that the analytical equations that have been developed in chapter 2 are actually valid.

3.3.1 Model Details

The finite element model was created using Abaqus 6.10, a commercial analysis software widely used in the aerospace industry and published by Dassault Systemes [9]. In Abaqus, the beam's walls are modeled as 2D shells using the S4R element, a 4-nodes quadrilateral reduced integration linear element. The structure is clamped at one end while at the other end a unit load is applied. The applied load is either a spanwise bending moment $M_c = 1$ or a torque $M_s = 1$. Several cases are tested for a variety of aspect ratios and layup angles as described in section 3.1. In order to find the optimal element size for the problem, a mesh convergence study was performed using the beam's tip displacement as the convergence criteria. The study showed that elements with a width of 12% the beam's total width were the largest that could be used without loss in solution quality. Using smaller elements would only increase the analysis time without improving the results.

Figure 3-1 and 3-2 illustrate an example of the finite element model for the beam of aspect ratio $\frac{W}{H} = 4$ and $\theta = 45°$ layup. The first figure shows the undeformed geometry while the second one illustrates the deformed shape under a unit bending load. The torsion of the cross section due to bend-twist coupling can clearly be seen.

3.3.2 FEA and Analytical Model Results Comparison

The predictions from the analytical model and the finite element analysis results are plotted on the next 4 figures. Figure 3-3 illustrates the validation of the spanwise bending stiffness EI_{cc}. The spanwise curvature κ_c due to a unit bending moment M_c at the tip of the sample beam is plotted for different layup angles. As expected,
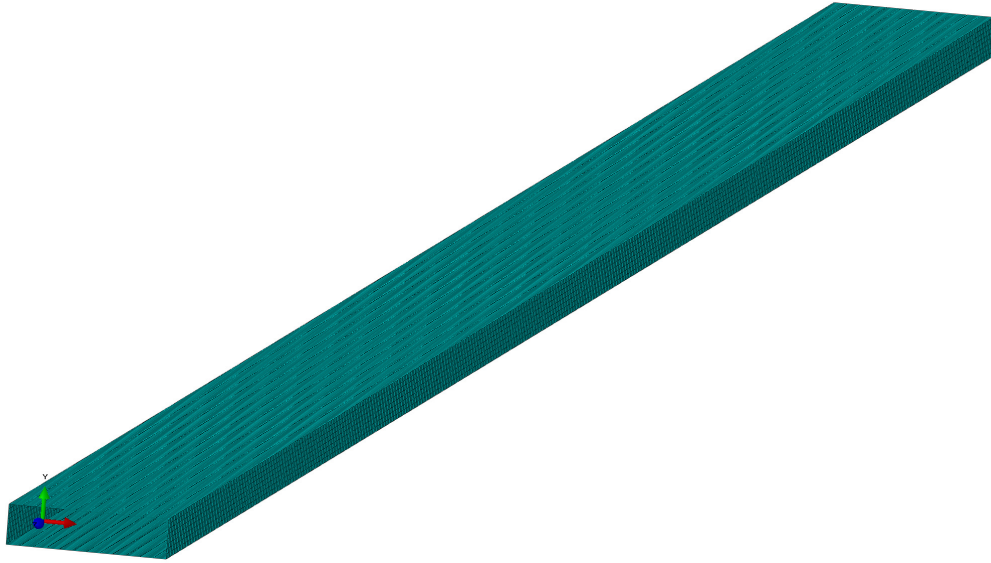
Figure 3-1: Undeformed isometric view of the beam of aspect ratio 4 in the Abaqus FEM illustrating the mesh.
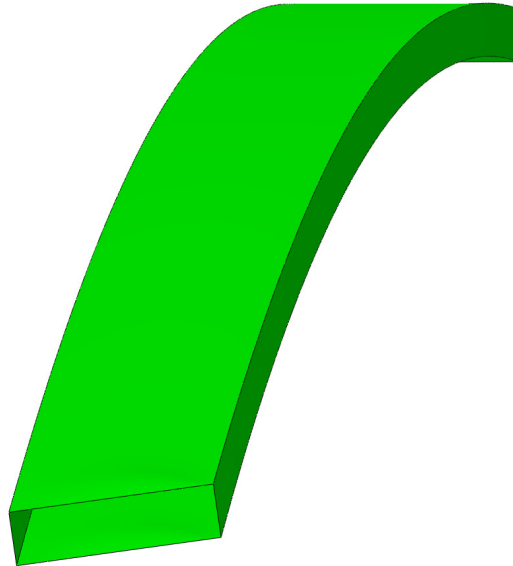
Figure 3-2: Deformed view of the beam of aspect ratio 4 due to a unit bending load $M_c = 1$ in the Abaqus FEM. The torsion of the section due to bend-twist coupling is easily noted.

the general trend for both models is that the bending stiffness decreases as the layup angle is increased. The correlation is excellent for the whole range of layup angles but seems to be slightly better at lower angles and for lower aspect ratios. The analytical

model underestimates the curvature when compared to the FEM for the whole range of layup angles, which implies that the equations slightly overestimate the beam's bending stiffness. It should be noted that at $\theta = 0$, there is no bend-twist coupling and in this case the analytical model matches exactly the FEM data.
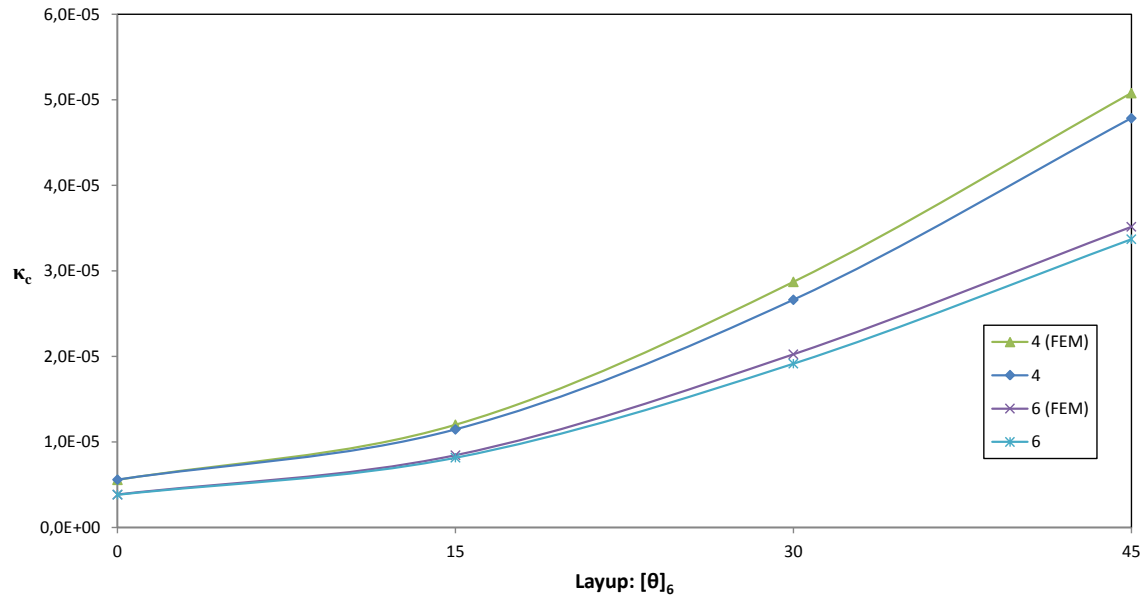
Figure 3-3: EI_{cc} validation against FEM for beams of aspect ratio 4 and 6 under a unit bending moment $M_c = 1$.

The next figure illustrates the twist slope ϕ' due to a unit bending moment M_c. This is effectively a measure of the quality of the bend-twist coupling coefficient EI_{cs} calculated by the analytical equations. At layup angles $\theta = 0$ there is obviously no coupling, which is why there is no twist. As the layup angle increases, larger coupling effects are observed, with a maximum coupling somewhere between 30 and 45 degrees layup angle. As for the bending stiffness, the analytical model always underestimates the twist slope compared to the FEM, specially at higher layup angles. At 15 and 30 degrees, the model predicts very nicely the coupling behavior of the beam. However, at 45 degrees it seems that the model diverges from the equations, particularly for beams of higher aspect ratios. This could be due to a nonlinear warping field for beams with high aspect ratios and high layup angles which is not captured by the linear warping field assumed by the present analytical model.

44

Figure 3-5 illustrates the curvature κ_c at the tip of the beam when subject to a unit torque $M_s = 1$. The figure is identical to figure 3-4 which is not surprising given the symmetric nature of the stiffness matrix and that a unit moment was applied in both cases. The analytical model can therefore predict coupling from torque or bending moments with the same solution quality.
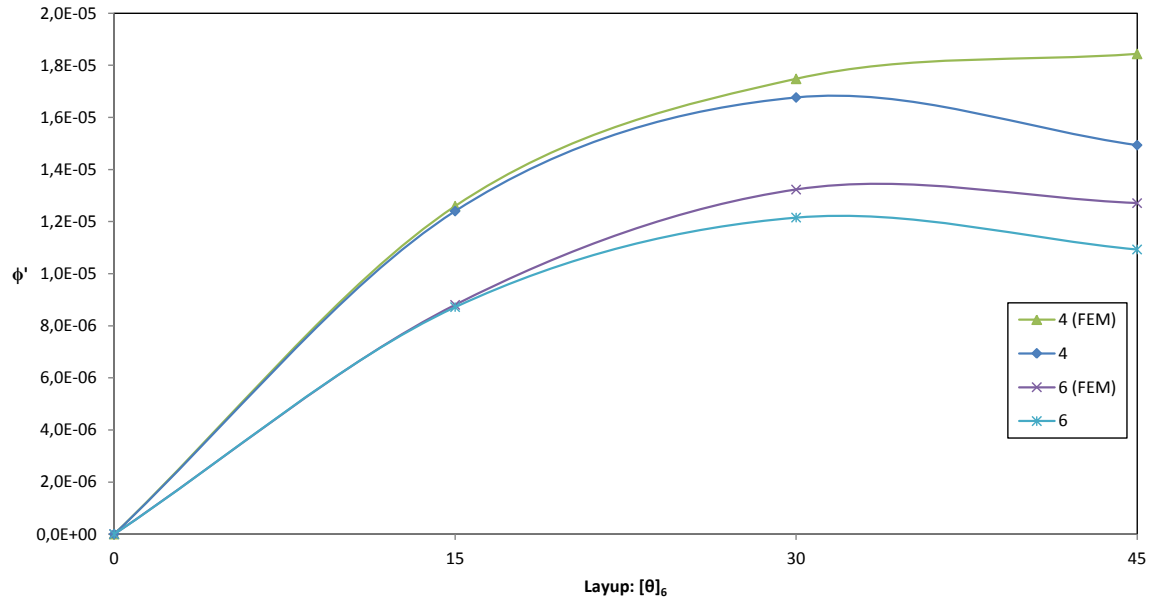
Figure 3-4: EI_{cs} validation against FEM for beams of aspect ratio 4 and 6 under unit moment $M_c = 1$.

Finally, figure 3-6 illustrates the twist slope ϕ' under a unit torque load $M_s = 1$ for the 4 layup angles. This is basically a measure of the torsion rigidity GJ as a function of the layup angle θ. From the plot, the torsion rigidity is maximum at a layup angle of 45 degrees which makes sense because the carbon fibers are then oriented in the direction of principal stress, which for a pure torque case is always at 45 degrees. Again the correlation between the analytical model and the FEM is excellent, specially at layup angles lower than 30 degrees. At 45 degrees, there is a larger difference between the two models particularly for the beams with an aspect ratio of 4. This is probably due again to nonlinear section warping effects at higher layup angles.
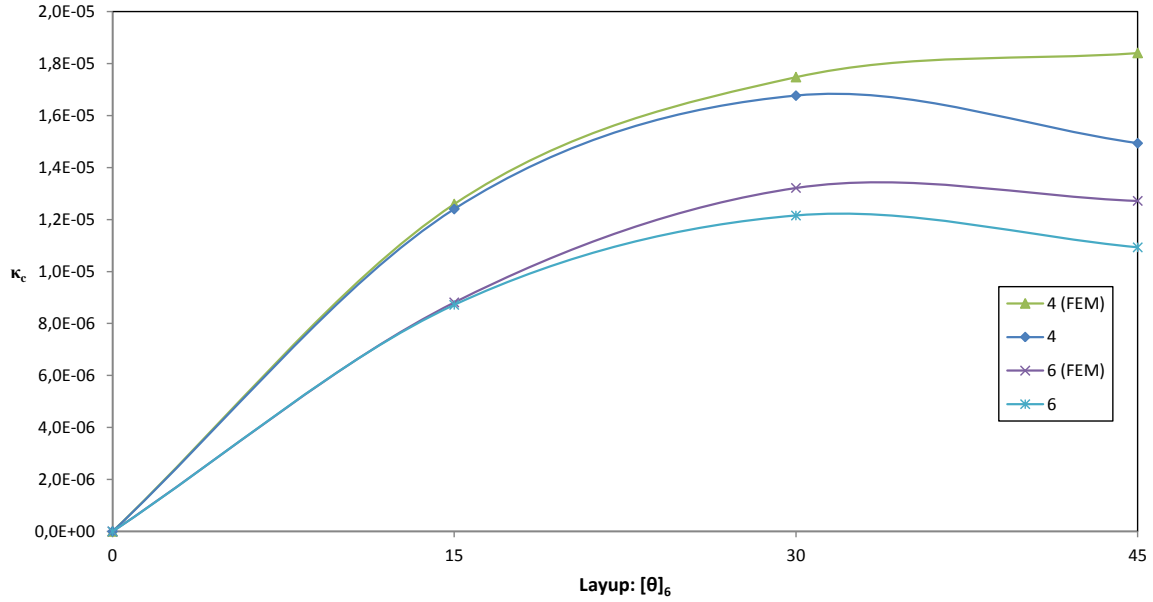
Figure 3-5: EI_{cs} validation against FEM for beams of aspect ratio 4 and 6 under a unit torque $M_s = 1$.
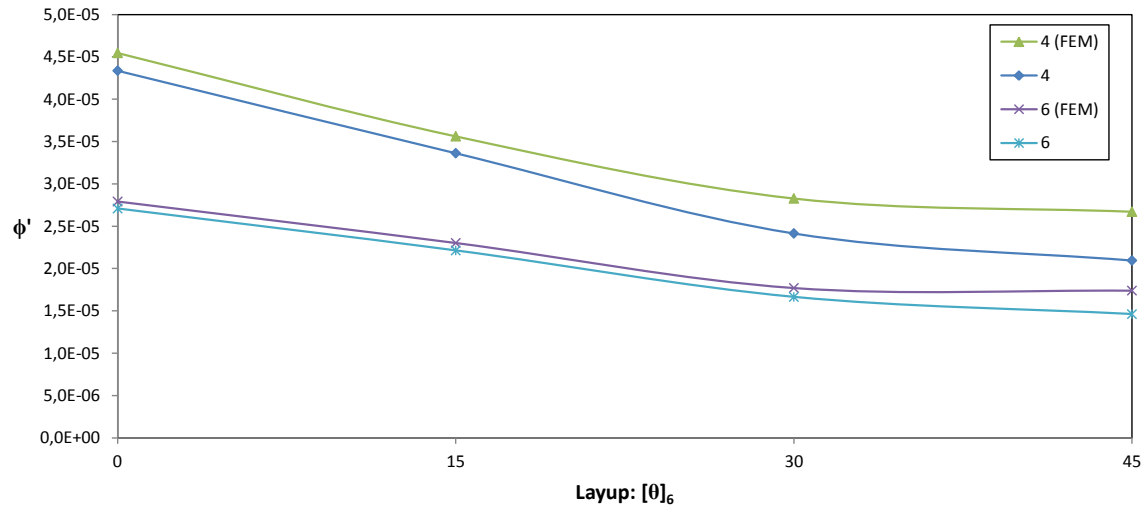
Figure 3-6: GJ validation against FEM for beams of aspect ratio 4 and 6 under unit torque $M_s = 1$.

3.4   Experimental Data

The data from the only paper which has published experimental results about bend-twist coupling of thin-walled orthotropic box beams will be used as a validation tool here [5]. In Chandra's paper, the twist and bending slopes of several beams of aspect

ratio 1.8 were measured under unit bending moments and torques. The beams had symmetric and balanced vertical walls and unbalanced horizontal walls to create the coupling. Even though most aircraft wings have a cross section aspect ratio above 3, it is still useful to compare the analytical model and the FEM results against this experimental data. The next two figures illustrate those results.

On figure 3-7, the twist angle ϕ at the tip of the beam, in radians, is plotted for different layup configurations. The difference between the analytical model and the finite element model results is greater than what was noted for beams of aspect ratios 4 and 6, as can be seen by comparing with figure 3-6. The trend is once again that the equations predict the stiffnesses more accurately for larger aspect ratio beams. Again, the difference between the two models is larger at higher layup angles. The experimental data matches closely the analytical equations at a layup angle of 15 degree but as the angle increases, the experimental data matches more closely the finite element model than the equations. It would have been interesting to see experimental data for beams with aspect ratios of 4 and 6 as it seems that the analytical model performs better in those cases. It would also have been more representative of a typical airplane wing geometry.
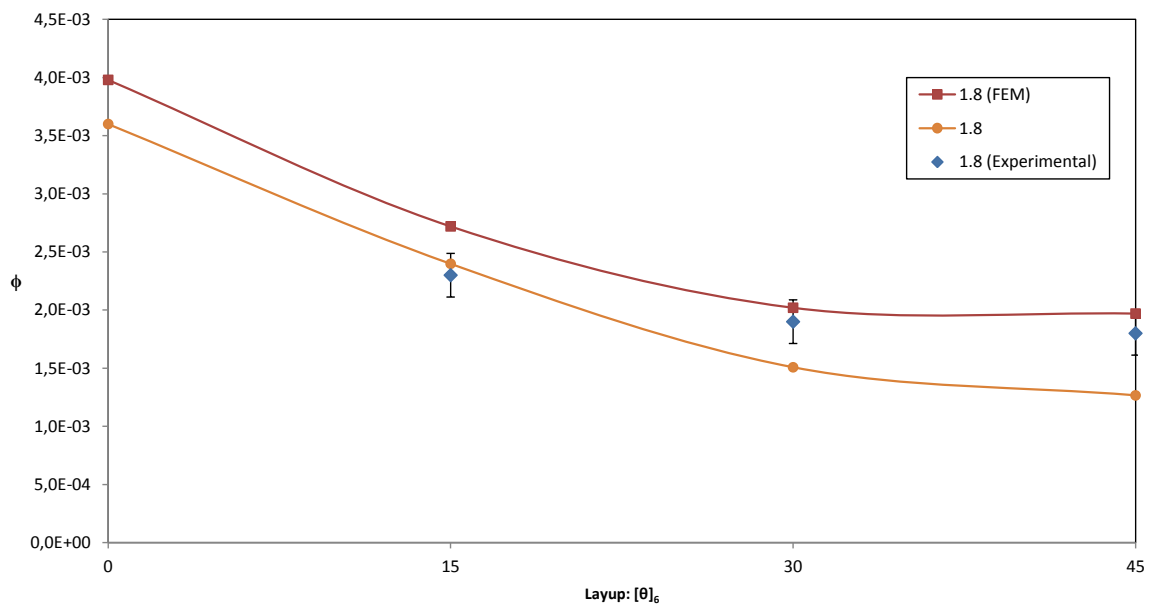
Figure 3-7: GJ validation against experimental data for beams of aspect ratio 1.8 under unit torque $M_s = 1$.

47

Finally, figure 3-8 displays the beam's bending slope at the tip for angles from 0 to 45 degrees. This is effectively a measure of the coupling coefficient EI_{cs}. In this case, the experimental data seems to match closely the analytical model for layup angles of 15 and 30 degrees but diverges at a layup angle of 45 degrees. It should be noted however that the experimental data has very large error bars. The fact that at 45 degrees the models and the experimental data do not match is not surprising as this trend was also observed previously for beams of higher aspect ratios.
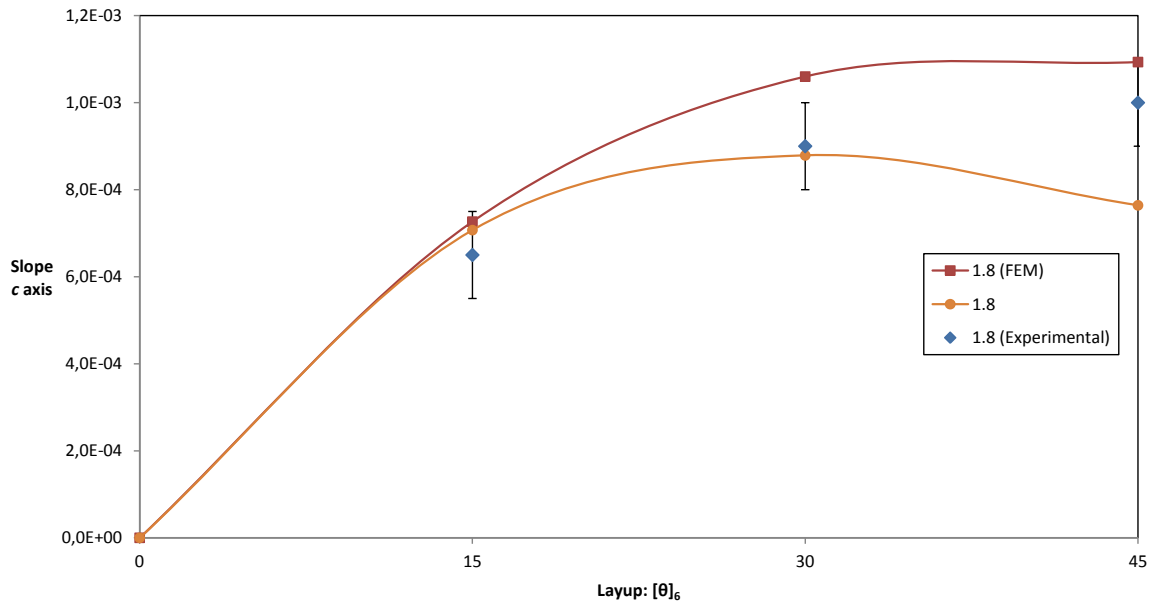
Figure 3-8: EI_{cs} validation against experimental data for beams of aspect ratio 1.8 under unit torque $M_s = 1$.

Based on the previous plots and comparisons, the analytical model developed in chapter 2 can accurately predict the bending stiffness matrix of an orthotropic box beam at different layup angles, within the limit of the assumptions presented in section 2.2. It performs best if the beam has an aspect ratio around 4 and if the layup angle is below 30 degrees.

Chapter 4

Aero-Structural Simulation Models

The intent of this chapter is to provide details about the aero-structural simulations which have been used to evaluate the performance of flexible wings with and without bend-twist coupling. First, some information about the simulation code and the different airplane models is provided. Then, the static and dynamic load cases are presented. Next, some explanations about the importance of the wing's initial twist angle distribution are given. The composite material properties used and the selected failure criteria are then described. Finally, the iterative sizing procedure of the wing is addressed.

4.1   ASWING Models

To evaluate the performance of the bend-twist coupled wings, the steady formulation of ASWING, a computer code developed by Mark Drela at MIT, is used. ASWING combines a nonlinear Euler-Bernoulli beam representation with an enhanced lifting-line model of the aerodynamic surfaces in order to predict the static loads and deformations of flexible aircraft [10].

In order to investigate the effects of aircraft scale on the coupling benefits, the ASWING simulations are performed on two aircraft models of different sizes. The first one is a Boeing 737-800 which is a short to medium range twin engine airliner. It is the best selling jet airliner in the history of commercial aviation, with over 7000

aircraft delivered so far. The second model is the Boeing 777-300ER, a long range wide body twin engine aircraft. It is one of the best selling long range passenger jet airplane in the world. Therefore, when combining the market segments of these two airplanes, most of the commercial air travel market is covered. A more detailed description of each airplane model is given in the next section.

4.1.1 Boeing 737-800

Table 4.1 provides some technical information about the Boeing 737-800. The maximum takeoff weight (MTOW), maximum zero fuel weight (MZFW) and maximum landing weight (MLW) will be required to evaluate the gust loads velocities on the wings in the next section.

Characteristic	Data
MTOW	174 200 lbs
MZFW	138 300 lbs
MLW	146 300 lbs
Passengers	108 - 177
Range	3050 - 5510 nmi
Mach	0.78
Wing Span	112.6 ft
Sweep Angle	25°

Table 4.1: Boeing 737-800 technical characteristics.

An isometric view of the 737 ASWING model is presented in figure 4-1.

4.1.2 Boeing 777-300ER

The same technical information is presented for the 777 in table 4.2. There are a few significant differences between it and the 737. In terms of mass properties, the takeoff weight of the 777 is more than 4 times larger than the 737's. Its wing is also much larger considering its wingspan is 100 feet longer than the 737's. Not only is this aircraft much bigger than the 737 but it also flies about 8% faster (Mach 0.84 vs 0.78). As a consequence, its wings have a higher sweep angle (32° vs 25°) in order

AZ = -135°
EL = 20°

ASWING 5.95
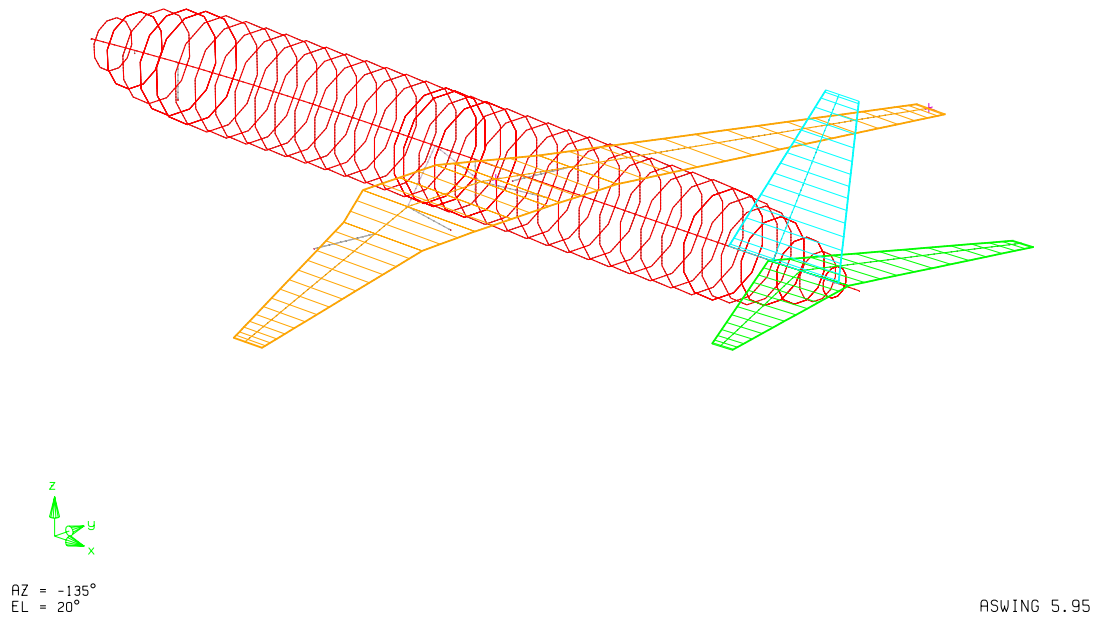
Figure 4-1: ASWING model of the Boeing 737-800.

to prevent the airflow on the top of the wings from reaching Mach, 1 which would otherwise lead to high sonic drag penalties.

Characteristic	Data
MTOW	775 000 lbs
MZFW	524 000 lbs
MLW	554 000 lbs
Passengers	365 - 550
Range	7930 nmi
Mach	0.84
Wing Span	212.6 ft
Sweep Angle	32°

Table 4.2: Boeing 777-300ER technical characteristics.

An isometric view of the ASWING model of the 777 is presented in figure 4-2.
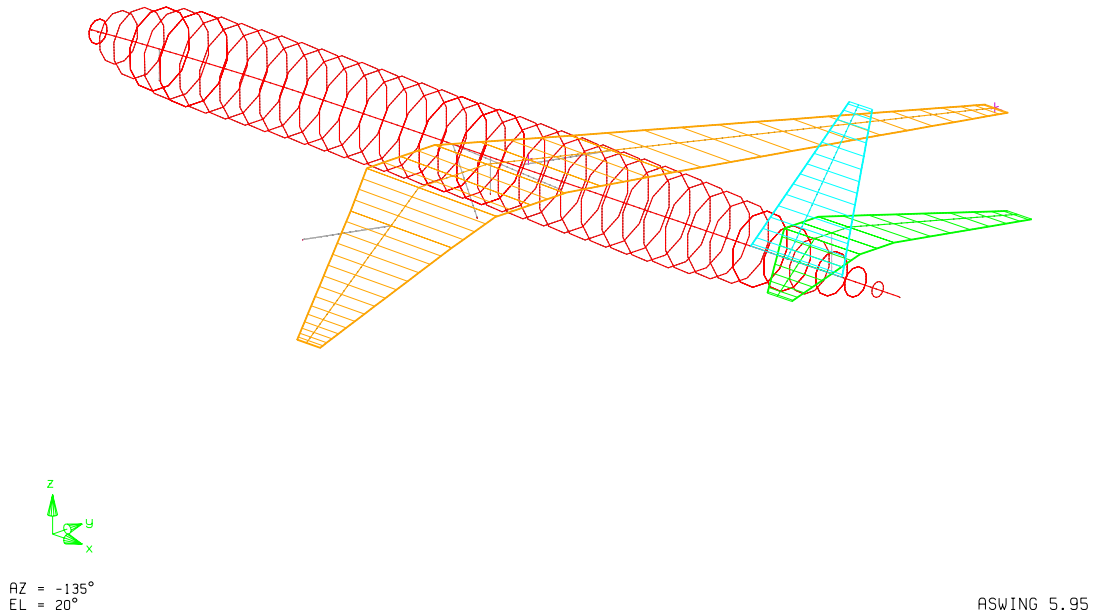
Figure 4-2: ASWING model of the Boeing 777-300ER.

4.2   Loading Scenarios

From the hundreds of different loading conditions a commercial airplane will experience during its lifespan, only the most extreme scenarios will actually be critical for the airplane's structure. Usually these critical load cases size particular areas of the aircraft. For example, the fuselage is dimensioned by, among other scenarios, ground cases such as hard landings and towing maneuvers. The wings, on the other hand, are typically sized by maneuvering loads and gust encounters. Since this thesis focuses on wing design, only the latter two loading scenarios will be considered for the aero-structural simulations.

More specifically, when a certificate of airworthiness is delivered to a new airplane type, the manufacturer must have thoroughly demonstrated that its design complies with the Federal Aviation Administration (FAA) rules. Both the 737 and the 777 are

certified under part 25 of the FAA regulations which covers transport category jet engine airplanes equipped with 10 or more seats. Consequently, the static maneuvering load factor and the gust velocities will be generated following the FAR 25 regulations [13].

4.2.1 Static Load Case

In chapter FAR 25.337, the static limit maneuvering load factor is defined as:

$$n = 2.1 + \frac{24000}{MTOW + 10000} \tag{4.1}$$

The FAA also specifies that the static load factor n may not be less than 2.5 and need not be greater than 3.8. Based on the maximum takeoff weight (MTOW) of the 737 and 777 and on equation 4.1, the calculated n for both airplanes is smaller than 2.5. Therefore, $n = 2.5$ will be used since it is the smallest value allowed by the FAA for this aircraft category. The ultimate static maneuvering load factor is then obtained by multiplying the limit load factor by 1.5 and is defined as $n_{ult} = 3.8$ for both airplanes.

4.2.2 Gust Cases

Sometimes, the static cases may not be critical for certain wing geometries, thus it is important to also look at dynamic cases. Gust encounters are highly stochastic events and it may not be obvious what is the critical gust for a given airplane [14]. The design case recommended by the FAA is an upgust where the air velocity profile inside the gust follows a $[1 - \cos]$ shape, as prescribed by FAR 25.341 regulations. The velocity U in feet per second at a distance s inside the gust is given by equation 4.2.

$$U = \frac{U_{ds}}{2} \left(1 - \cos \frac{\pi s}{H}\right) \tag{4.2}$$

with $0 \leq s \leq 2H$

It is important to note that the loads generated by this gust profile are limit loads and a factor of 1.5 must be applied on these in order to get the ultimate design load. Equation 4.2 depends on a few parameters which are defined in the FAA chapter 25.341 but their definition is reprinted here for convenience.

U_{ds} is the peak gust velocity and is defined by equation 4.3. H is the gust length, varying from 30 to 350 feet. This is a very important parameter since the critical gust length H may change depending on the geometry and stiffness of the wing. U_{ref} is the reference gust velocity and it is set to the maximum possible value allowed by the FAA in order to be conservative (56 ft/s). Z_{mo} is the maximum operating altitude of the airplane, in feet. The other parameters are defined in the following equations and depend mainly on different weight ratios of the airplane.

$$U_{ds} = U_{ref} F_g \left(\frac{H}{350} \right)^{1.6} \tag{4.3}$$

Where:

$$F_g = 0.5(F_{gs} + F_{gm}) \tag{4.4}$$

$$F_{gs} = 1 - \frac{Z_{mo}}{250000} \tag{4.5}$$

$$F_{gm} = \sqrt{R_2 \tan \left(\frac{\pi R_1}{4} \right)} \tag{4.6}$$

$$R_1 = \frac{MLW}{MTOW} \tag{4.7}$$

$$R_2 = \frac{MZFW}{MTOW} \tag{4.8}$$

The gust velocities evaluated with equation 4.3 are presented in table 4.3. Gust lengths of 30, 100, 200, 300 and 350 feet have been chosen to cover the full span of gust lengths prescribed by the FAA. They will be used to evaluate the response of

the different 737 and 777 composite wings to the gust scenario.

H	U_{ds}	
	737	777
30	30.1	27.7
100	36.8	33.8
200	41.3	38.0
300	44.2	40.6
350	45.4	41.7

Table 4.3: Limit gust velocities in feet per second for gust lengths between 30 and 350 feet, following FAR 25.341 rules.

4.3   Wing Twist Distribution

One of the inputs required by ASWING is the initial spanwise wing twist distribution (refered to as $Twist$ or Tw_0). There usually exists an optimal zero load twist angle distribution which will result in a minimum drag coefficient C_D in 1g flight conditions. Usually this in-flight twist target is known based on aerodynamic analysis while the optimal zero load twist, required to obtain the proper deformed wing shape, is unknown.

This initial twist angle distribution depends mainly on the wing's stiffness. More compliant wings will require a greater initial twist than stiffer wings in order to compensate for the additional in-flight twist deformation. If a given wing is modified such that it becomes more compliant without changing its geometry, its loading will naturally shift towards the inboard portion of the wing unless its initial twist is modified accordingly. This load shift would ultimately lead to a reduction of the wing's root spanwise bending moment M_{c0}, which from a structural point of view would be beneficial. However, from an aerodynamic point of view, this is not really desired since an increase in induced drag is observed as a consequence of the non-optimal twist distribution. Generally this drag penalty is greater than the benefits of the weight savings from the reduced moment and thus leads to increased fuel burn. Therefore, to make a fair comparison between the different designs, all the wings

should have the same deformed shape and root bending moment M_{c0} when flying in steady and level flight. This is obtained by adjusting the wing's initial twist.

Figure 4-3 compares the section lift coefficients distribution along the span of a 737 wing for two different initial twist scenarios. The first curve shows the wing loading when the optimal twist distribution is applied, while the second curve illustrates a non optimal configuration. Even though both wings generate the same amount of total lift, the second scenario clearly generates more lift inboard of the wing compared to the optimal case. This has the obvious consequence of reducing the wing's spanwise root bending moment. Moreover, the wing's total drag coefficient has been shown to be 30% lower when the twist angle was optimized, a consequence of the lower wing induced drag coefficient C_{Di}.
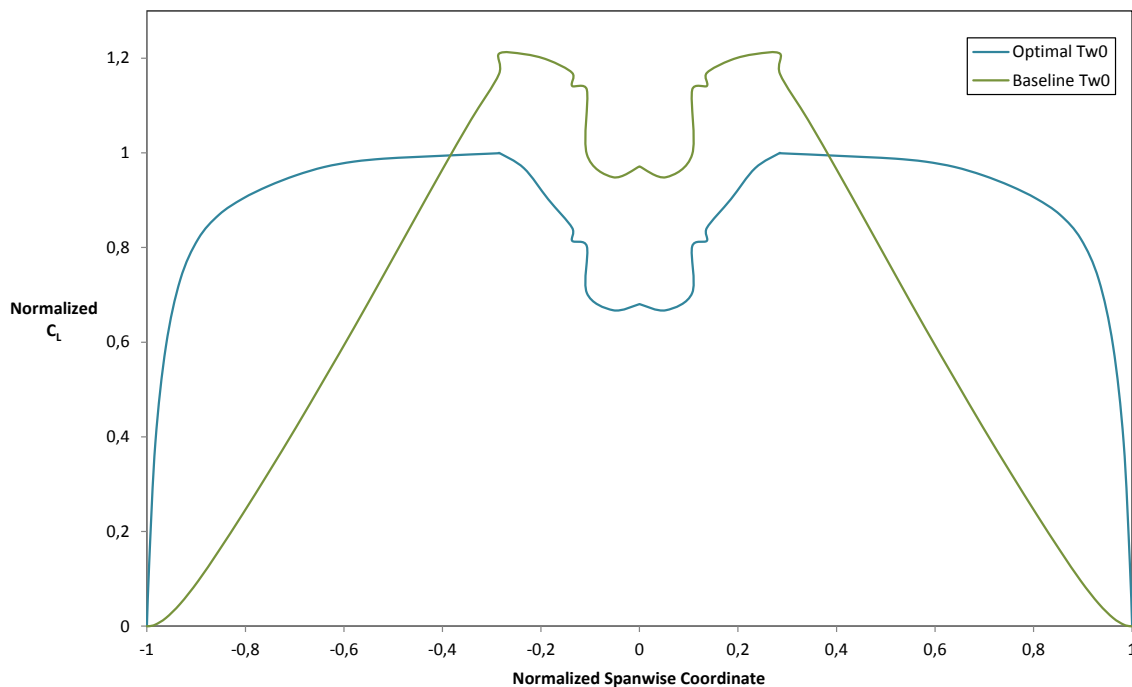
Figure 4-3: Effect of initial twist on lift distribution over the 737 wing in cruise conditions.

Because of the importance of this parameter, a Fortran computer code (Twist.f) was developed in order to automatically find the optimal wing zero load twist distribution. Through an iterative process, the code modifies the wing's $Twist$ parameter until the in-flight twist matches a specific optimal target deformation. The targets

are based on the baseline aluminum wings of the 737 and 777 and are shown in table 4.4. Having the composite wings match the in-flight twist of the aluminum wings ensures that the wings share the same drag coefficients and the same root bending moments, which makes their comparison easier and more relevant. Appendix A.2 presents the "Twist.f" code listing developed for this purpose.

(a) 737		(b) 777	
x (m)	Tw (°)	x (m)	Tw (°)
0.	1.22	0.	1.31
1.80	1.22	3.05	1.31
2.80	1.09	5.31	1.07
3.80	0.95	7.58	0.81
4.80	0.78	9.84	0.52
7.80	0.34	15.07	-0.10
10.81	-0.11	20.30	-0.91
13.82	-0.45	25.53	-1.71
16.83	-0.64	30.76	-2.53

Table 4.4: Wing twist targets for the 737 and the 777 based on aluminum wing in 1g cruise flight.

4.4 Material Properties

Another important feature of any simulation model is obviously the choice of the material properties. The lamina elastic properties used for the aero-structural simulations are the same ones used for the validation of the bend-twist coupling equations. They were for the AS4/3501 unidirectional tape and were presented in table 3.1. Since the strength properties of this particular material were not available, numbers from a different carbon fiber material had to be used. The unidirectional tape T700/2510 was chosen since it is similar to the AS4/3501. Just like the AS4/3501, it is a unidirectional tape and has similar ply thickness and elastic properties. Also, the ply properties of the T700/2510 are publicly available through the Advanced General Aviation Transport Experiments (AGATE) initiative [1]. This is a publicly funded project started by the FAA and NASA which was aiming at making composite ma-

terials more accessible to smaller airplane manufacturers. It is doing so by providing a standardized database of material properties which have been tested and approved following the FAA's standards. This had the impact of significantly reducing the cost and time required for general aviation manufacturers who wanted to use those materials as they did not have to go through the complex FAA material qualification process.

To be conservative, the 3 in-plane strength properties have been measured at elevated temperatures (180° F) and under wet conditions (85% relative humidity). The statistical variability of the material properties is also taken into account through a B-Basis statistical knockdown factor. Typically, composite material strengths will be slightly different between compression and tension. To simplify the analysis and to be conservative the lowest number between tension or compression values was chosen for all the properties. The resulting strength allowables are therefore representative of the worst case scenario for this material and are very conservative. Table 4.5 shows the final strength values in the material coordinate system.

Property	Value
F_1^u	155 ksi
F_2^u	3.3 ksi
F_{12}^u	12.9 ksi

Table 4.5: Lamina strength properties accounting for B-Basis and elevated temperature wet conditions.

As can be noted from the strength numbers, the material is much weaker in the transverse direction (Axis 2) than in the fiber direction. This is typical of unidirectional tapes since this axis is not reinforced by fibers and therefore only reflects the tensile strength of the resin. This is why unless a part is always loaded in the same direction, most composite laminates will be made of plies of different angles in order to have a more uniform resistance.

4.5   Composite Failure Criteria

To evaluate the failure of a composite laminate, there exists a wide choice of failure criteria to choose from. Unfortunately, none of them can accurately predict all the failure modes of a laminate [16]. For the purpose of this study, a combination between the maximum strain and the maximum stress failure criteria was chosen due to their simplicity and their wide usage in the aeronautics industry. For the type of structure and loading this thesis is concerned about, only the in-plane failure modes are relevant. These failure modes are fiber failure, matrix failure and shear failure.

To evaluate if a laminate fails in any of these modes using the maximum stress criteria, the laminate stresses have to be rotated into the ply's coordinate system. Then, the ply stresses are compared to the material's design allowables to evaluate if they exceed or not their limit. Once one of the plies reaches its maximum stress, the ply stresses can be rotated back into the laminate coordinate system to generate an equivalent laminate axial failure stress. This axial failure stress can then be converted into an equivalent laminate axial strain which then becomes the laminate failure strain ε_{cr}. This is a convenient metric since ASWING already calculates the wing strains along the span of the wing. Given that the axial strain is typically highest at the wing root, the maximum strain criteria only needs to be verified at that location. A detailed Matlab script has been written in order to perform the task of finding the laminate's critical axial strain ε_{cr} and the code listing is provided in appendix A.3.

The laminate failure strains and loads were evaluated for a family of laminates with layup angles ranging from 0 to 45 degrees. Both balanced and unbalanced configurations were evaluated in order to find the influence of coupling on laminate strength. The layup families studied are presented in table 4.6.

Unbalanced (Coupling)	Balanced (No coupling)
-	$[\,0\,]_n$
$[\,\theta\,]_n$	$[\,\pm\theta\,]_{n/2}$

Table 4.6: The different layup types evaluated, where n is the total number of plies in the laminate and θ ranges from 5 to 45 degrees with 5 degree intervals.

Because the laminate failure strain does not depend on the laminate thickness, it can be calculated beforehand and used as a target for the ASWING models. This requires knowing the repartition between the axial, transverse and shear loads on wings. From the initial problem statement, the transverse load has been set to zero, therefore the only remaining unknown is the distribution between shear and axial loads.

The typical loading of the 737 and 777 wings was examined in order to find the importance of the shear load versus the axial load in the wing. ASWING simulations under typical 1g flight conditions were performed and the loads at the root of the wings were extracted. On the 737, the shear load was about 10% of the total spanwise axial load while on the 777 this number was more around 20%. The increased proportion of shear on the 777 wing can be partly explained by the increased wing sweep (from 25° to 32°) which has the consequence of increasing significantly the moment arm of the lift about the s axis, especially at the wing tip. Ultimately this creates higher torques on the wing for the same applied load at the tip.

Knowing the typical load distribution on each wings, the critical strains of the various laminates can now be evaluated using the "Laminate Failure" Matlab script listed in appendix A.3. Table 4.7 shows the resulting critical strain values. These critical strains will ultimately be used as targets for the wing's root axial strains in ASWING in order to size the wing structure.

Theoretically, the optimal angle at which the fibers should be oriented in order to benefit from the maximum strength of the material should be close the principal stress direction. From Mohr circle theory under plane stress conditions [32], the principal stress angle θ_p can be evaluated as:

$$\tan(2\theta_p) = \frac{2\tau_{xy}}{\sigma_x - \sigma_y} \tag{4.9}$$

Based on the initial problem assumptions, the transverse stress is zero and the shear stress is a percentage of the axial load as specified in the previous paragraphs. More specifically $\sigma_y = 0$, $\tau_{xy} = 0.1\sigma_x$ for the 737 and $\tau_{xy} = 0.2\sigma_x$ for the 777. Finally,

	(a) 737 (10% shear)			(b) 777 (20% shear)	
θ	Coupling	No Coupling	θ	Coupling	No Coupling
0	0.00625	0.00625	0	0.00318	0.00318
5	0.00724	0.00653	5	0.00462	0.0035
10	0.00946	0.00646	10	0.00678	0.0047
15	0.00708	0.00715	15	0.00996	0.0059
20	0.00684	0.00789	20	0.00784	0.0065
25	0.00588	0.00728	25	0.00759	0.0066
30	0.00484	0.00702	30	0.00797	0.0067
35	0.00425	0.00715	35	0.00622	0.007
40	0.00384	0.00761	40	0.00502	0.0076
45	0.00353	0.0084	45	0.00435	0.0084

Table 4.7: Layup critical axial strains ε_{cr}.

the principal stress angles can be evaluated for the 737 and 777 wings.

$$\theta_{p\,737} = \tan^{-1}(0.1) \approx 6° \tag{4.10}$$

$$\theta_{p\,777} = \tan^{-1}(0.2) \approx 11° \tag{4.11}$$

A similar process to the one used to evaluate the critical strains can be employed to find the critical failure loads of the laminates. Unlike the strains, the failure loads are a function of the laminate thickness. Even though the absolute strength number will vary with thickness, some useful information can be pulled out by normalizing the critical loads of the laminates against the critical load for $\theta = 0°$ laminates. In fact, no matter what the thickness is, the normalized strength curve will always be the same as long as the thickness is increased by repeating the same stacking sequence multiple times. For example, if a laminate of the type $[15/-15]_n$ is studied, the normalized failure load compared to the $[0]_n$ will be the same for all the values of n.

Figures 4-4 and 4-5 illustrate the variation of the normalized laminate strength as a function of the laminate angle θ. The first figure covers the 737 wing's loading conditions, it shows the strengths of laminates with a proportion of 10% shear with

respect to the applied axial load. The second one reproduces the loading of the 777 as the shear proportion is 20% of the axial load. Both graphs also show the impact of bend-twist coupling on strength by plotting curves for balanced (no coupling) and unbalanced (coupling) laminates.

Some useful information can be extracted from those two charts. First, the peak strengths in both figures are relatively close to the principal stress angles which have been evaluated previously. Secondly, the optimal layup angle is the same whether or not the laminates are balanced or unbalanced. The balanced laminates seem to be less sensitive to angle variations about that optimal angle. In both cases, the unbalanced laminates are stronger at small layup angles, basically because the fibers are oriented in a direction closer to the principal stress direction. Beyond the laminate's principal stress angle, there is a transition point where the strength of the coupled laminates quickly falls below the strength of the uncoupled laminates. For most of the layup angles, the laminates without coupling are stronger than the ones with coupling. The benefits of balanced laminate is that their strength stays relatively high for a wider range of layup angles since there are fibers in two directions which can compensate for the weakness of the resin in the transverse direction.
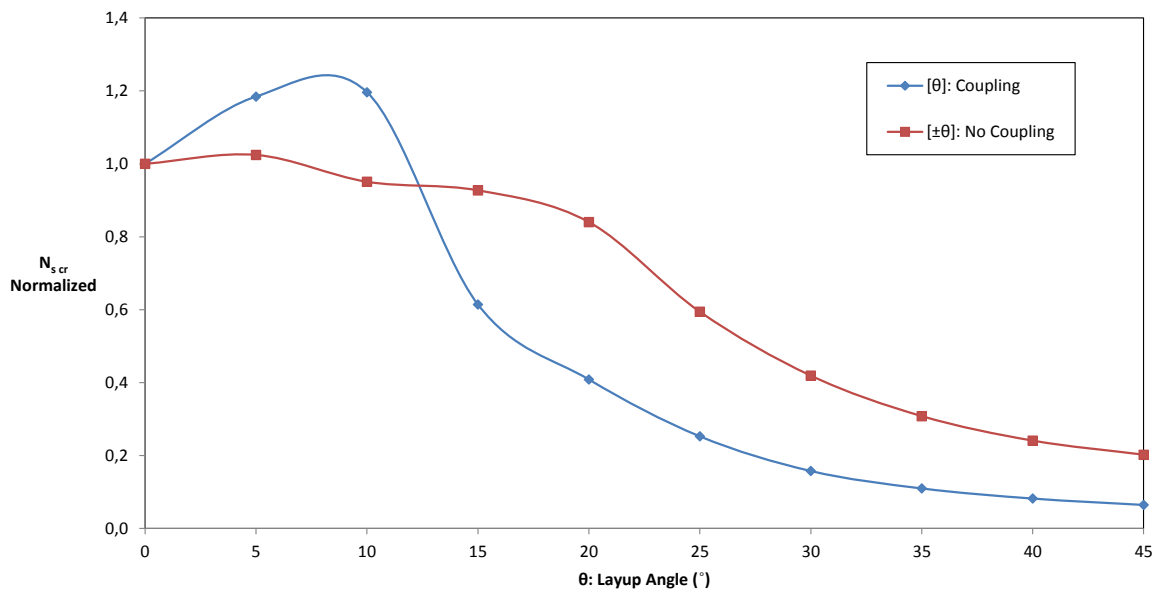
Figure 4-4: Normalized critical laminate axial load with 10% shear.
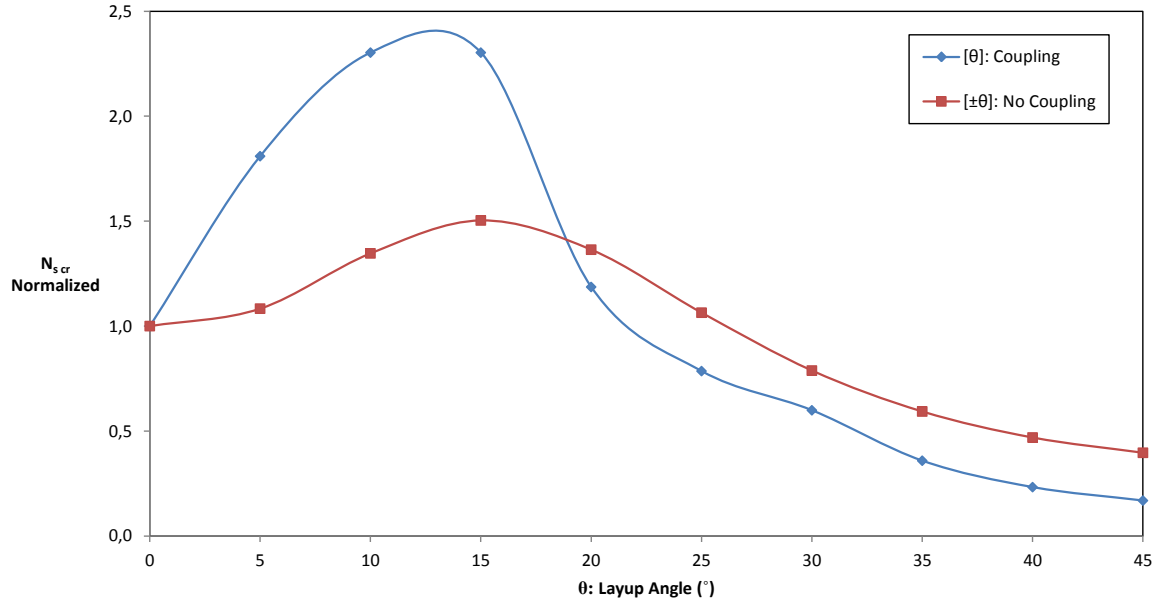
Figure 4-5: Normalized critical laminate axial load with 20% shear.

4.6   Iterative Wing Sizing Procedure Summary

In the previous sections, the different tools and technical details required to perform an evaluation of the effect of bend-twist coupling on commercial airplane wings have been presented. This section presents a step by step summary of the overall wing sizing process.

The first step of the process is to define the aircraft that will be analyzed. Several technical characteristics are needed to build the ASWING models. Airplane dimensions, performance data, aerodynamics properties, structural properties and weights are all required. More information on this is provided in the ASWING user manual. Once all the necessary airplane data has been gathered, the laminate failure strains of different layup configurations are evaluated following the process presented in section 4.5.

The next step is to choose a reasonable initial laminate thickness (based on the bending moments of the metallic wing) and then calculate the wing's initial bending stiffness matrix $[\bar{E}]$. The bending stiffnesses are evaluated only at the root section of the wing. The root stiffness is then scaled along the span of the wing following the scaling curves of the baseline metallic wing as shown in figure 4-6. Because the

wing's geometric shape is not modified, the thickness reduction along the span will follow the same trend as the metallic wing, therefore the various EI and GJ terms should follow the metallic wing's scaling. Since the metallic wing does not exhibit any coupling effects, the coupling term is scaled based on the spanwise bending stiffness curve. Previous structural simulations have shown that for various beam dimensions, the coupling term EI_{cs} usually scales with the spanwise bending stiffness term EI_{cc}.
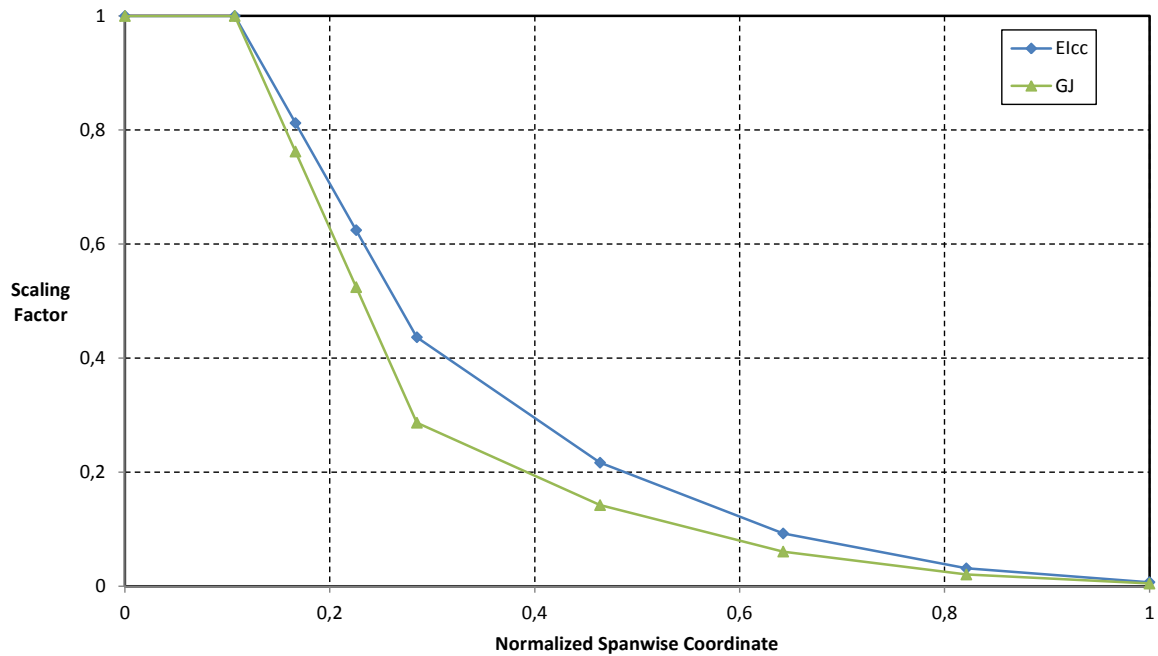
Figure 4-6: Bending and torsion rigidity scaling factors along the span of the 737 metallic wing.

The next step is to export the data into the ASWING model input file. Then, the "Twist.f" Fortran code is used to adjust the wing's initial twist in order to minimize the wing's drag coefficient in cruise conditions. Once this is done, the ASWING simulations of the static or dynamic cases can be performed. After the simulation are completed, the spanwise bending moment M_{c0} and the axial strain ε_s are extracted from the ASWING output files. The wing root's strain is compared against the critical laminate strain ε_{cr}. Finally, the laminate thickness is modified if needed and the process is started over until convergence is reached. The laminate thickness must be modified by multiples of 2 plies so that the laminate remains symmetric

64

and respects the initial assumptions of the bend-twist coupling equations derived in chapter 2.

For better clarity, figure 4-7 illustrates the complete sizing process diagram, starting from the initial wing geometry and ending with the final layup details and wing weight.

Figure 4-7: Wing sizing procedure diagram.

Bend-Twist Coupling Evaluation

Aircraft & Wing Parameters

Wing Span	Payload
Aspect Ratio	Mach
Sweep	...
Laminate Angle	

Evaluate Laminate Failure Strain ε_{cr}

Wing Sizing

Evaluate Wing Bending Stiffness Matrix

Create ASWING Model

Adjust Wing Twist (T*wist.f*)

Simulate Static or Dynamic Cases

Evaluate Spanwise Root Bending Moment *Mc0*

$\varepsilon = \varepsilon_{cr}$?

N

$\varepsilon < \varepsilon_{cr}$

$\varepsilon > \varepsilon_{cr}$

Remove Plies

Add Plies

Y

Output:
Laminate Information
Wing weight

Chapter 5

Bend-Twist Coupling Load Alleviation Results

This chapter presents the results of the ASWING simulations performed on the 737 and 777 airplane models created following the details provided in chapter 4. The critical load cases for each configurations are highlighted and the final wing sizings are described. The effects of bend-twist coupling on the wing's weight and root bending moments is estimated by comparing those metrics against results for uncoupled wings. But first, the effects of bend-twist coupling on individual laminates strength are presented in the next section.

5.1 Effects of Bend-Twist Coupling on Laminate Strength

In this first section, an analysis of the relationship between the beam's bend-twist coupling and the critical laminate load is presented. Figure 5-1 and 5-2 show the laminate strength as a function of the amount of bend-twist coupling. The first figure presents data for typical 737 wings while the second one covers the 777. The laminate's failure load has been normalized by the critical load of 0 degree laminates. Instead of presenting the coupling in terms of an absolute EI_{cs} value, the ratio between

the bend-twist coupling coefficient and the spanwise bending coefficient EI_{cc} is used. As it has been seen in the equation validations in chapter 3, the bend-twist coupling effect is maximum around 30 degrees. However, this behavior is not observed for the absolute EI_{cs} parameter. In fact, the ratio between EI_{cs} and EI_{cc} is much more representative of the amount of coupling present in a beam. As the layup angle is increased, the bending stiffness of the laminates gets smaller, therefore the relative importance of the coupling coefficient gets larger even though in absolute numbers it is not increasing.
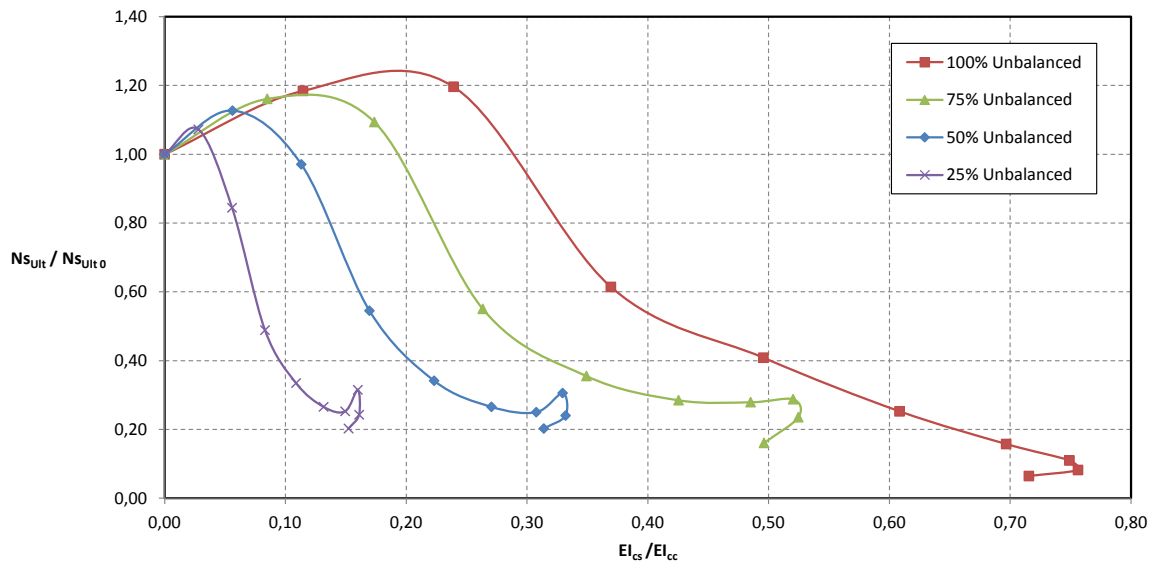
Figure 5-1: Laminate strength as a function of coupling, $N_{xy} = 0.1N_x$ (737)

Each data point on the strength-coupling curves measures the efficiency of a different layup angle. The angles start at 0 degree, on the extreme left of the curves, and go all the way to 45 degrees for the last point on the curves. An increment of 5 degrees was used between each data point. Around $\theta = 30°$, all configurations reach a maximum amount of bend-twist coupling. Beyond this point, the bend-twist coupling effects get lower. This explains the strange looking end of the curves.

Furthermore, in order to understand the impact of reducing the unbalanced proportion in the layup, four levels of unbalance are plotted for each airplane. For a given layup angle, reducing the unbalance amount has the effect of reducing the coupling of the beam without improving its strength. Indeed, for any amount of bend-twist cou-
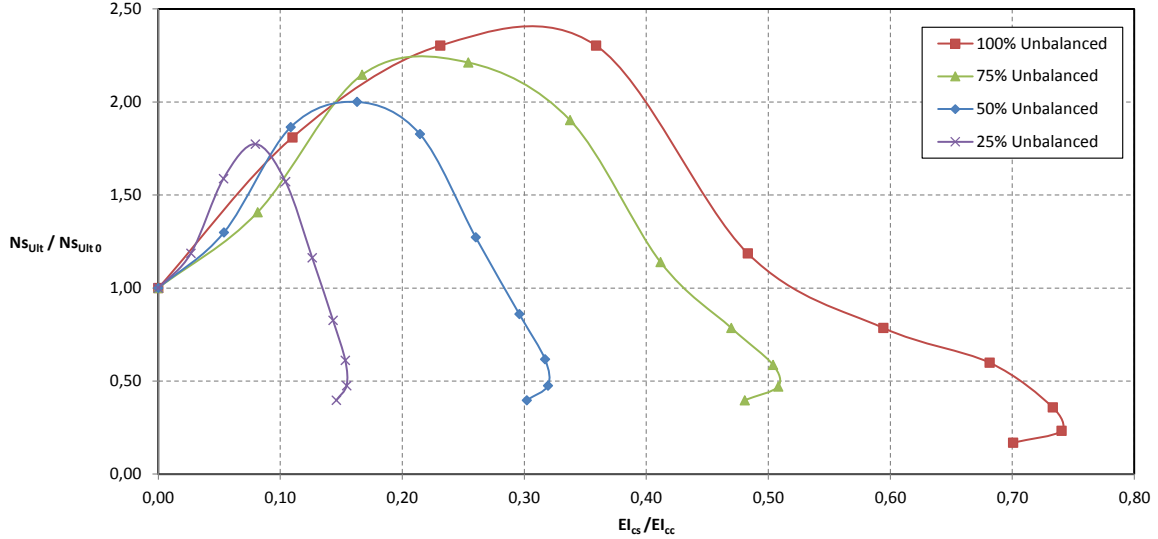
Figure 5-2: Laminate strength as a function of coupling, $N_{xy} = 0.2N_x$ (777)

pling, the 100% unbalanced layups are always stronger than the other configurations. Since the ultimate goal is to maximize both the coupling and the strength, there is then no benefit in reducing the amount of unbalance in the laminates and the fully unbalanced configuration will be the one evaluated in the ASWING simulations.

Interesting information is found when comparing the plots for both airplanes. The main difference between the 737 and 777 curves is that their peak strength is reached at different layup angles. The peak is between 10 and 15 degrees for the 777 while it is between 5 and 10 degrees on the 737 wings. This is due to the principal stress orientation being different as explained in chapter 4. A common feature found on both graphs is that layups at angles over 30 degrees have reduced bend-twist coupling and significantly lower strength compared to layups of lower angles (80% reduction in strength). For those reasons, they will not be considered for the next steps of the study as they are obviously suboptimal configurations.

Since the layups with the greatest bend-twist coupling effects are not optimal in terms of strength, it is not clear which configuration will be the best for the airplane. The question is whether or not the benefits of bend-twist coupling at the aircraft level will be large enough to compensate for the reduced strength at the laminate level. This is what the next sections will seek to answer.

5.2 Critical Load Cases

This section compares the resulting loads on the wings from the static and dynamic cases. The goal is to find which cases are actually critical for each airplane and wing type. Based on this information, the wings will then be sized using those critical loading conditions.

5.2.1 Gust Loads

As explained in chapter 4, the wings are analyzed for various gusts lengths ranging from 30 to 350 feet. In order to cover the full length of the dynamic event, a time step of 0.1 second with 70 integration points was used. Those settings lead to a 7 seconds time domain which was long enough to cover the dynamic effects of all the gust lengths and configurations studied. A convergence study was performed to make sure that the 0.1 second time step was small enough to provide valid physical results. The main goal for all these simulations was to identify the critical gust for each layup and airplane type. In order to find that critical gust length, the spanwise bending moment at the wing root was extracted from the ASWING output file for each time step. The ratio between the actual moment M and the 1g moment M_{1g} was then plotted as a function of time and is shown in the next two figures. This ratio provides a good non dimensional measure of the bending moment increase in the wing. The lower the moment ratio is, the less sensitive the aircraft is to that particular gust.

Figure 5-3 illustrates those metrics for the 737 wing while figure 5-4 shows the results for the 777. For the 737, the critical gust length is 200 feet although most of the time the 300 feet gust yielded similar bending moments. The critical gust length of the 737 was not sensitive to the presence or not of bend-twist coupling. On the 777, the critical gust length shifts towards the higher gust lengths (300-350 ft) for the uncoupled wings. However, the 777 wings with coupling have a critical gust length of 200 feet, just like the 737. The bending moment ratios are higher on the 777 than on the 737 and the wings seem to return to their 1g state a little bit faster on the larger airplane. Layup configurations of $\theta = 5°$ and $\theta = 10°$ without bend-twist

coupling were chosen as examples for these two plots but graphs were generated for all layup angles between 0 and 30 degrees with and without bend-twist coupling. Those additional figures can be seen in appendix B.1.1 for the 737 and in appendix B.2.1 for the 777.
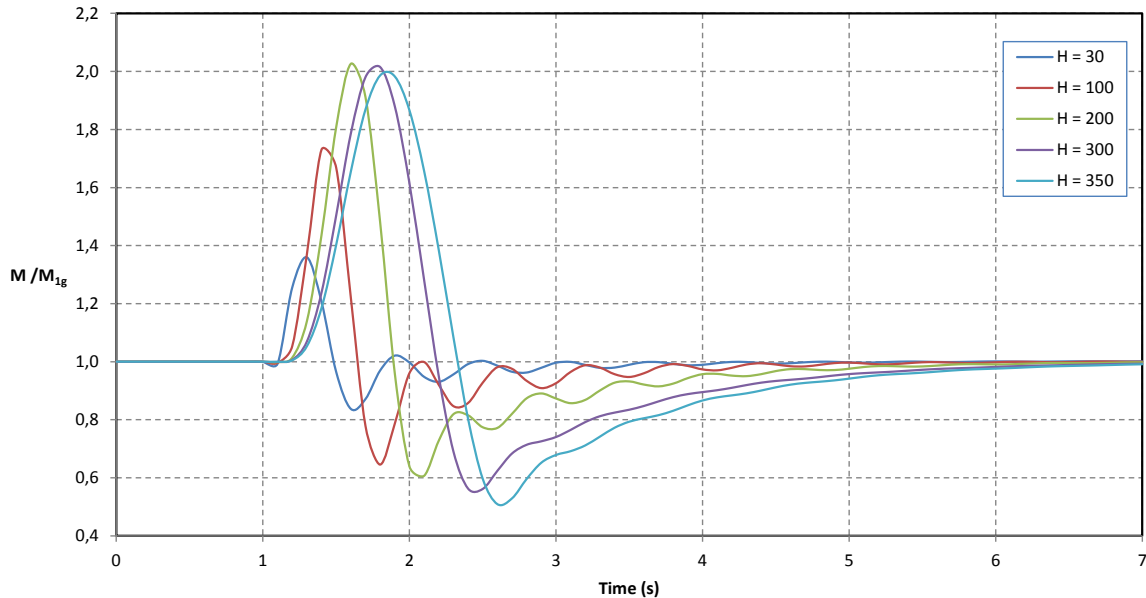
Figure 5-3: 737 Bending moment ratio for various gust lengths, $\theta = 5°$ (Without coupling).

5.2.2   Static Load

The next step is to find out whether the static lift increase condition($n = 3.8$) is more severe than the critical gusts identified in the previous section. The baseline ASWING simulations for 1g flight have been performed with a cruise speed of 150 m/s for the 737 and 200 m/s for the 777. These speeds resulted in cruising angles of attack between 2 and 2.5 degrees, which are reasonable for those types of airplanes.

The static load increase load case is simulated in ASWING by increasing the 1g lift by a factor of 3.8. In order to generate that extra lift, the airplane's angle of attack had to be increased significantly, leading to aerodynamic stalls if the reference velocity was kept constant. To avoid the wing stalls, all the static load increase simulations other than the 1g case required an increased airplane velocity. On the
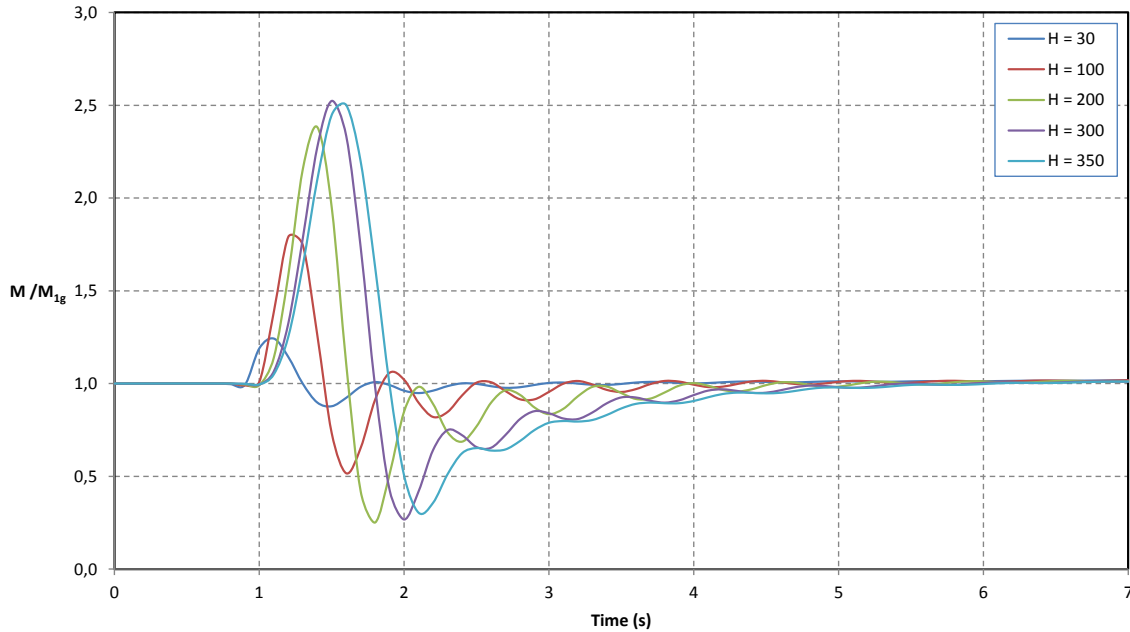
Figure 5-4: 777 Bending moment ratio for various gust lengths, $\theta = 10°$ (Without coupling).

737, it was increased up to 225 m/s while on the 777 it had to be increased up to 250 m/s. The next two plots illustrate the critical gust bending moment increase as well as the static load increase under limit load conditions for both airplanes. Again, the plots for $\theta = 5°$ and $\theta = 10°$ are illustrated as an example. For further references, the figures for the other layup angles are provided in appendix B.1.2 for the 737 and appendix B.2.2 for the 777.

In those figures, the dashed horizontal lines show the limit bending moment increase resulting from the static load case while the continuous curves represent the evolution in time of the bending moment for the critical gust case. The results are plotted for both the coupled and uncoupled cases.

There are a couple of interesting features in those charts. First, it is clear that the bending moment increase is much smaller when the wing exhibits some bend-twist coupling (about 60% less for the plotted cases). Second, if the dashed line is lower than the continuous line's peak, like in figure 5-5, it means that the static load increase is less critical than the gust case for that configuration. This is a pattern that has been observed only on the 737's wings with layup angles of 5 and 10 degrees.
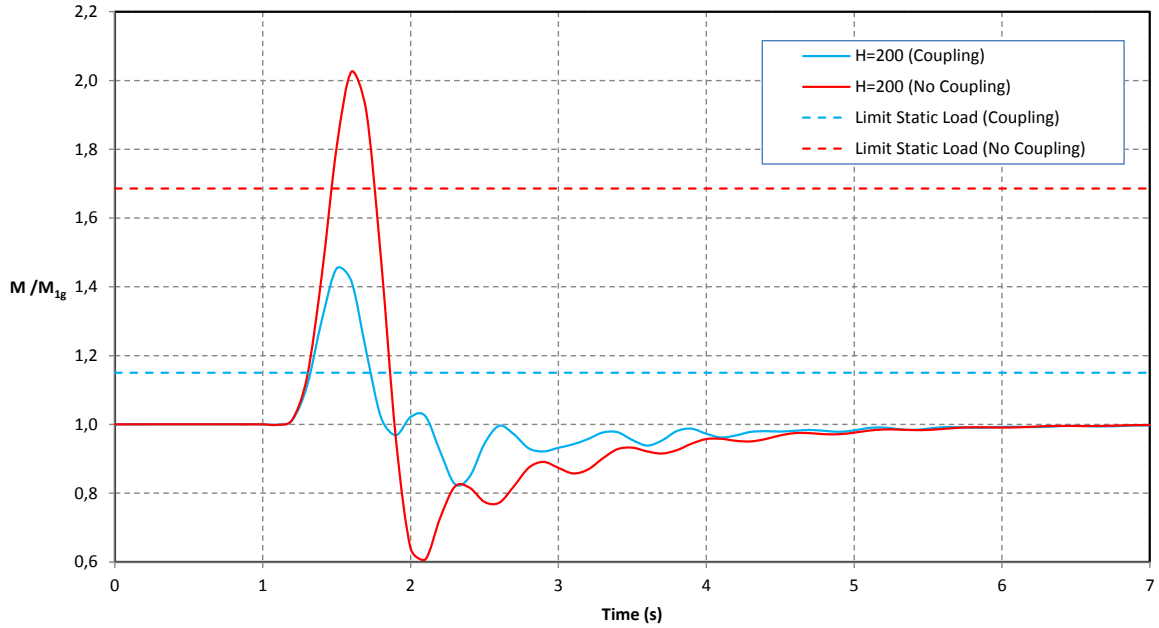
Figure 5-5: 737 Bending moment ratio for the critical gust and static load cases, $\theta = 5°$.
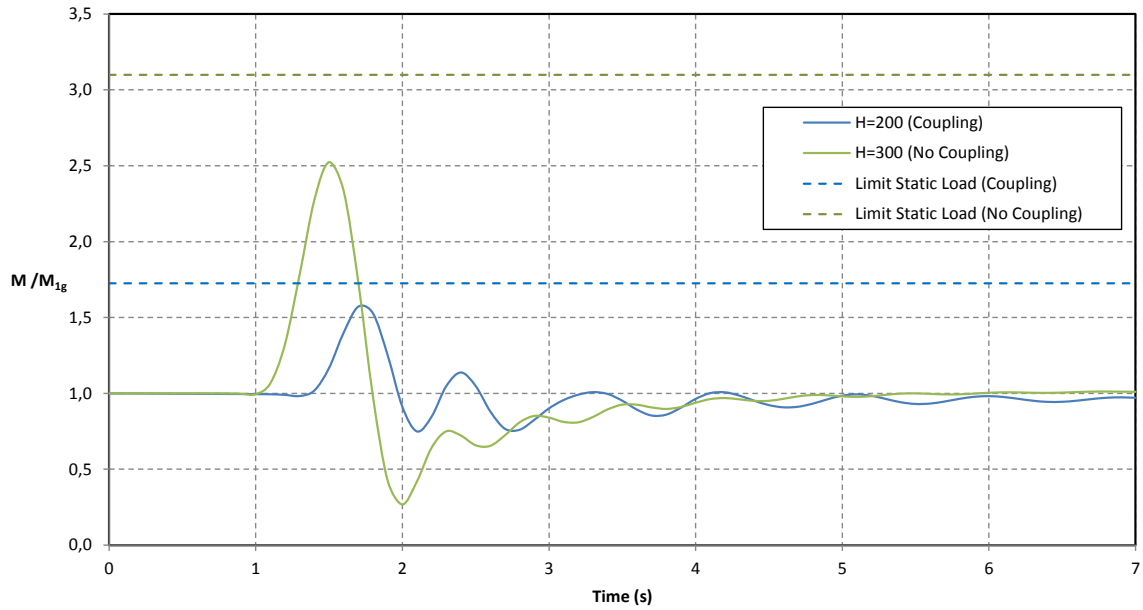
Figure 5-6: 777 Bending moment ratio for the critical gust and static load cases, $\theta = 10°$.

The other 737 wings were actually sized by the static cases. This was also the case for all the 777 wings as the gust cases were never critical for that aircraft. For example, figure 5-6 clearly indicates that this wing is sized by the static case since the bending

moment increase is much larger for that load case.

Another interesting feature of those graphs is noticed when looking at the configurations sized by the static loads. The wings without bend-twist coupling seem to have a higher margin of safety when it comes to dynamic gusts. In other words, the wings with coupling have almost the same bending moment peak for the static case or the dynamic gust case. This means the uncoupled wing could theoretically be able to handle stronger gusts than the ones with bend-twist coupling without breaking. However, since both wings have to be sized using FAA's rules, this would only be a benefit in the eventuality that the airplane flies into a gust much stronger than what the FAA prescribes. Another way to see this would be to claim that the wings with bend-twist coupling are more optimized since their margin of safety is close to zero for both load cases.

5.3 Effects of Bend-Twist Coupling on Wing Root Bending Moment

This section presents the effects of bend-twist coupling on the spanwise bending moment at the root of the wing. It will also try to explain the mechanisms behind these effects by looking at the wing tip's twist and displacement as the airplane flies into the gust.

5.3.1 Spanwise Bending Moment Ratio

As part of the preparation of the models, the wings had their initial twist distribution adjusted so that they all shared the same initial root bending moment M_{1g} as explained in chapter 4. For this reason, the bending moment ratio, defined as the ratio between the critical bending moment at a specific layup angle and the moment in 1g conditions, can be used as an indicator of the impact of bend-twist coupling on the wing's structural response. This ratio is plotted for each layup angle between 0 and 30 degrees.

As can be noted on the 737 and 777 plots in figures 5-7 and 5-8, the wings with coupling actually experience a much smaller increase in bending moment than the ones without coupling for the same layup angle. On both airplanes, when $\theta = 0°$ the wing has no coupling effect and this is why the bending moment is the same for both curves.
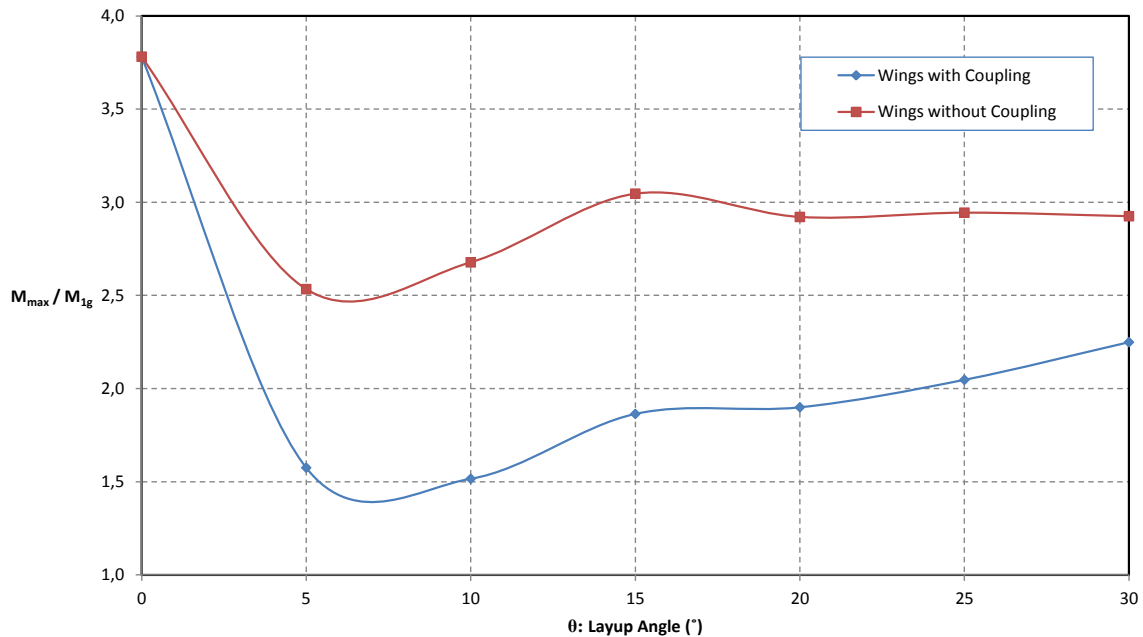
Figure 5-7: 737 Wing root spanwise critical bending moment ratio. This represents the largest ratio due to either the static case or the gust case for each layup angle.

For the 737 wing, the largest difference between the two curves occurs between 5 and 10 degrees, which coincides with the wing's principal stress direction. For example, at $\theta = 5°$, the moment ratio goes from 2.5 for uncoupled wings to around 1.5 for coupled wings. This is a 40% reduction in the peak bending moment for exactly the same gust case. As the layup angle increases, the difference between the two curves gets smaller. In fact, beyond 20 degrees, the bending moment ratio is rather constant for the coupled wings while this ratio gets larger for the uncoupled wings.

On the 777, the difference between the coupled and uncoupled wings is the greatest for layups between 10 and 15 degrees, as seen on figure 5-8. Those angles also coincide with the principal stress and maximum strength orientation of the laminates. At 10
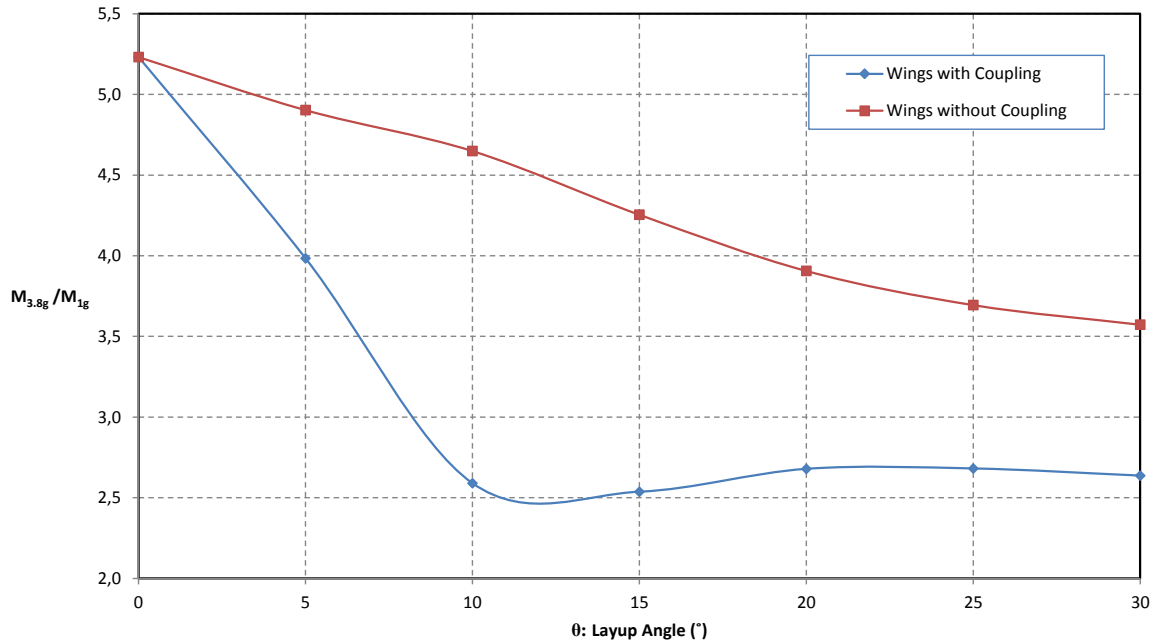
Figure 5-8: 777 Wing root spanwise critical bending moment ratio. This represents the largest ratio due to either the static case or the gust case for each layup angle.

degrees, for example, the bending moment increases by more than 4.5 times the 1g moment for the uncoupled wing while this number is only around 2.5 when there is bend twist coupling. This represents a 45% reduction in the peak bending moment experienced by the wing, which is about 5% more than what was noted on the 737. The uncoupled wing's bending moment ratio decreases almost linearly with layup angle. For coupled wings, this ratio seems to stabilize itself at 10 degrees. Just like on the 737, as the layup angle is increased, the difference in bending moment gets smaller. The large reductions in peak bending moments observed on both the 737 and 777 should have a positive impact on the wing's weight.

5.3.2   Wing Tip Twist and Displacement

In order to understand where the bending moment reduction comes from, the wing tip's twist and vertical displacements have been extracted as a function of time from the ASWING output files. The wing tip's movements can be compared against the uncoupled wing for a given layup angle.

Figure 5-9 and 5-10 illustrates the 737's wing tip movements when flying into the

critical gust for the $\theta = 5°$ configuration. When looking at the wing tip twist plot, there are two important features that come out of this graph. First, the magnitude and sign of the maximum twist angle are very different between the coupled wings and the uncoupled ones. Even though the wings initially start twisting in the same direction, the coupled wing's tip quickly twists nose-down and reaches maximum twist values almost 3 times larger than the uncoupled one. The nose-down twist reduces the wing tip's local angle of attack, and thus reduces the increase in bending moment. The other interesting feature on this chart is that the twisting motion of the wings with bend-twist coupling is clearly less damped than for the wings without coupling. In other words, the wing tip oscillates around its original twist angle for a longer time until it stabilizes.
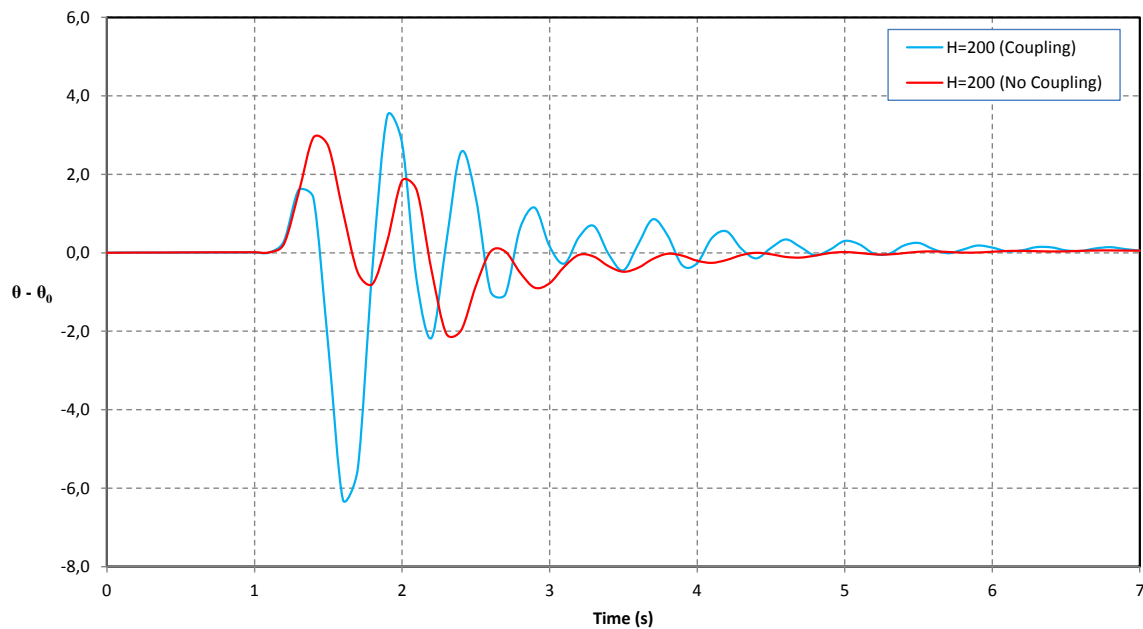
Figure 5-9: 737 Wing tip twist versus time in the critical gust case, $\theta = 5°$.

Figure 5-10 shows the 737's wing tip displacements magnitude. As opposed to the wing twist behavior, the displacements are smaller on the wing with bend-twist coupling and the difference in magnitude is not nearly as large as what was noticed for the twist. The damping of the displacement motion does not seem to be affected by bend-twist coupling. This can be interpreted as a different mechanism in the way the gust energy is absorbed by the wings with coupling. In fact, most of the gust

energy seems to be absorbed by twisting motion rather than vertical displacement of the wing. The increased nose-down twist of the wing tip reduces the effective angle of attack of the wing tips which in the end generates less loading outboard of the wing. This smaller outboard load consequently reduces the tip's vertical displacement and the spanwise bending moment of the wing.
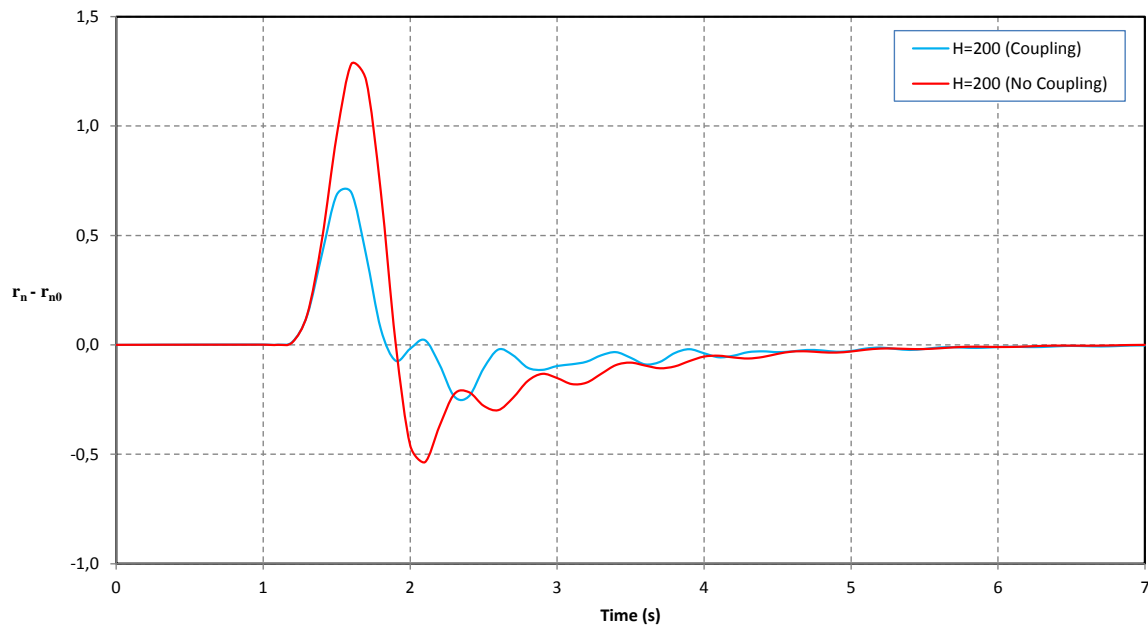
Figure 5-10: 737 Wing tip displacement versus time in the critical gust case, $\theta = 5°$.

The next two charts, figure 5-11 and 5-12, plot the same wing tip parameters for the larger 777 airplane.

The behavior of the 777 wing tip in the gust is similar to what was observed for the 737 wing, the only difference being the relative importance of the twist and displacement motions. The 777 wing's twist at the tip is about 8 times greater when there is bend-twist coupling than when there is not. This is a much larger difference than what was noted on the 737. The reduction in vertical displacement is less significant than on the 737, but it is compensated by the additional twisting of the wing. Because of the larger wing span and sweep angle, the reduction of the wing's outboard loading ultimately has a larger impact on the wing's root bending moment than on the 737. The damping of the twisting motion, although still smaller than the uncoupled wing, seems to be better than the one on the 737, probably due to the
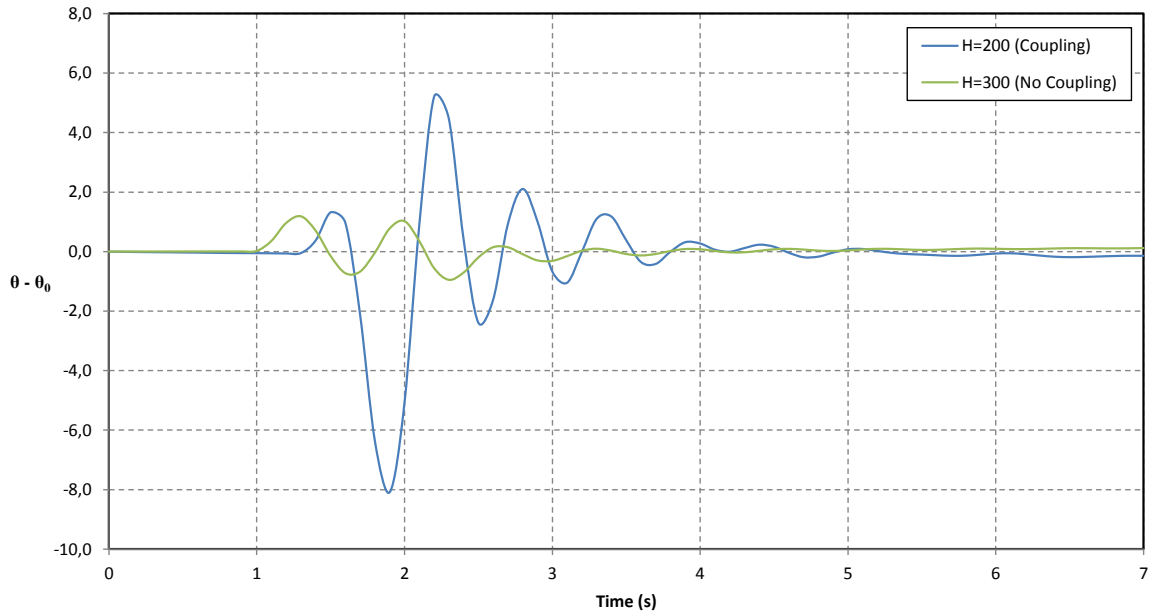
Figure 5-11: 777 Wing tip twist versus time in a typical gust case, $\theta = 10°$.
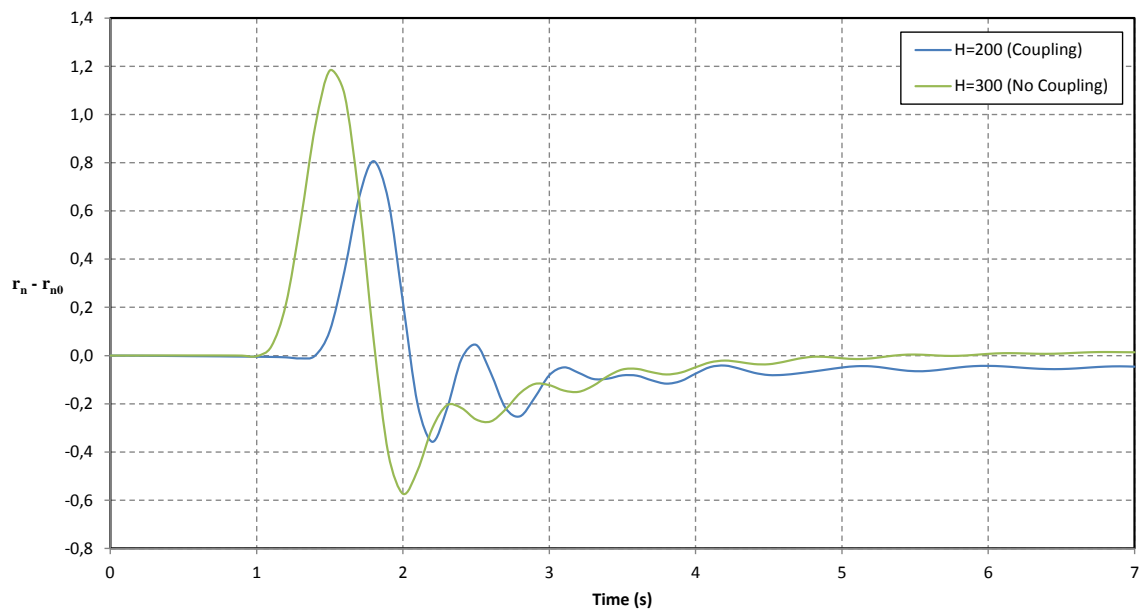
Figure 5-12: 777 Wing tip displacement versus time in a typical gust case, $\theta = 10°$.

larger bending inertia of the heavier wing. The damping of the tip's displacement is relatively unchanged just like on the 737.

5.4 Effects of Bend-Twist Coupling on Wing Weight

Finally, this section presents the effects of bend-twist coupling on the weight of the wings. For each particular layup angle between 0 and 30 degrees, the wings have been dimensioned using their respective critical load cases. To compute the effects of bend-twist coupling, this process has been performed for unbalanced and balanced layups. For each case the total wing weight was extracted from ASWING and plotted as a function of the layup angle θ. The results for the 737 and 777 are presented in figures 5-13 and 5-14.
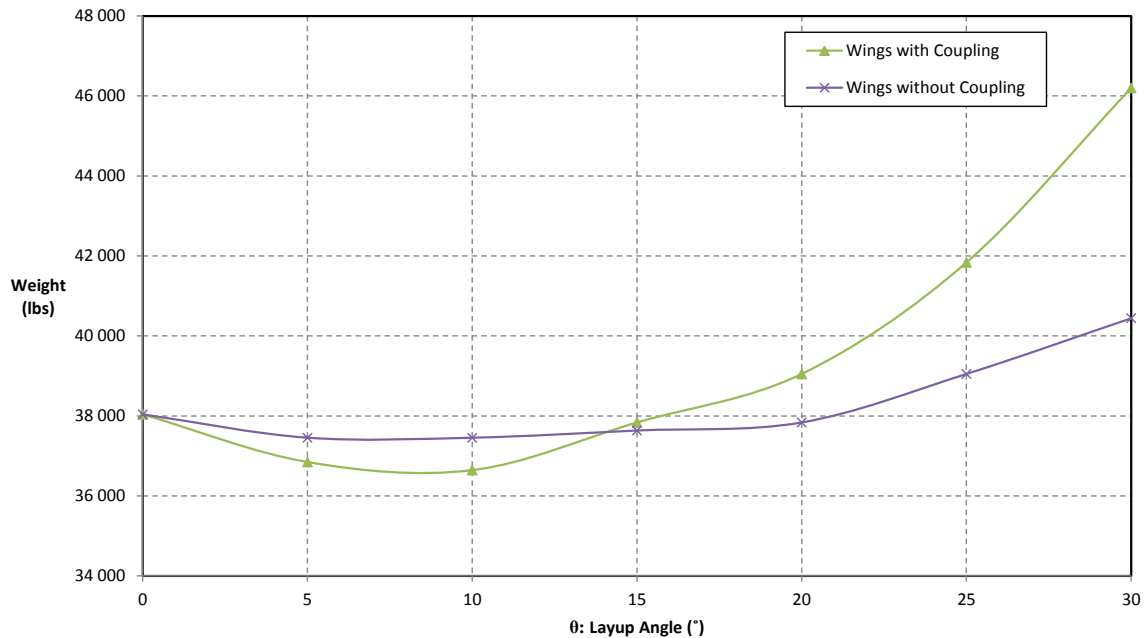
Figure 5-13: 737 composite wing weight with and without bend-twist coupling.

As stated in previous sections, it is impossible to obtain bend-twist coupling with a 0 degree layup which is why there is no weight difference for this particular laminate. A common feature of both charts is that the minimum weight wing is found at the layup angle for which the fibers are aligned with the load case's principal stress direction, whether or not there is bend-twist coupling. The minimum weight point for the 737 is between 5 and 10 degrees while it is around 15 degrees for the 777.

Another interesting feature of the weight charts is that there exists a transition point where the coupled wings actually become heavier than the uncoupled ones.
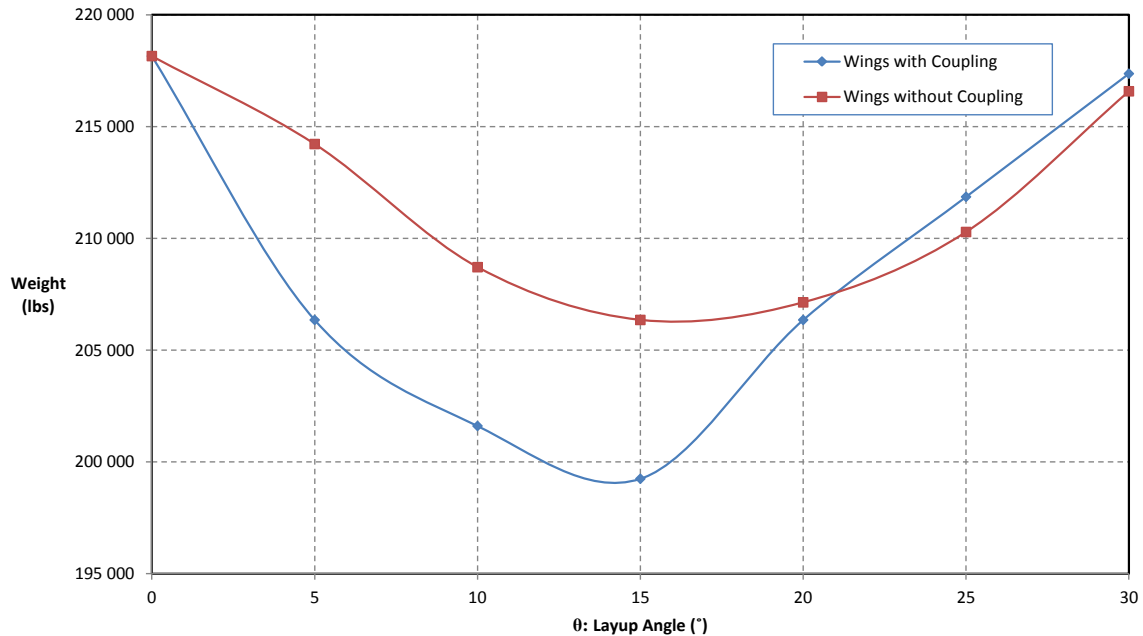
Figure 5-14: 777 composite wing weight with and without bend-twist coupling.

This transition occurs at layup angles a few degrees higher than the optimal weight configuration. Because the strength of unbalanced laminates is significantly reduced when the layup angle is greater than the principal stress direction, it implies that the wings will need a larger amount of plies to sustain the design loads. As shown in section 5.1, the larger the difference between the fiber angle and the principal stress direction is, the bigger the penalty on laminate strength will be. This effect is even worse for the highly unbalanced laminates required to create bend-twist coupling of the beam. Such layups can really only be efficient if the fibers are oriented in a direction close to the principal stress direction, which is not the case beyond the transition point. Moreover, as the layup angle is increased, the difference in bending moment between the coupled and uncoupled wings gets smaller, as seen in section 5.3. The two factors of the reduced strength of the laminates and the less significant bending moment reduction provide a rational explanation for the increased weight of the coupled wings after the transition point.

Finally, figure 5-15 shows the weight saving potential of each particular layup angle on both aircraft. Each point on this chart represents the efficiency of using

81
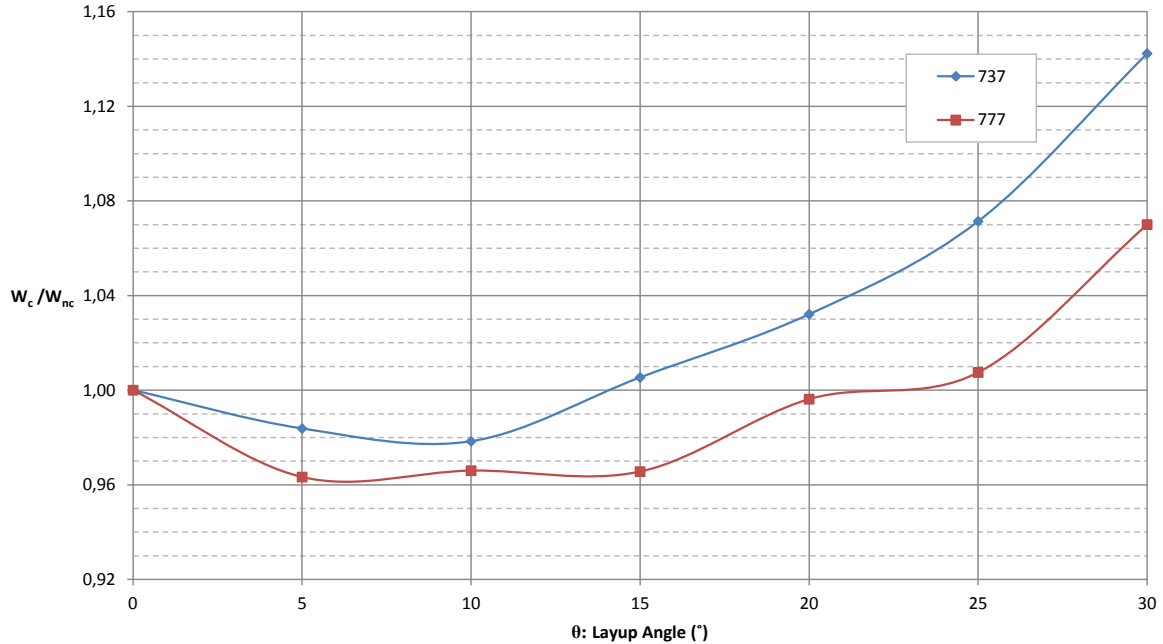
Figure 5-15: 737 and 777 wing weight ratio due to bend-twist coupling for each layup angle.

bend-twist coupling on different wing designs (737 or 777). At each layup angle, the ratio between the weight of the coupled wing W_c and the weight of the uncoupled wing W_{nc} is plotted. On this plot, if the ratio is above 1 it means there is a weight penalty associated to using bend-twist coupling at that specific layup angle.

The maximum weight reduction for the 777 wing is 4% as for the 737 it is about 2%. In both cases, the maximum weight savings coincide with the principal stress angle of the wing. Furthermore, since the 777 curve is always below the one from the 737, it indicates that bend-twist coupling has a greater impact on the heavier 777 wing for the whole range of layup angles. This can be explained by the influence of the classical geometric cube-square law. Therefore, one of the important conclusions drawn from this chart is that using bend-twist coupling on larger airplanes seems to provide more weight savings opportunities than on lighter airplanes with smaller wings.

Even though those preliminary weight reduction numbers may seem small in terms of percentage, within the context of rising fuel prices, any weight saving opportunities are welcomed. Each pound saved on an airplane means fuel and money savings on

every flights for the airliners. Also, the manufacturers are often struggling to meet the performance targets of their new airplanes driven by very aggressive modern marketing requirements. Every bit of technology or innovation that can lead to a few pounds of weight savings is then worth considering.

Chapter 6

Conclusions

6.1 Summary of Findings

A methodology to compute the effects of bend-twist coupling on commercial airplanes wings was presented. The coupling is hypothesized to provide potential weight savings for the wings by working as a passive load alleviation mechanism. To verify this, an analytical beam model was developed to evaluate the deflection and twist of orthotropic box beams. The orthotropic beam bending equations were derived based on the standard isotropic beam bending equations combined with the classical laminated plate theory. The transverse load in the beam walls was assumed to be zero. It was demonstrated previously in the literature that warping plays an important role in the generation of bend-twist coupling at the beam level, therefore a bilinear warping function was used.

The analytical model was then validated against finite element analysis and experimental data from the literature. Beams of various aspect ratios (1.8, 4 and 6) and layup angles (0° to 45°) were evaluated in order to understand the effect of those parameters on the solution quality. A simple cantilevered beam model with a unit torque or bending moment was used. In each case, the deflection and twist of the beam due to the unit load was calculated using both the analytical model and the finite element model. The analytical model predicted the deflection and twist of all the test cases within 15% of the finite element analysis results with a tendency to

slightly overestimate the beam's stiffnesses. The best results were observed for beams of higher aspect ratios and with layup angles under 30 degrees. The finite element analysis showed that beams with high layup angles had stronger warping effects which the bilinear warping function was not able to capture properly.

A fully non-linear set of aero-structural simulations were performed using the ASWING simulation code to evaluate the impact of bend-twist coupling at the airplane level. The simulations models represented a 737 and a 777, two Boeing airplanes of very different sizes which together cover most of the market segments of modern commercial aviation. To size the composite wings, two different loading scenarios were defined. A static load increase and a set of different gust lengths were used as prescribed by the rules of FAA's FAR 25. The initial twist of each wing was adjusted in order to standardize the 1g bending moment at the root of the wing. Finally, a combination between the maximum stress and maximum strain failure criteria was used to evaluate the strength of the laminates. A target margin of safety of 0 was used to size the wings at ultimate load.

Following the aero-structural simulations, a number of interesting conclusions were found. First, the critical load case for most wings was the static load increase. The dynamic gusts scenario was critical only on the 737 wings with layup angles of 5 and 10 degrees. Therefore, most of the wings have been sized using the bending moment due to the static load increase.

Second, a strong reduction in the wing's root spanwise bending moment was observed for all wings with bend-twist coupling. This reduction was in the order of 20% to 45% depending on the layup angle and wing model. The reduction in peak bending moment was most significant at the principal stress angle of the wing and on the 777. The mechanism behind this reduction in bending moment was associated to a reduced vertical displacement of the wing tip and an increased wing tip twist in the critical load case. The increased wing tip twists reduces the outboard wing loading due to the lower angle of attack of the tip which ultimately leads to a smaller root bending moment.

Third, the damping of the twisting motion of the wings seems to be reduced

significantly by the presence of bend-twist coupling while the damping of the tip displacement is unaffected.

Last, the maximum weight saving benefits of bend-twist coupling are evaluated to be around 2% of the wing's weight on the 737 and 4% on the 777. The optimal layup angle for maximum weight saving coincides with the wing's principal stress angle. Even if at higher layup angles the wings exhibit more bend-twist coupling, the load alleviation properties of the coupling terms are not large enough to compensate for the large reductions in strength due to the unbalanced laminates.

In summary, the findings of this thesis suggest that there may be some benefits of using bend-twist coupling on airplane wings as it reduces the wing's peak root bending moment and weight, specially on larger and heavier airplanes. However, these are still preliminary findings and, in order to fully evaluate the true potential of structural coupling, some more detailed topics would need to be investigated in the future. Some of those points are discussed in the next section.

6.2 Future Work

Most importantly, there is a need to generate more experimental data on composite box beams as only a few set of experiments were available in the public literature at the moment this thesis was written. To be more representative of typical wing geometries, experimental data for beams of aspect ratios between 3 and 6 are needed. The analytical model developed in this thesis could then be validated against those more representative results.

Another research direction would be to evaluate the impact of bend-twist coupling on the flutter response of the wings. As mentioned in chapter 5, the wing's twist motion damping is affected by bend-twist coupling and it could potentially have adverse effects on the flutter response of the airplane.

In terms of the aero-structural ASWING simulations, the study could be broaden to include more aircraft types. Since the benefits of coupled wings seem to be larger when heavier airplanes are considered, the study should be repeated with models of

the Boeing 747 or the new Airbus A380 for example. Following the cube-square law, the weight savings on those heavy airplanes is expected to be larger than the 4% found on the 777.

In terms of material sciences, the usage of very unbalanced laminates is something that aerospace design guidelines usually do not recommend. For this reason, there is not a great deal of experimental data on these types of laminates. Recently, Pawar has demonstrated numerically that microcracking on composite helicopter blades could significantly affect the elastic stiffness properties of the blades [24]. On unbalanced laminates such as those studied in this thesis, it is very likely that micrcocracking will occur due to the lack of laminate transverse stiffening. What would then be the impacts on the wing's strength and elastic properties? Some other material sciences related topics to explore could be, for example, unbalanced laminates resistance to fatigue and environmental cycling or even damage resistance studies. All those topics should be investigated before such laminates are going to be used on primary structures of future airplanes.

Finally, this study is based on wings sizings performed in isolation of the rest of the airplane but, a lighter wing could probably change the overall aircraft configuration. Therefore, the whole airplane should be adapted in order to accommodate this lighter wing. Since the weight savings claimed in this thesis did not include potential contributions from other major components of the airplane, ultimately the weight reduction potentials could be larger than expected initially.

Bibliography

[1] Advanced General Aviation Transport Experiments. A-basis and B-basis design allowables for epoxy-based prepreg Toray T700GC-12K-31 2510 unidirectional tape. Technical report, National Institute for Aviation Research, Wichita, KS, November 2002.

[2] J. Alkahe. Analytic extraction of the elastic coupling mechanisms in composite blades. *Composite Structures*, 49(4):399–413, August 2000.

[3] W.J. Cantwell and J. Morton. The impact resistance of composite materials – a review. *Composites*, 22(5):347 – 362, 1991.

[4] Carlos E. S. Cesnik and D. H. Hodges. VABS: A new concept for composite rotor blade cross-sectional modeling. *Journal of the American Helicopter Society*, 42(1):12, 1997.

[5] Ramesh Chandra, Alan D. Stemple, and Inderjit Chopra. Thin-walled composite beams under bending, torsional, and extensional loads. *AIAA Journal*, 27(7):619–626, 1990.

[6] Inderjit Chopra. Aeroelastic analysis of a composite bearingless rotor in forward flight using an improved warping model. *Journal of the American Helicopter Society*, 40(3):12, 1995.

[7] The Boeing Company. Boeing 777 composite materials, (accessed May 15, 2012). http://www.boeing.com/commercial/777family/background/back5.html.

[8] The Boeing Company. Boeing 787 composite materials, (accessed May 15, 2012). http://www.boeing.com/commercial/787family/background.html.

[9] Dassault Systemes. Abaqus FEA, (accessed May 15, 2012). http://www.3ds.com/products/simulia/portfolio/abaqus/overview/.

[10] Mark Drela. Integrated simulation model for preliminary aerodynamic, structural, and control-law design of aircraft. In *40th AIAA SDM Conference*, Reston, Virginia, 1999. AIAA.

[11] Mark Drela. Design Drivers of Energy-Efficient Transport Aircraft. *SAE International Journal of Aerospace*, 4:602–618, 2011.

[12] FAA. *Metallic Materials Properties Development and Standardization MMPDS-04*. Federal Aviation Administration, fourth edition, April 2008.

[13] FAA. *Code of Federal Regulations 14 CFR 25*. Office of the Federal Register National Archives and Records Administration, Washington, DC, 2012.

[14] Krzysztof J. Fidkowski, Frode Engelsen, Karen E. Willcox, and Ilan M. Kroo. Stochastic gust analysis techniques for aircraft conceptual design. In *12th AIAA/ISSMO Multidisciplinary Analysis and Optimization Conference*, Reston, Virginia, 2008. AIAA.

[15] Peretz P. Friedmann. Rotary-wing aeroelasticity - Current status and future trends. *Aerospace Engineering*, (January), 2001.

[16] M.J. Hinton, A.S. Kaddour, and P.D. Soden. *Failure Criteria in Fibre Reinforced Polymer Composites: The World-Wide Failure Exercise*. Elsevier, 2004.

[17] S. Jeon. Static and dynamic analysis of composite box beams using large deflection theory. *Computers & Structures*, 57(4):635–642, November 1995.

[18] Robert M. Jones. *Mechanics of Composite Materials*. Taylor & Francis, New York, NY, second edition, 1999.

[19] Sung Nam Jung, V. T. Nagaraj, and Inderjit Chopra. Refined structural model for thin and thick walled composite rotor blades. *AIAA Journal*, 40(1), 2002.

[20] L. Librescu and O. Song. On the static aeroelastic tailoring of composite aircraft swept wings modelled as thin-walled beam structures. *Composites Engineering*, 2(5-7):497–512, 1992.

[21] Gerald E. Mabson. Fracture analysis for bondlines and interfaces of composite structures. In *4th International conference of composites testing and modeling identification*, Dayton, Ohio, 2008. The Boeing Company.

[22] Pierre J.A. Minguet. *Static and dynamic behavior of composite helicopter rotor blades under large deflections*. PhD thesis, MIT, 1989.

[23] M. Mitra. A new super convergent thin walled composite beam element for analysis of box beam structures. *International Journal of Solids and Structures*, 41(5-6):1491–1518, March 2004.

[24] P. Pawar and R. Ganguli. On the effect of matrix cracks in composite helicopter rotor blade. *Composites Science and Technology*, 65(3-4):581–594, March 2005.

[25] B. Popescu. On asymptotically correct Timoshenko-like anisotropic beam theory. *International Journal of Solids and Structures*, 37(36):535–558, September 2000.

[26] O. Rand. On the importance of cross-sectional warping in solid composite beams. *Composite Structures*, 49(4):393–397, August 2000.

[27] Lawrence W. Rehfield. A refined simple model for tailoring box beams. *AIAA Journal*, 2001.

[28] Hubert Ronan. Aircraft Crashes Record Office Press Release, January 2008 (accessed May 15, 2012). http://www.baaa-acro.com/Communique%20de%20presse-UK-010108.htm.

[29] A. Sheikh and O. Thomsen. An efficient beam element for the analysis of laminated composite beams of thin-walled open and closed cross sections. *Composites Science and Technology*, 68(10-11):2273–2281, August 2008.

[30] Edward C. Smith and Inderjit Chopra. Formulation and evaluation of an analytical model for composite box-beams. *Journal of the American Helicopter Society*, 36(3):13, 1991.

[31] Alan D. Stemple and Sung W. Lee. Finite-element model for composite beams with arbitrary cross-sectional warping. *AIAA Journal*, 26(12):1512–1520, December 1988.

[32] Ansel C. Ugural and Saul K. Fenster. *Advanced Strength and Applied Elasticity*. Prentice Hall, Upper Saddle River, New Jersey, fourth edition, 2003.

[33] V. Volovoi. Assessment of beam modeling methods for rotor blade applications. *Mathematical and Computer Modelling*, 33(10-11):1099–1112, May 2001.

Appendix A

Code Listings

A.1 Matlab Script to Evaluate the Bending Stiffness Matrix of Orthotropic Box Beams

```
1  %————————————————————————————————————————————————
2  %
3  %       Orthotropic  Box Beam Bending  Stiffness  Matrix
4  %       Sebastien  Gauthier  Perron
5  %       Fall  2011
6  %
7  %
     .........................................................................
8  %   Given  material  properties  and beam  geometry  as  an  input ,  this
       function
9  %   will  return  the  equivalent  EI ,  GJ and  Coupling  factors  for  the  beam.
10 %   These  are  written  in  typical  stiffness  matrix  format :
11 %
12 %                EIcc    Kcs     0
13 %       E =     Kcs     GJ      0
14 %                0       0      EInn
15 %
16 %   Assumes  there  is  no  coupling  between  lateral  bending  and  twist  (
       Balanced
17 %   beam  webs ) , therefore :  Ksn = 0  and  also  assumed  c ,n  axes  are  aligned
       with
18 %   principal  bending  axis  of  the  beam:  EIcn = 0.
```

93

```
19  %    Assumes Uniform Thickness around the cross section
20  %
         _____

21  %    Inputs:
22  %    − W, H : Beam geometric dimensions (Width and Height)
23  %    − E1, E2, G12, v12, v21 : Ply elastic properties
24  %    − tply : Ply thickness
25  %    − Layup: The stacking sequence and ply orientations of the beam's
         layup
26
27  function [E EA A_Skins Q]=Beam_Stiffness(W,H,E1, E2, G12, v12,v21,tply,
         Layup);
28
29  Lam_Repeat = Layup(1,1);
30  nbply_base = size(Layup,1)−1;
31  nbply = nbply_base∗Lam_Repeat;
32  t = tply∗nbply;
33
34  % Calculation of ply reduced stiffness matrix Q, in material coordinate
35  % system under plane stress conditions
36  % 1 = Longitudinal
37  % 2 = Transverse
38  % 6 = Shear
39  Q11 = E1/(1−v12∗v21);
40  Q22 = E2/(1−v12∗v21);
41  Q12 =  v12∗E2/(1−v12∗v21);
42  Q66 = G12;
43  Q=[Q11 Q12 0; Q12 Q22 0; 0 0 Q66];
44
45  % Calculation of Rotated Reduced Stiffness (Qbar(k)) for kth ply in the
46  % layup of the beam
47  % Qbar11(1,4) = Qbar11 of 4th ply of Top or Bottom Layup
48  % Qbar12(2,3) = Qbar12 of 3rd ply of web layup
49
50  for i=[2,3]
51      % i=2 : Skins
52      % i=3 : Webs
53       Theta_Index=0;
54       for j = 1:nbply
55           % Ply Coordinates Calculation
56           % Returns laminate (Top Skin, Rear Spar) distance from
                    coordinate origin
```

```matlab
57              %Skins
58              if i==2
59                  ply_mid(1,j)= H/2 - tply*(j-0.5);
60                  ply_bottom(1,j)= ply_mid(1,j) - tply/2;
61                  ply_top(1,j)= ply_mid(1,j) + tply/2;
62              else
63                  %Webs
64                  ply_mid(2,j)= W/2 - tply*(j-0.5);
65                  ply_bottom(2,j)= ply_mid(2,j) - tply/2;
66                  ply_top(2,j)= ply_mid(2,j) + tply/2;
67              end
68
69              if Theta_Index == nbply_base
70                  Theta_Index=1;
71              else
72                  Theta_Index=Theta_Index+1;
73              end
74
75              Theta = Layup(Theta_Index+1,i)*3.14159/180;
76              Qbar11(i-1,j)= Q11*cos(Theta)^4 + 2*(Q12 + 2*Q66)*(sin(Theta)^2)
                    *(cos(Theta)^2) + Q22*sin(Theta)^4;
77              Qbar12(i-1,j) = (Q11+Q22-4*Q66)*(sin(Theta)^2)*(cos(Theta)^2) +
                    Q12*((sin(Theta)^4) + cos(Theta)^4);
78              Qbar22(i-1,j) = Q11*(sin(Theta)^4) + 2*(Q12 + 2*Q66)*(sin(Theta)
                    ^2)*(cos(Theta)^2) + Q22*cos(Theta)^4;
79              Qbar16(i-1,j) = (Q11 - Q12 - 2*Q66)*sin(Theta)*cos(Theta)^3 + (
                    Q12 - Q22 + 2*Q66)*(sin(Theta)^3)*cos(Theta);
80              Qbar26(i-1,j) = (Q11 - Q12 - 2*Q66)*(sin(Theta)^3)*cos(Theta) +
                    (Q12 - Q22 + 2*Q66)*sin(Theta)*cos(Theta)^3;
81              Qbar66(i-1,j) = (Q11 + Q22 -2*Q12 -2*Q66)*(sin(Theta)^2)*(cos(
                    Theta)^2) + Q66*(sin(Theta)^4 + cos(Theta)^4);
82
83              A11(i-1,j) = Qbar11(i-1,j)*tply;
84              A12(i-1,j) = Qbar12(i-1,j)*tply;
85              A22(i-1,j) = Qbar22(i-1,j)*tply;
86              A16(i-1,j) = Qbar16(i-1,j)*tply;
87              A26(i-1,j) = Qbar26(i-1,j)*tply;
88              A66(i-1,j) = Qbar66(i-1,j)*tply;
89
90              % Calculation of total Laminate Extensional Stiffness (A Matrix)
91              A11lam(i-1)=A11lam(i-1)+A11(i-1,j);
92              A12lam(i-1)=A12lam(i-1)+A12(i-1,j);
93              A22lam(i-1)=A22lam(i-1)+A22(i-1,j);
```

```matlab
94              A16lam(i-1)=A16lam(i-1)+A16(i-1,j);
95              A26lam(i-1)=A26lam(i-1)+A26(i-1,j);
96              A66lam(i-1)=A66lam(i-1)+A66(i-1,j);
97
98              % Calculate Cbar for kth ply. Cbar is the reduced Qbar matrix
99              % assuming Ny = 0, therefore reducing the plate equations to a
100             % uniaxial + shear loading condition.
101             Cbar11(i-1,j) = Qbar11(i-1,j) - ((Qbar12(i-1,j)^2)/Qbar22(i-1,j)
                    );
102             Cbar16(i-1,j) = Qbar16(i-1,j) - (Qbar12(i-1,j)*Qbar26(i-1,j)/
                    Qbar22(i-1,j));
103             Cbar66(i-1,j) = Qbar66(i-1,j) - ((Qbar26(i-1,j)^2)/Qbar22(i-1,j)
                    );
104         end
105  end
106
107  % Integral Variables Definition:
108  % Example: Qbar26n2(1,i)
109  % Integral over ith ply (j=1 : Skin) of Qbar26*n^2
110  for i=1:nbply
111
112      %Top and Bottom Laminates
113      Qbar26n2(1,i)= Qbar26(1,i)*W*(ply_top(1,i)^3- ply_bottom(1,i)^3)/3;
114      Qbar22n2(1,i)= Qbar22(1,i)*W*(ply_top(1,i)^3- ply_bottom(1,i)^3)/3;
115      Qbar12n2(1,i)= Qbar12(1,i)*W*(ply_top(1,i)^3- ply_bottom(1,i)^3)/3;
116      Qbar16n2(1,i)= Qbar16(1,i)*W*(ply_top(1,i)^3- ply_bottom(1,i)^3)/3;
117      Qbar66n2(1,i)= Qbar66(1,i)*W*(ply_top(1,i)^3- ply_bottom(1,i)^3)/3;
118      Qbar22dA(1,i)= Qbar22(1,i)*W*(tply);
119      Cbar11n2(1,i)= Cbar11(1,i)*W*(ply_top(1,i)^3- ply_bottom(1,i)^3)/3;
120      Cbar11c2(1,i)= Cbar11(1,i)*(W^3)*(tply)/12;
121      Cbar11dA(1,i)= Cbar11(1,i)*W*(tply);
122      Qbar26n2_Sum(1)= Qbar26n2_Sum(1)+ Qbar26n2(1,i);
123      Qbar22n2_Sum(1)= Qbar22n2_Sum(1)+ Qbar22n2(1,i);
124      Qbar12n2_Sum(1)= Qbar12n2_Sum(1)+ Qbar12n2(1,i);
125      Qbar16n2_Sum(1)= Qbar16n2_Sum(1)+ Qbar16n2(1,i);
126      Qbar66n2_Sum(1)= Qbar66n2_Sum(1)+ Qbar66n2(1,i);
127      Qbar22dA_Sum(1)= Qbar22dA_Sum(1)+ Qbar22dA(1,i);
128      Cbar11n2_Sum(1) = Cbar11n2(1,i) + Cbar11n2_Sum(1);
129      Cbar11c2_Sum(1) = Cbar11c2(1,i) + Cbar11c2_Sum(1);
130      Cbar11dA_Sum(1) = Cbar11dA(1,i) + Cbar11dA_Sum(1);
131
132      %
            ************************************************************
```

```matlab
133        % Side Laminates (Webs)
134        Qbar22n2(2,i)= Qbar22(2,i)*(H^3)*(tply)/12;
135        Qbar12n2(2,i)= Qbar12(2,i)*(H^3)*(tply)/12;
136        Qbar16n2(2,i)= Qbar16(2,i)*(H^3)*(tply)/12;
137        Qbar66c2(2,i)= Qbar66(2,i)*H*(ply_top(2,i)^3- ply_bottom(2,i)^3)/3;
138        Qbar22dA(2,i)= Qbar22(2,i)*H*(tply);
139        Cbar11n2(2,i)= Cbar11(2,i)*(H^3)*(tply)/12;
140        Cbar11c2(2,i)= Cbar11(2,i)*H*(ply_top(2,i)^3- ply_bottom(2,i)^3)/3;
141        Cbar11dA(2,i)= Cbar11(2,i)*H*(tply);
142        Qbar22n2_Sum(2)= Qbar22n2_Sum(2)+ Qbar22n2(2,i);
143        Qbar12n2_Sum(2)= Qbar12n2_Sum(2)+ Qbar12n2(2,i);
144        Qbar16n2_Sum(2)= Qbar16n2_Sum(2)+ Qbar16n2(2,i);
145        Qbar66c2_Sum(2)= Qbar66c2_Sum(2)+ Qbar66c2(2,i);
146        Qbar22dA_Sum(2)= Qbar22dA_Sum(2)+ Qbar22dA(2,i);
147        Cbar11n2_Sum(2) = Cbar11n2(2,i) + Cbar11n2_Sum(2);
148        Cbar11c2_Sum(2) = Cbar11c2(2,i) + Cbar11c2_Sum(2);
149        Cbar11dA_Sum(2) = Cbar11dA(2,i) + Cbar11dA_Sum(2);
150    end
151
152    % Skin Laminate A Matrix Definition
153    A_Skins=[A11lam(1) A12lam(1) A16lam(1); A12lam(1) A22lam(1) A26lam(1);
           A16lam(1) A26lam(1) A66lam(1)];
154
155    % Uniaxial & Shear A Matrix (Assume Ny = 0)
156    for i=1:2
157        Aprime11(i)= A11lam(i)-(A12lam(i)^2)/A22lam(i);
158        Aprime16(i)= A16lam(i)-(A12lam(i)*A26lam(i)/A22lam(i));
159        Aprime66(i)= A66lam(i)-(A26lam(i)^2)/A22lam(i);
160    end
161
162    % Laminate Equivalent Shear Modulus:
163    G(1) = (Aprime66(1)-(Aprime16(1)^2/Aprime11(1)))/t;
164    G(2) = (Aprime66(2)-(Aprime16(2)^2/Aprime11(2)))/t;
165    Alpha = (W/H)*(t/t)*(G(2)/G(1));
166
167    % Warping Coefficient
168    Beta = -(1-Alpha)/(1+Alpha);
169
170    d2=(1+Beta)*(2*Qbar26n2_Sum(1))/(2*(Qbar22n2_Sum(1)+Qbar22n2_Sum(2)));
171
172
173
```

```matlab
174  %————————————————————————————————————————————————
175  % Stiffness Matrix Calculations
176
177  % Bending Stiffness around C axis
178  EIcc = 2*(Cbar11n2_Sum(1) + Cbar11n2_Sum(2));
179
180  % Bending Stiffness around N axis
181  EInn = 2*(Cbar11c2_Sum(1) + Cbar11c2_Sum(2));
182
183  % Bend−Twist Coupling
184  EIcs = (1+Beta)*2*(Qbar16n2_Sum(1)+Qbar16n2_Sum(2)) − d2*2*(Qbar12n2_Sum
         (1)+Qbar12n2_Sum(2));
185
186  % Torsionnal Stiffness
187  GJ = ((1+Beta)^2)*2*(Qbar66n2_Sum(1)) + ((1−Beta)^2)*2*Qbar66c2_Sum(2) −
         d2*(1+Beta)*2*Qbar26n2_Sum(1);
188
189  % Axial Stiffness
190  EA = 2*(Cbar11dA_Sum(1) + Cbar11dA_Sum(2));
191
192  % Bending Stiffness Matrix Definition
193  E = [EIcc EIcs 0; EIcs GJ 0; 0 0 EInn];
194
195  % Reduced A matrix
196  Aprime_Skins = [Aprime11(1) Aprime16(1); Aprime16(1) Aprime66(1)];
197
198  end
```

A.2 Fortran Wing Twist Adjusment Script Twist.f

```fortran
1   c
2   c————————————————————————————————————————
3   c
4   c        Wing Twist Calculator
5   c        Sebastien Gauthier Perron
6   c        January 2012
7   c
8   c........................................................
9   c      Description:
10  c      This program will perform iterations with Aswing on a given
11  c      model in order to find the initial wing twist required to match
12  c      a certain wing deformation in 1g flight. Typically the 1g
13  c      deformed shape should result in a minimum wing drag condition.
14  c
15  c      Details:
16  c      − *.asw input file and Aswing launching script should be in same
17  c         directory as this script.
18  c      − Modify launching script (Aswing_Script.sh) to match Aswing
19  c         executable's location on your computer.
20  c      − In the Aswing input file, the twist should not be on the same
21  c         line as other parameters.
22  c
23  c————————————————————————————————————————
24          PROGRAM Twist
25          IMPLICIT NONE
26          CHARACTER*125 file_name, buffer, asw_file(500)
27          CHARACTER*8 temp_file
28          INTEGER stat, max_iter, col, i, j, nline_wing, nline, Tw_loc(2)
29          INTEGER niter
30          REAL Delta_Tw(11), Tw0(11), Tw_Target(11), Tw(11), Tw0_mod(11)
31          REAL wing_data(60,9), Delta, t(11), conv
32
33          temp_file = 'temp.asw'
34          niter = 0
35
36  c      Convergence Criteria:
37          conv = 0.1
38
39  c——— Target Twist based on Aluminum 737 in 1g Flight
40          Tw_Target(1) = 1.21982
41          Tw_Target(2) = 1.21982
```

```fortran
42          Tw_Target(3) = 1.21982
43          Tw_Target(4) = 1.08665
44          Tw_Target(5) = 0.95348
45          Tw_Target(6) = 0.78031
46          Tw_Target(7) = 0.78031
47          Tw_Target(8) = 0.34028
48          Tw_Target(9) = -0.10974
49          Tw_Target(10) = -0.44976
50          Tw_Target(11) = -0.63978
51    c————————————————————————————————————————————————
52    c———— Target Twist based on Aluminum 777 in 1g Flight
53    c        Tw_Target(1) = 1.30648
54    c        Tw_Target(2) = 1.30648
55    c        Tw_Target(3) = 1.30648
56    c        Tw_Target(4) = 1.07019
57    c        Tw_Target(5) = 0.8139
58    c        Tw_Target(6) = 0.51761
59    c        Tw_Target(7) = 0.51761
60    c        Tw_Target(8) = -0.09736
61    c        Tw_Target(9) = -0.90732
62    c        Tw_Target(10) = -1.70728
63    c        Tw_Target(11) = -2.53224
64    c————————————————————————————————————————————————
65
66          WRITE (*,*) 'Enter Aswing (.asw) file name:'
67          READ (*,*) file_name
68          WRITE (*,*) 'Enter Maximum Number of Iterations:'
69          READ (*,*) max_iter
70
71    c     Add ".asw" extension to file name
72          DO i=1,125
73              IF (file_name(i:i) == ' ') THEN
74                  GOTO 500
75              END IF
76          END DO
77    500   file_name = file_name(1:i-1)//'.asw'
78          CALL system('cp '//file_name//' '//file_name(1:i-1)//'.bak')
79          CALL system('cp '//file_name//' '//temp_file)
80          CALL system('rm '//file_name)
81
82          DO 5000 WHILE (niter <= max_iter)
83              i = 1
84              niter = niter+1
```

```fortran
85   c        Start Aswing Analysis
86              CALL system ('./Aswing_Script.sh temp')
87
88              OPEN( unit = 1, file = 'Twist_Results', STATUS='OLD')
89              DO
90              READ (1,'(A)', IOSTAT=stat) buffer
91              IF (stat<0) THEN
92   c                Stat<0 => End of File
93                  GOTO 1000
94              ELSE
95                  IF (buffer(22:26)=='Wing') THEN
96   c---- Read Heading Lines
97                      READ (1,'(A)', IOSTAT=stat) buffer
98                      READ (1,'(A)', IOSTAT=stat) buffer
99                      READ (1,'(A)', IOSTAT=stat) buffer
100                     DO
101  c---- Store all wing parameters in array wing_data
102                         READ (1,'(A)', IOSTAT=stat) buffer
103                         IF (buffer(2:6)=='.....') THEN
104                             GOTO 1000
105                         END IF
106                         READ (buffer,*) (wing_data(i, col), col=1,9)
107                         i=i+1
108                     END DO
109                 END IF
110             END IF
111         END DO
112   1000 CLOSE (1)
113         nline_wing = i - 1
114
115         Delta_Tw(1) = wing_data(25,4)
116         Delta_Tw(2) = wing_data(27,4)
117         Delta_Tw(3) = wing_data(28,4)
118         Delta_Tw(4) = wing_data(30,4)
119         Delta_Tw(5) = wing_data(32,4)
120         Delta_Tw(6) = wing_data(33,4)
121         Delta_Tw(7) = wing_data(34,4)
122         Delta_Tw(8) = wing_data(37,4)
123         Delta_Tw(9) = wing_data(40,4)
124         Delta_Tw(10) = wing_data(43,4)
125         Delta_Tw(11) = wing_data(50,4)
126
127   c        Get Initial Twist (Tw0) from .asw file
```

```fortran
128          i = 1
129          nline = 0
130          OPEN( unit = 2, file = temp_file, STATUS='OLD')
131          DO
132              READ (2,'(A)', IOSTAT=stat) buffer
133              IF (stat<0) THEN
134  c              Stat<0 => End of File
135                  GOTO 2000
136              ELSE
137                  nline = nline+1
138                  asw_file(nline) = buffer
139                  IF (buffer(1:4) == 'Wing') THEN
140                      DO
141                          nline = nline+1
142                          READ (2,'(A)', IOSTAT=stat) buffer
143                          asw_file(nline) = buffer
144
145                          IF (INDEX(buffer,'twist') .NE. 0) THEN
146  c------                     Read Heading Lines
147                              Tw_loc(1) = nline + 2
148                              nline = nline+1
149                              READ (2,'(A)', IOSTAT=stat) buffer
150                              asw_file(nline) = buffer
151
152                              DO
153                                  nline = nline+1
154                                  READ (2,'(A)', IOSTAT=stat) buffer
155                                  asw_file(nline) = buffer
156                                  IF (INDEX(buffer,'------') .NE. 0) THEN
157                                      Tw_loc(2) = nline-1
158                                      GOTO 1500
159                                  END IF
160                                  READ (buffer,*) (wing_data(i, col),
161      &                                                       col=1,2)
162                                  t(i) = wing_data(i,1)
163                                  Tw0(i) = wing_data(i,2)
164                                  i=i+1
165                              END DO
166                          END IF
167                      END DO
168                  END IF
169              END IF
170  1500 END DO
```

```fortran
171    2000 CLOSE (2)
172
173          Delta_Tw(1) = 0
174          Delta_Tw(2) = 0
175          Delta_Tw(3) = 0
176          Tw = Delta_Tw + Tw0
177          Tw0_mod = Tw_Target - Tw + Tw0
178 c        Wing Tip Convergence Check
179          Delta = ABS(Tw0_mod(11) - Tw0(11))
180
181 c    Write Tw0_mod to temp.asw file
182          j = 1
183          OPEN (UNIT=3, FILE = temp_file, ACTION="write", STATUS="replace")
184          DO i=1,nline
185              IF (i >= Tw_loc(1) .AND. i <= Tw_loc(2)) THEN
186                  WRITE(3,20) t(j), Tw0_mod(j)
187    20            FORMAT (4X, F8.5, 7X, F8.5)
188                  j = j+1
189              ELSE
190                  WRITE(3,'(A)') asw_file(i)
191              END IF
192          END DO
193          CLOSE (3)
194 c    Iterate until convergence or max iter
195          IF (Delta < conv) THEN
196              GOTO 6000
197          END IF
198
199    5000 CONTINUE
200
201    6000 CALL system('cp '//temp_file//' '//file_name)
202          CALL system('rm '//temp_file)
203          CALL system('rm Twist_Results')
204          WRITE(*,*) 'Process stopped after ', niter,' iterations'
205          WRITE(*,*) 'Tip twist change after last iteration:', Delta
206          STOP
207          END
```

A.3 Laminate Failure Matlab Script

```matlab
1
2  %─────────────────────────────────────────────────────
3  %
4  %       Laminate Failure
5  %       Sebastien Gauthier Perron
6  %       January 2012
7  %
8  %............................................................
9  %   Description:
10 %    This script is used to find the critical load (Nx) and
11 %    critical strain (Epsxx_Cr) of a given laminate. It will also
12 %    return the critical ply (Crit_Ply) and the failure mode
13 %    (Fail_Mode) associated to it.
14 %
15 %    It requires the in−plane stress allowables and
16 %    information about the geometry and layup as input
17 %    parameters.
18 %──────────────────────────────────────────────────────────
19
20 function [FI_Max Mc Nx Crit_Ply Crit_Angle Fail_Mode Epsxx_Cr]=
       Lam_Max_Load(FTU1, FTU2, FSU12, A_Skins, Layup, M, W, H, Q)
21
22 FI_Target = 1.;
23 Residual = 100;
24
25 nbply=size(Layup)−1;
26 FI=zeros(nbply);
27
28 while abs(Residual)>0.01
29
30     Nx=(M(1)/H)/W;
31     Ny=0;
32     Nxy=(M(3)/H)/W;
33     N=[Nx;Ny;Nxy];
34     Strain_Skins = A_Skins\N;
35     FI_Max=0;
36
37     %Evaluate failure index for each ply in the laminate
38     for i = 1:nbply
39         Theta = Layup(i+1,2)*3.14159/180;
40         Qbar11 = Q(1,1)*cos(Theta)^4 + 2*(Q(1,2) + 2*Q(3,3))*(sin(Theta)
```

```matlab
                    ^2)*(cos(Theta)^2) + Q(2,2)*sin(Theta)^4;
41              Qbar12 = (Q(1,1)+Q(2,2)-4*Q(3,3))*(sin(Theta)^2)*(cos(Theta)^2)
                    + Q(1,2)*((sin(Theta)^4) + cos(Theta)^4);
42              Qbar22 = Q(1,1)*(sin(Theta)^4) + 2*(Q(1,2) + 2*Q(3,3))*(sin(
                    Theta)^2)*(cos(Theta)^2) + Q(2,2)*cos(Theta)^4;
43              Qbar16 = (Q(1,1) - Q(1,2) - 2*Q(3,3))*sin(Theta)*cos(Theta)^3 +
                    (Q(1,2) - Q(2,2) + 2*Q(3,3))*(sin(Theta)^3)*cos(Theta);
44              Qbar26 = (Q(1,1) - Q(1,2) - 2*Q(3,3))*(sin(Theta)^3)*cos(Theta)
                    + (Q(1,2) - Q(2,2) + 2*Q(3,3))*sin(Theta)*cos(Theta)^3;
45              Qbar66 = (Q(1,1) + Q(2,2) -2*Q(1,2) -2*Q(3,3))*(sin(Theta)^2)*(
                    cos(Theta)^2) + Q(3,3)*(sin(Theta)^4 + cos(Theta)^4);
46
47          % Compute Stresses in laminate and ply axis
48          Sigmaxx = Qbar11*Strain_Skins(1) + Qbar12*Strain_Skins(2) +
                    Qbar16*Strain_Skins(3);
49          Sigmayy = Qbar12*Strain_Skins(1) + Qbar22*Strain_Skins(2) +
                    Qbar26*Strain_Skins(3);
50          Sigmaxy = Qbar16*Strain_Skins(1) + Qbar26*Strain_Skins(2) +
                    Qbar66*Strain_Skins(3);
51          Sigma11 = (cos(Theta)^2)*Sigmaxx + (sin(Theta)^2)*Sigmayy + 2*
                    sin(Theta)*cos(Theta)*Sigmaxy;
52          Sigma22 = (sin(Theta)^2)*Sigmaxx + (cos(Theta)^2)*Sigmayy - 2*
                    sin(Theta)*cos(Theta)*Sigmaxy;
53          Sigma12 = -sin(Theta)*cos(Theta)*Sigmaxx + sin(Theta)*cos(Theta)
                    *Sigmayy + ((cos(Theta)^2)-(sin(Theta)^2))*Sigmaxy;
54
55      % Compute failure index based on Max Stress Criteria
56          Max_Stress(1) = abs(Sigma11)/FTU1;
57          if Sigma22 >=0
58              Max_Stress(2) = Sigma22/FTU2;
59          else
60              Max_Stress(2) = abs(Sigma22)/(FTU2);
61          end
62          Max_Stress(3) = abs(Sigma12)/FSU12;
63          FI(i)=max(Max_Stress);
64
65          if FI(i)>FI_Max
66              FI_Max = FI(i);
67              Crit_Ply = i;
68              Crit_Angle = Theta*180/3.14159;
69              Epsxx_Cr = Strain_Skins(1);
70
71              %Failures Modes
```

```matlab
72                    % 1: Fiber Tension
73                    % 2: Matrix Cracking
74                    % 3: Shear
75
76                    if max(Max_Stress)==Max_Stress(1)
77                        Fail_Mode=1;
78                    elseif max(Max_Stress)==Max_Stress(2)
79                        Fail_Mode=2;
80                    elseif max(Max_Stress)==Max_Stress(3)
81                        Fail_Mode=3;
82                    end
83              end
84        end
85
86        % Compute residual and adjust bending moment if needed
87        Residual = (FI_Max-FI_Target)/FI_Target;
88        if Residual < -0.01
89            M(1)=M(1)*1.01;
90        elseif Residual >0.01
91            M(1)=M(1)*0.99;
92        end
93
94      % Compute Shear load as % of axial load
95      %737
96       M(3)=0.1*M(1);
97
98      %777
99       %M(3)=0.2*M(1);
100  end
101  Mc=M(1);
102  end
```

A.4 Matlab Script to Generate Aswing Input

```matlab
1
2  %————————————————————————————————————————
3  %
4  %        Aswing Beam Structural Properties Input
5  %        Sebastien Gauthier Perron
6  %        January 2012
7  %
8  %..........................................................
9  %    Description:
10 %    This script ouputs the wing's structural properties in the format
        required by Aswing.
11 %    It also evaluates the properties along the span of the wing based on
         the supplied properties at the root of the wing.
12 %  In order to do so, the metalic 737 and 777 scaling factors are
        provided
13 %
14 %    INPUTS:
15 %        - Beam's Bending Stiffness Matrix calculated at the wing's root
16 %        - Wing height (H) and width (W) at the root
17 %        - Wing layup at the root (Layup)
18 %        - Ply thickness (tply) and material density (Rho)
19 %
20 %    OUTPUT: Aswing input text file with the following beam properties
        along the wing span:
21 %    - t
22 %    - mg, mgnn
23 %    - Cshell, Nshell, Atshell
24 %    - EIcc, EInn, GJ, EA
25 %    - EIcs
26 %————————————————————————————————————————————
27
28  function Write_ASWING_Input(EIcc, EInn, EIcs, GJ, EA, Layup, W, H, tply,
        Rho)
29  k=0.001;
30  kEIcc=0;
31  kEInn=0;
32  kEIcs=0;
33  kGJ=0;
34  kEA=0;
35  kmg=0;
36  kmgnn=0;
```

```matlab
37  kCshell=0;
38  kNshell=0;
39  kAtshell=0;
40  %
41  nbply =size(Layup) - 1;
42  nbply = nbply(1);
43  t=tply*nbply;
44  A= t*(2*W + 2*(H-2*t));
45  % mg Scaling (1.66) to account for leading/trailing edge, flaps,
46  % actuators...
47  % mgnn Scaling (2.5)
48  mg_root = A*Rho*9.81*1.66;
49  Inn_root = (H*W^3)/12 - (H-2*t)*((W-2*t)^3)/12;
50  mgnn_root = Inn_root*Rho*9.81*2.5;
51  Cshell_root=W/2;
52  Nshell_root=H/2;
53  Atshell_root = W*H*t;
54  while kEIcc==0 || kEInn==0 || kEIcs==0 || kGJ==0 || kEA==0 || kmg==0 ||
        kmgnn==0
55      if EIcc/k <10 && kEIcc==0
56          kEIcc=k;
57      end
58      if EInn/k <10 && kEInn==0
59          kEInn=k;
60      end
61      if EIcs/k <10 && kEIcs==0
62          kEIcs=k;
63      end
64      if GJ/k <10 && kGJ==0
65          kGJ=k;
66      end
67      if EA/k <10 && kEA==0
68          kEA=k;
69      end
70      if mg_root/k<10 && kmg==0
71          kmg=k;
72      end
73      if mgnn_root/k <10 && kmgnn==0
74          kmgnn=k;
75      end
76      if Cshell_root/k <10 && kCshell==0
77          kCshell=k;
78      end
```

```matlab
79          if  Nshell_root/k <10 && kNshell==0
80              kNshell=k;
81          end
82          if  Atshell_root/k <10 && kAtshell==0
83              kAtshell=k;
84          end
85          k=k*10;
86  end
87  EIcc=EIcc/kEIcc;
88  EInn=EInn/kEInn;
89  EIcs=EIcs/kEIcs;
90  GJ=GJ/kGJ;
91  EA=EA/kEA;
92  mg_root=mg_root/kmg;
93  mgnn_root=mgnn_root/kmgnn;
94  Cshell_root = Cshell_root/kCshell;
95  Nshell_root = Nshell_root/kNshell;
96  Atshell_root = Atshell_root/kAtshell;
97  % 777-300ER Stiffness Scaling Factor along wing span (based on Metallic
98  % version)
99  % Assumes Stiffness properties were evaluated at root of wing.
100 % Could be imported from 2nd text file?
101 % 777-300ER Spanwise Coordinate definition (t)
102 % tAswing(1)=0;
103 % tAswing(2)=3.048;
104 % tAswing(3)=3.048;
105 % tAswing(4)=5.31259;
106 % tAswing(5)=7.57718;
107 % tAswing(6)=9.84177;
108 % tAswing(7)=9.84177;
109 % tAswing(8)=15.0702;
110 % tAswing(9)=20.2986;
111 % tAswing(10)=25.5271;
112 % tAswing(11)=30.7555;
113 % % EIcc, EInn, EIcs Spanwise Scaling Factors
114 % EI_Ratio(1)=1.00;
115 % EI_Ratio(2)=1.00;
116 % EI_Ratio(3)=1.00;
117 % EI_Ratio(4)=8.19E-01;
118 % EI_Ratio(5)=6.38E-01;
119 % EI_Ratio(6)=4.58E-01;
120 % EI_Ratio(7)=4.58E-01;
121 % EI_Ratio(8)=1.93E-01;
```

```
122  % EI_Ratio(9)=6.43E-02;
123  % EI_Ratio(10)=1.4E-02;
124  % EI_Ratio(11)=1.160E-03;
125  % % GJ Spanwise Scaling Factors
126  % GJ_Ratio(1)=1.00;
127  % GJ_Ratio(2)=1.00;
128  % GJ_Ratio(3)=1.00;
129  % GJ_Ratio(4)=7.61E-01;
130  % GJ_Ratio(5)=5.03E-01;
131  % GJ_Ratio(6)=2.54E-01;
132  % GJ_Ratio(7)=2.54E-01;
133  % GJ_Ratio(8)=1.07E-01;
134  % GJ_Ratio(9)=3.57E-02;
135  % GJ_Ratio(10)=7.79E-03;
136  % GJ_Ratio(11)=6.48E-04;
137  % % EA Spanwise Scaling Factors
138  % EA_Ratio(1)=1.00;
139  % EA_Ratio(2)=1.00;
140  % EA_Ratio(3)=1.00;
141  % EA_Ratio(4)=9.27E-01;
142  % EA_Ratio(5)=8.54E-01;
143  % EA_Ratio(6)=7.81E-01;
144  % EA_Ratio(7)=7.81E-01;
145  % EA_Ratio(8)=5.08E-01;
146  % EA_Ratio(9)=2.93E-01;
147  % EA_Ratio(10)=1.37E-01;
148  % EA_Ratio(11)=3.93E-02;
149  % % mg Spanwise Scaling Factors
150  % mg_Ratio(1)=1.00E+00;
151  % mg_Ratio(2)=1.00E+00;
152  % mg_Ratio(3)=1.00E+00;
153  % mg_Ratio(4)=9.27E-01;
154  % mg_Ratio(5)=8.54E-01;
155  % mg_Ratio(6)=7.81E-01;
156  % mg_Ratio(7)=7.81E-01;
157  % mg_Ratio(8)=5.08E-01;
158  % mg_Ratio(9)=2.93E-01;
159  % mg_Ratio(10)=1.37E-01;
160  % mg_Ratio(11)=3.93E-02;
161  % % Cshell & Nshell Spanwise Scaling Factor
162  % Cshell_Ratio(1)=1.00;
163  % Cshell_Ratio(2)=1.00;
164  % Cshell_Ratio(3)=1.00;
```

```matlab
165   % Cshell_Ratio(4)=0.93;
166   % Cshell_Ratio(5)=0.85;
167   % Cshell_Ratio(6)=0.78;
168   % Cshell_Ratio(7)=0.78;
169   % Cshell_Ratio(8)=0.63;
170   % Cshell_Ratio(9)=0.48;
171   % Cshell_Ratio(10)=0.33;
172   % Cshell_Ratio(11)=0.17;
173   % % Atshell Scaling Factor
174   % Atshell_Ratio(1)=1.00;
175   % Atshell_Ratio(2)=1.00;
176   % Atshell_Ratio(3)=1.00;
177   % Atshell_Ratio(4)=0.88;
178   % Atshell_Ratio(5)=0.73;
179   % Atshell_Ratio(6)=0.55;
180   % Atshell_Ratio(7)=0.55;
181   % Atshell_Ratio(8)=0.29;
182   % Atshell_Ratio(9)=0.13;
183   % Atshell_Ratio(10)=0.04;
184   % Atshell_Ratio(11)=0.01;
185   %————————————————————————————————————
186   % 737-800 Stiffness Scaling Factor along wing span (based on Metallic
187   % version)
188   % % 737-800 Spanwise Coordinate definition (t)
189   tAswing(1)=0;
190   tAswing(2)=1.8034;
191   tAswing(3)=1.8034;
192   tAswing(4)=2.801;
193   tAswing(5)=3.79859;
194   tAswing(6)=4.79619;
195   tAswing(7)=4.79619;
196   tAswing(8)=7.80432;
197   tAswing(9)=10.8125;
198   tAswing(10)=13.8206;
199   tAswing(11)=16.8287;
200   % EIcc, EInn, EIcs Spanwise Scaling Factors
201   EI_Ratio(1)=1.00;
202   EI_Ratio(2)=1.00;
203   EI_Ratio(3)=1.00;
204   EI_Ratio(4)=8.12E-01;
205   EI_Ratio(5)=6.24E-01;
206   EI_Ratio(6)=4.37E-01;
207   EI_Ratio(7)=4.37E-01;
```

```
208  EI_Ratio(8)=2.17E−01;
209  EI_Ratio(9)=9.26E−02;
210  EI_Ratio(10)=3.14E−02;
211  EI_Ratio(11)=7.10E−03;
212  % GJ Spanwise Scaling Factors
213  GJ_Ratio(1)=1.00;
214  GJ_Ratio(2)=1.00;
215  GJ_Ratio(3)=1.00;
216  GJ_Ratio(4)=7.62E−01;
217  GJ_Ratio(5)=5.24E−01;
218  GJ_Ratio(6)=2.87E−01;
219  GJ_Ratio(7)=2.87E−01;
220  GJ_Ratio(8)=1.42E−01;
221  GJ_Ratio(9)=6.08E−02;
222  GJ_Ratio(10)=2.06E−02;
223  GJ_Ratio(11)=4.67E−03;
224  % EA Spanwise Scaling Factors
225  EA_Ratio(1)=1.00;
226  EA_Ratio(2)=1.00;
227  EA_Ratio(3)=1.00;
228  EA_Ratio(4)=9.83E−01;
229  EA_Ratio(5)=9.66E−01;
230  EA_Ratio(6)=9.49E−01;
231  EA_Ratio(7)=9.49E−01;
232  EA_Ratio(8)=6.68E−01;
233  EA_Ratio(9)=4.37E−01;
234  EA_Ratio(10)=2.54E−01;
235  EA_Ratio(11)=1.21E−01;
236  % mg Spanwise Scaling Factors
237  mg_Ratio(1)=1.00E+00;
238  mg_Ratio(2)=1.00E+00;
239  mg_Ratio(3)=1.00E+00;
240  mg_Ratio(4)=9.83E−01;
241  mg_Ratio(5)=9.66E−01;
242  mg_Ratio(6)=9.49E−01;
243  mg_Ratio(7)=9.49E−01;
244  mg_Ratio(8)=6.68E−01;
245  mg_Ratio(9)=4.37E−01;
246  mg_Ratio(10)=2.54E−01;
247  mg_Ratio(11)=1.21E−01;
248  % Cshell & Nshell Spanwise Scaling Factor
249  Cshell_Ratio(1)=1.00;
250  Cshell_Ratio(2)=1.00;
```

```matlab
251   Cshell_Ratio(3)=1.00;
252   Cshell_Ratio(4)=0.90;
253   Cshell_Ratio(5)=0.80;
254   Cshell_Ratio(6)=0.70;
255   Cshell_Ratio(7)=0.70;
256   Cshell_Ratio(8)=0.59;
257   Cshell_Ratio(9)=0.48;
258   Cshell_Ratio(10)=0.36;
259   Cshell_Ratio(11)=0.25;
260   % Atshell Scaling Factor
261   Atshell_Ratio(1)=1.00;
262   Atshell_Ratio(2)=1.00;
263   Atshell_Ratio(3)=1.00;
264   Atshell_Ratio(4)=0.91;
265   Atshell_Ratio(5)=0.80;
266   Atshell_Ratio(6)=0.65;
267   Atshell_Ratio(7)=0.65;
268   Atshell_Ratio(8)=0.38;
269   Atshell_Ratio(9)=0.20;
270   Atshell_Ratio(10)=0.09;
271   Atshell_Ratio(11)=0.03;
272   %
         ****************************************************************************

273   %Write Output to EIGJ.txt in ASWING format
274   stack_top=' ';
275   stack_webs=' ';
276   nbply_base=2;
277   Lam_Repeat=nbply/nbply_base;
278   for j=2:3
279       for i=2:nbply_base+1
280           if j==2
281               if i==nbply_base+1
282                   ply_angle=sprintf('%2.0f',Layup(i,j));
283               else
284                   ply_angle=sprintf('%2.0f/',Layup(i,j));
285               end
286               stack_top= strcat(stack_top,ply_angle );
287           else
288               if i==nbply_base+1
289                   ply_angle=sprintf('%2.0f',Layup(i,j));
290               else
291                   ply_angle=sprintf('%2.0f/',Layup(i,j));
```

```matlab
292                end
293                stack_webs= strcat(stack_webs, ply_angle);
294            end
295        end
296 end
297 % use sprintf to convert the numeric data to text, using %E
298 k_str = sprintf('*      %2.1E         %2.1E      %2.1E      %2.1E      %2.1E\r\n'
        ,1.0, kEIcc, kEInn,kGJ, kEA);
299 k_str_mg = sprintf('*      %2.1E         %2.1E      %2.1E\r\n',1.0, kmg, kmgnn
        );
300 k_str_Cshell = sprintf('*     %2.1E         %2.1E      %2.1E      %2.1E\r\n'
        ,1.0, kCshell, kNshell, kAtshell);
301 % use strrep to replace Windows exponent prefix with Unix 2 digits
        Version
302 k_str = strrep(k_str, 'E+0','E+');
303 k_str = strrep(k_str, 'E-0','E-');
304 k_str_mg=strrep(k_str_mg, 'E+0','E+');
305 k_str_mg=strrep(k_str_mg, 'E-0','E-');
306 k_str_Cshell=strrep(k_str_Cshell, 'E+0','E+');
307 k_str_Cshell=strrep(k_str_Cshell, 'E-0','E-');
308 % Open and Write to text File
309 Filename = strcat('EIGJ_',num2str(Layup(2,2)),'_', num2str(nbply),'.txt
        ');
310 fid = fopen(Filename, 'w');
311 % Header / Description of Beam Dimensions
312 fprintf(fid, '# Beam Section Properties (at Wing Root)\r\n');
313 fprintf(fid, '# Width: %3.2f\r\n',W);
314 fprintf(fid, '# Height: %3.2f\r\n',H);
315 fprintf(fid, '# Number of plies: %2.0f\r\n',nbply);
316 fprintf(fid, '# Wall Thickness: %2.1E\r\n',t);
317 fprintf(fid, '# Stacking Sequence (Top)  : [%s]%2.0f\r\n',stack_top,
        Lam_Repeat);
318 fprintf(fid, '# Stacking Sequence (Sides): [%s]%2.0f\r\n',stack_webs,
        Lam_Repeat);
319 fprintf(fid, '#————————————————————————\r\n');
320 fprintf(fid, '       t               mg          mgnn\r\n');
321 fprintf(fid, '%s',k_str_mg);
322 for i=1:11
323    if tAswing(i)<10
324        fprintf(fid, '    % 7.5f        %7.5f    %7.5f\r\n', tAswing(i),
                mg_root*mg_Ratio(i), mgnn_root*EI_Ratio(i));
325    else
326        fprintf(fid, '    %8.5f        %7.5f    %7.5f\r\n', tAswing(i),
```

114

```matlab
                            mg_root*mg_Ratio(i), mgnn_root*EI_Ratio(i));
327         end
328     end
329     fprintf(fid, '#————————————————————\r\n');
330     fprintf(fid, '          t                Cshell       Nshell       Atshell\r\n');
331     fprintf(fid, '%s',k_str_Cshell);
332     for i=1:11
333         if tAswing(i)<10
334             fprintf(fid, '    % 7.5f        %7.5f      %7.5f      %7.5f\r\n',
                    tAswing(i),Cshell_root*Cshell_Ratio(i), Nshell_root*
                    Cshell_Ratio(i), Atshell_root*Atshell_Ratio(i));
335         else
336             fprintf(fid, '    %8.5f        %7.5f      %7.5f      %7.5f\r\n',
                    tAswing(i),Cshell_root*Cshell_Ratio(i), Nshell_root*
                    Cshell_Ratio(i), Atshell_root*Atshell_Ratio(i));
337         end
338     end
339     fprintf(fid, '#————————————————————\r\n');
340     fprintf(fid, '          t                EIcc         EInn         GJ          EA\r
            \n');
341     fprintf(fid, '%s',k_str);
342     for i=1:11
343         if tAswing(i)<10
344             fprintf(fid, '    % 7.5f        %7.5f      %7.5f      %7.5f      %7.5f\
                    r\n', tAswing(i),EIcc*EI_Ratio(i), EInn*EI_Ratio(i), GJ*
                    GJ_Ratio(i), EA*EA_Ratio(i));
345         else
346             fprintf(fid, '    %8.5f        %7.5f      %7.5f      %7.5f      %7.5f\r
                    \n', tAswing(i),EIcc*EI_Ratio(i), EInn*EI_Ratio(i), GJ*
                    GJ_Ratio(i), EA*EA_Ratio(i));
347         end
348     end
349     fprintf(fid, '#————————————————————\r\n');
350     fprintf(fid, '          t                EIcs\r\n');
351     k_str = sprintf('*     %2.1E        %2.1E\r\n',1.0, kEIcs);
352     k_str = strrep(k_str,'E+0','E+');
353     k_str = strrep(k_str,'E-0','E-');
354     fprintf(fid, '%s',k_str);
355     for i=1:10
356         if tAswing(12-i)<10
357             fprintf(fid, '    %7.5f        %7.5f\r\n', -tAswing(12-i),-EIcs*
                    EI_Ratio(12-i));
358         else
```

```matlab
359            fprintf(fid, '     %8.5f           %7.5f\r\n', -tAswing(12-i),-EIcs*
                  EI_Ratio(12-i));
360        end
361    end
362    for i=1:11
363        if tAswing(i)<10
364            fprintf(fid, '      %7.5f           %7.5f\r\n', tAswing(i),EIcs*
                  EI_Ratio(i));
365        else
366            fprintf(fid, '     %8.5f           %7.5f\r\n', tAswing(i),EIcs*
                  EI_Ratio(i));
367        end
368    end
369    fclose(fid);
370    end
```

Appendix B

Wing Critical Load Cases

This appendix presents the various plots which were used to identify the critical load cases of the wings. The time-dependent data is plotted for every layup angles simulated as well as every gust length. Those dynamic loads are also compared against the static load cases in order to identify which one is more critical for each wing design.

B.1   737

The following plots were generated from the 737 ASWING model.

B.1.1   737 Critical Gust Cases for Various Layup Angles

This section presents the dynamic gust response of the 737 wings by plotting the root spanwise bending moment as a function of time for various gust lengths. For each specific layup angle tested, a comparison between the coupled and uncoupled wing responses is presented. The critical gust length can be identified for each wing design by finding the peak bending moment on their respective charts. As seen on charts B-1 to B-5, the critical gust length and peak bending moment change slightly due to the variation of layup angles and the presence or not of coupling which affect the wing's overall stiffness.
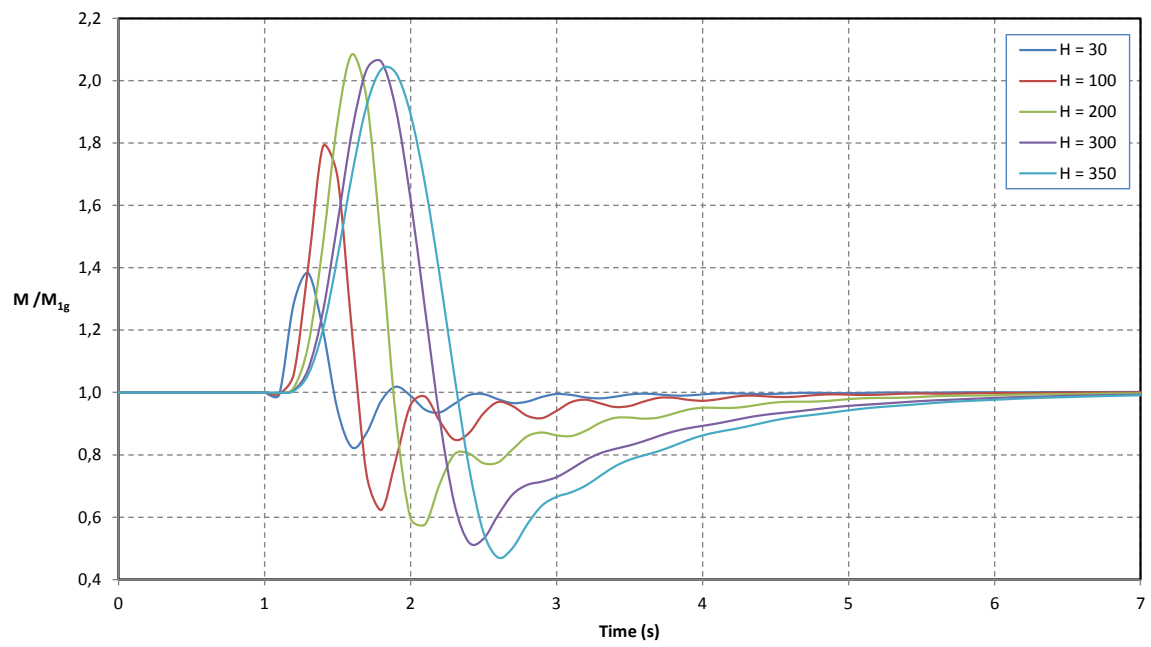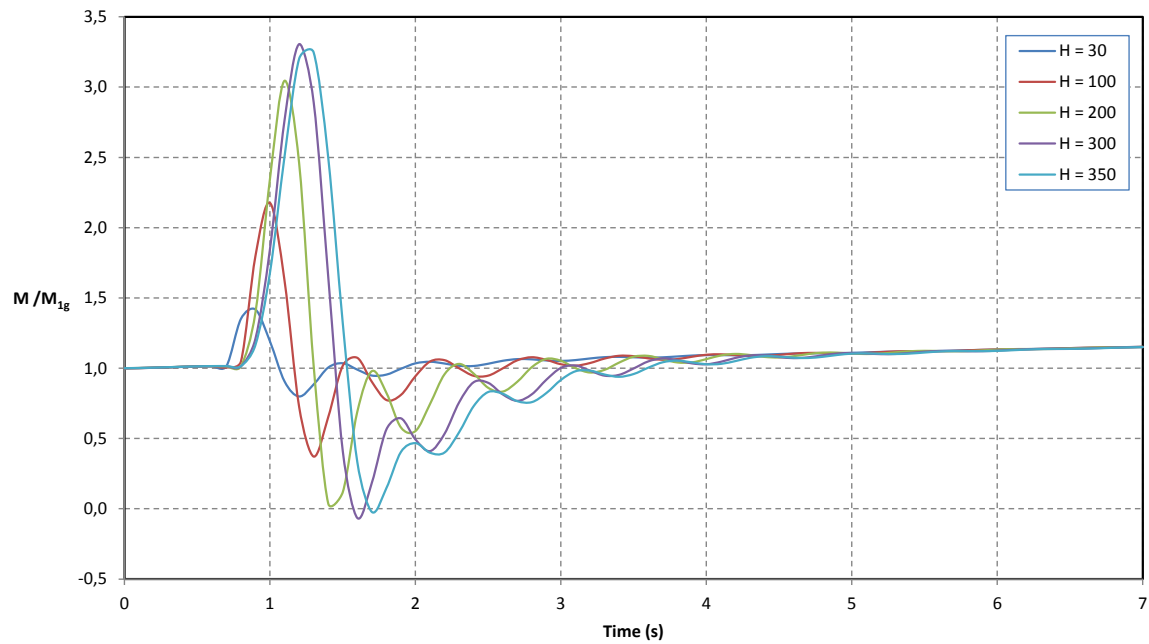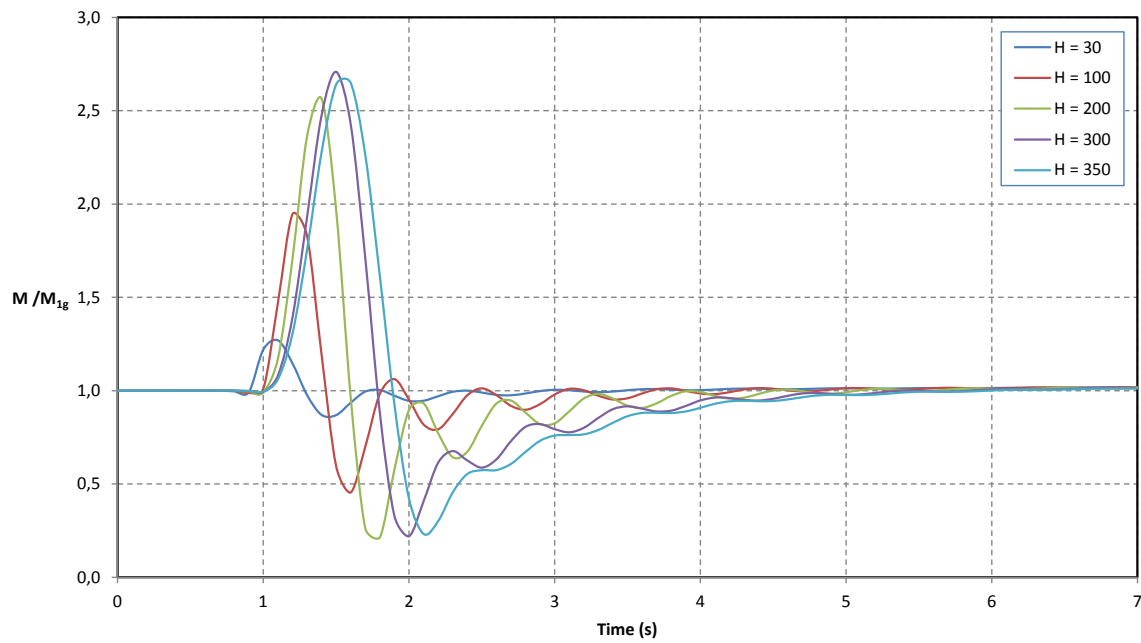
Figure B-1: 737 Bending moment ratio for various gust lengths, $\theta = 0°$.
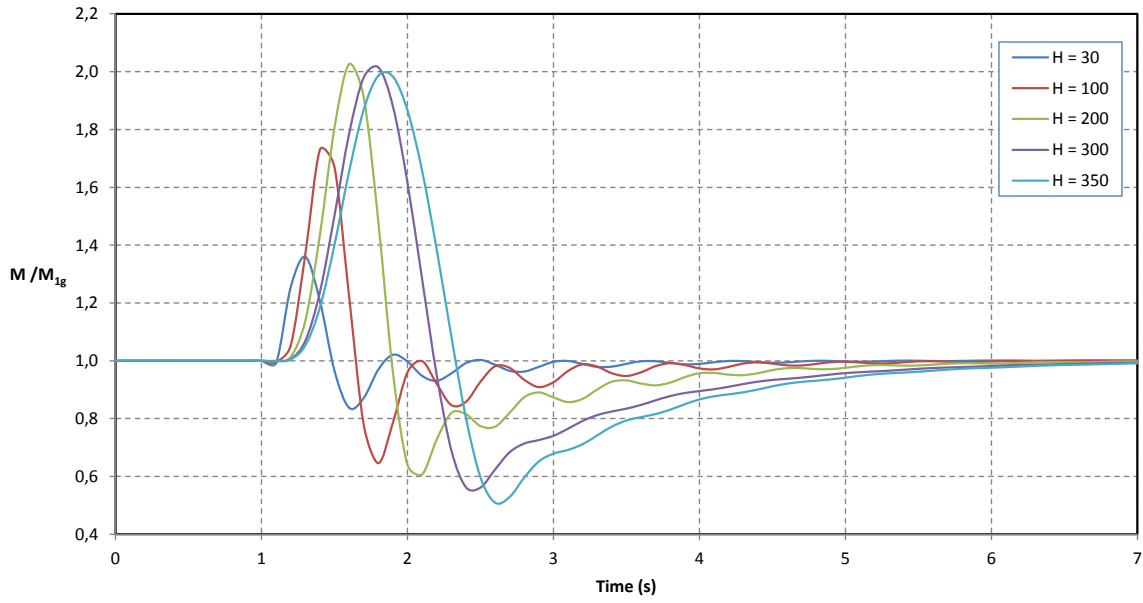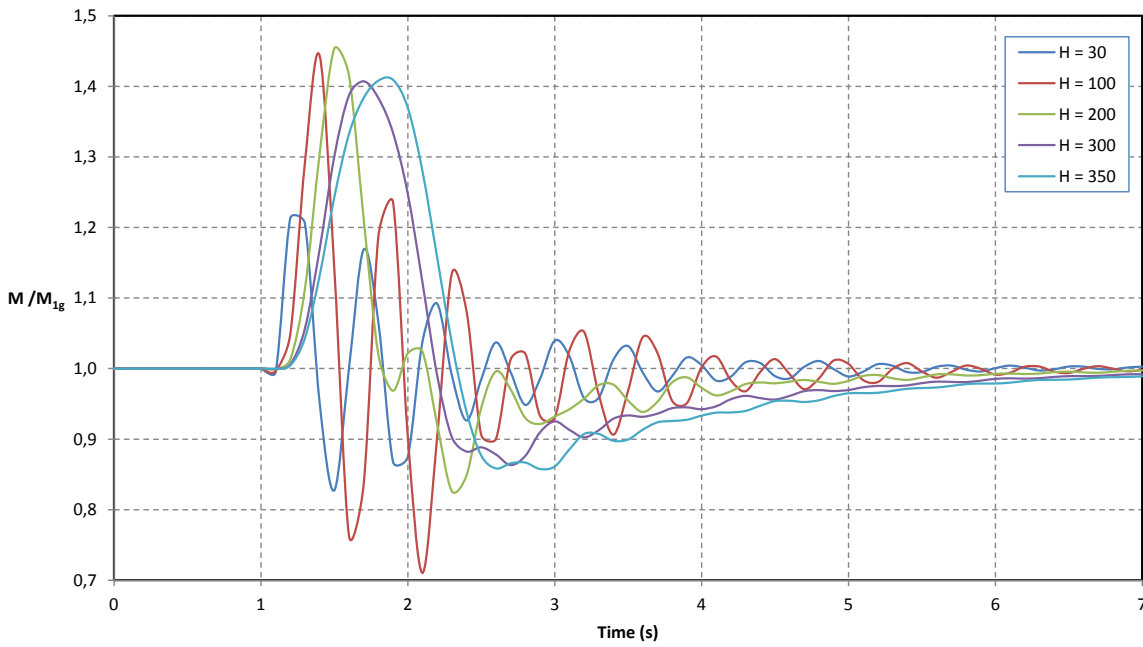
(a) Without Coupling

(b) With Coupling

Figure B-2: 737 Bending moment ratio for various gust lengths, $\theta = 5°$.
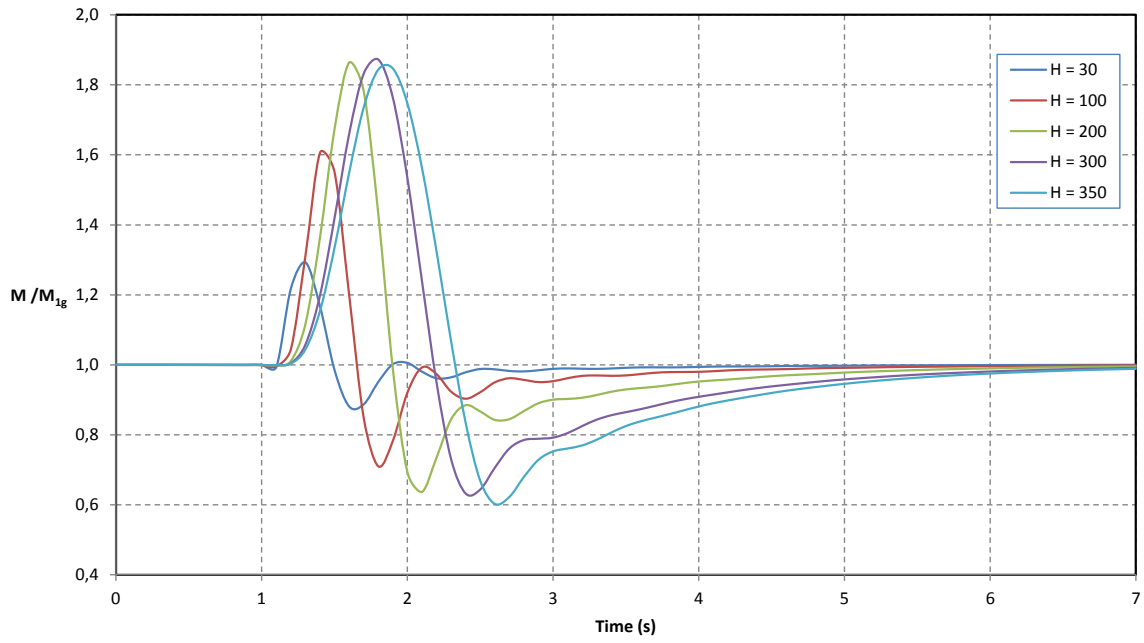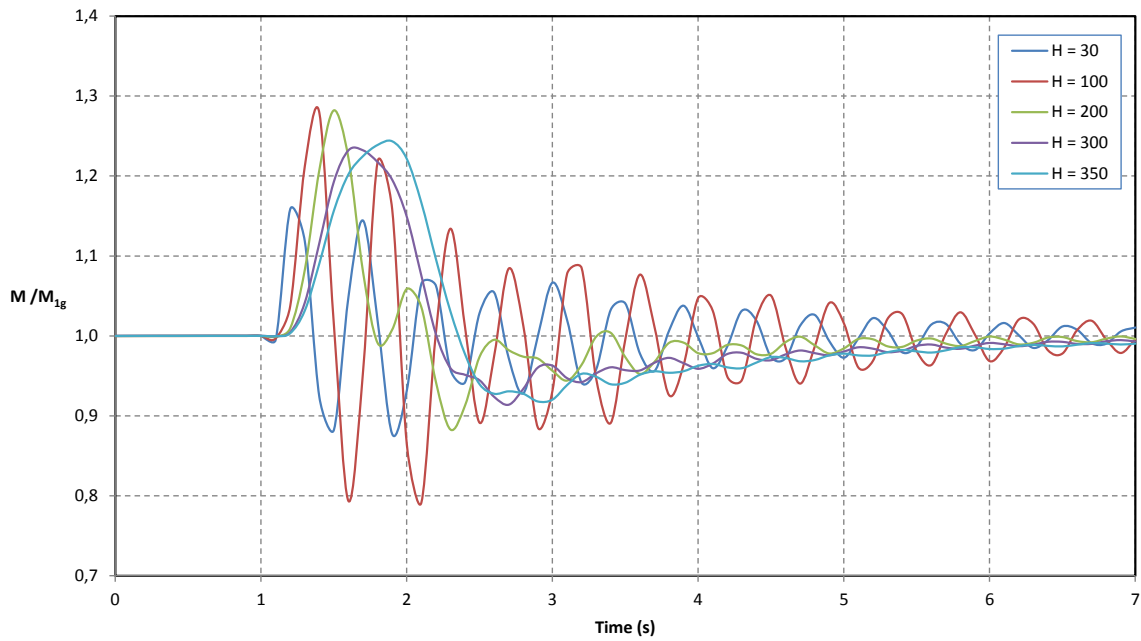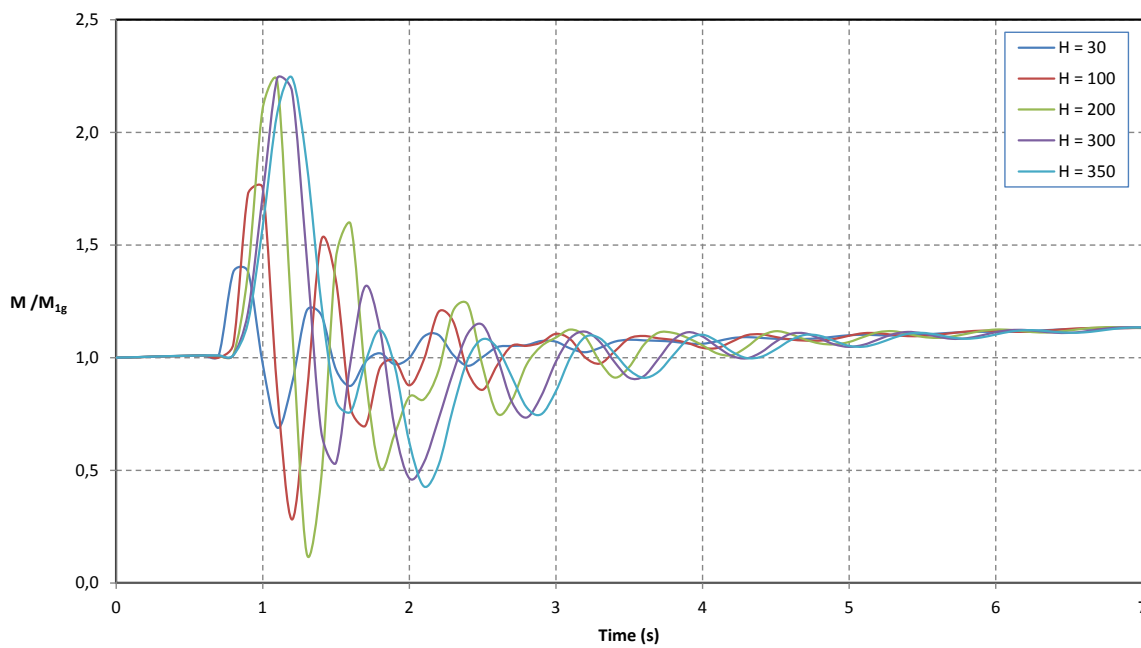
(a) Without Coupling

(b) With Coupling

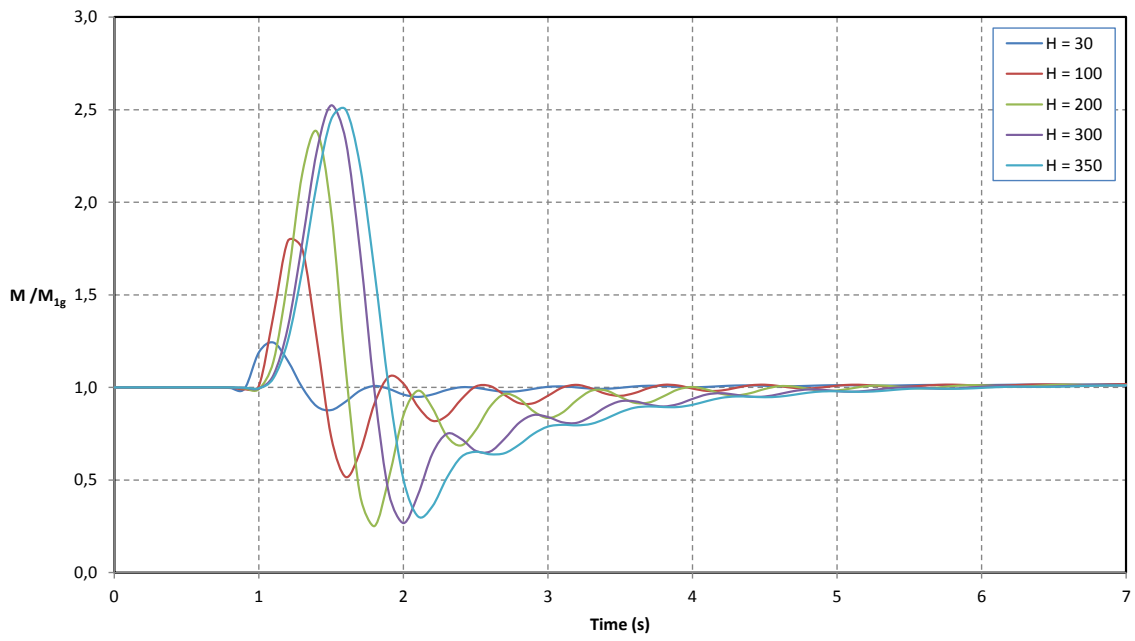Figure B-3: 737 Bending moment ratio for various gust lengths, $\theta = 10°$.
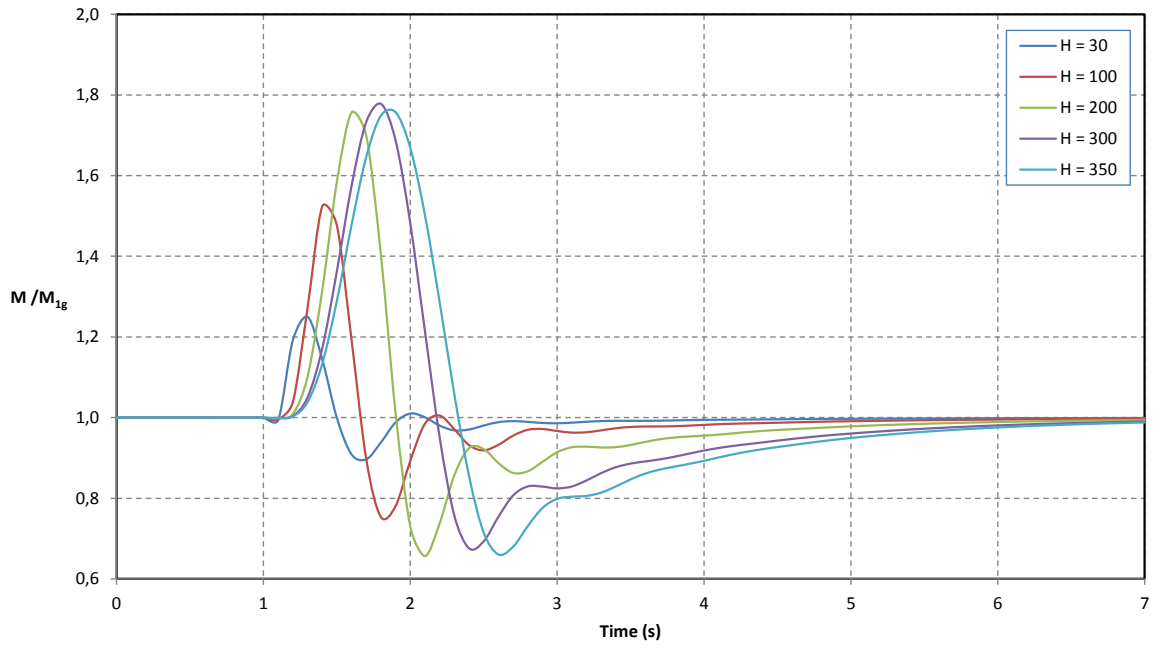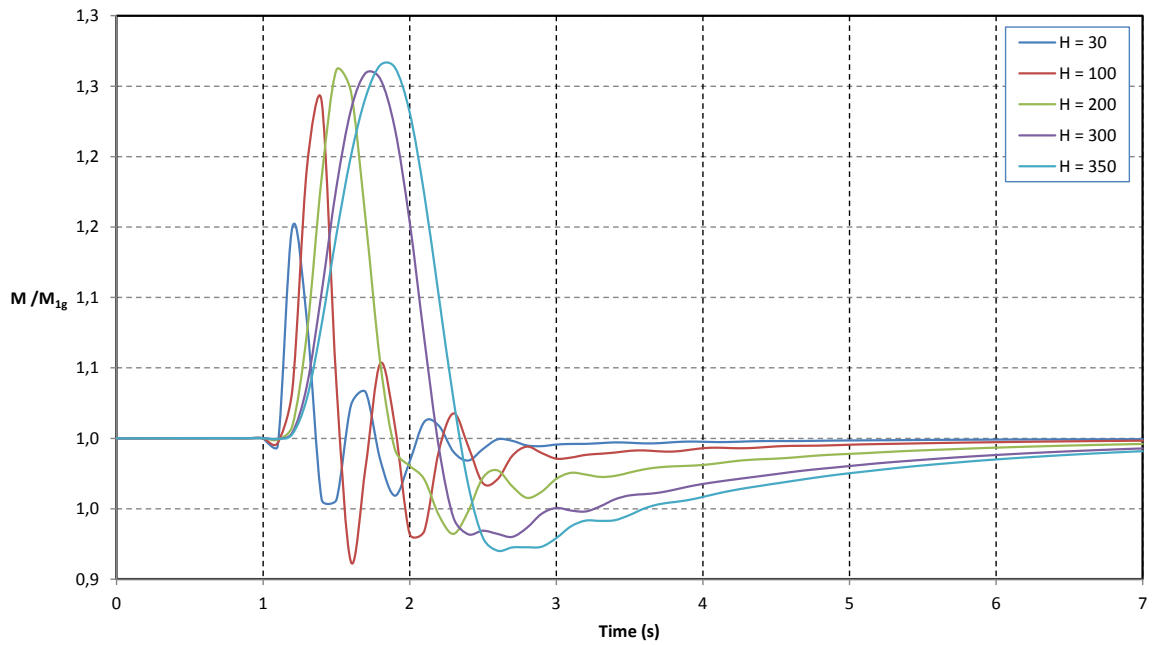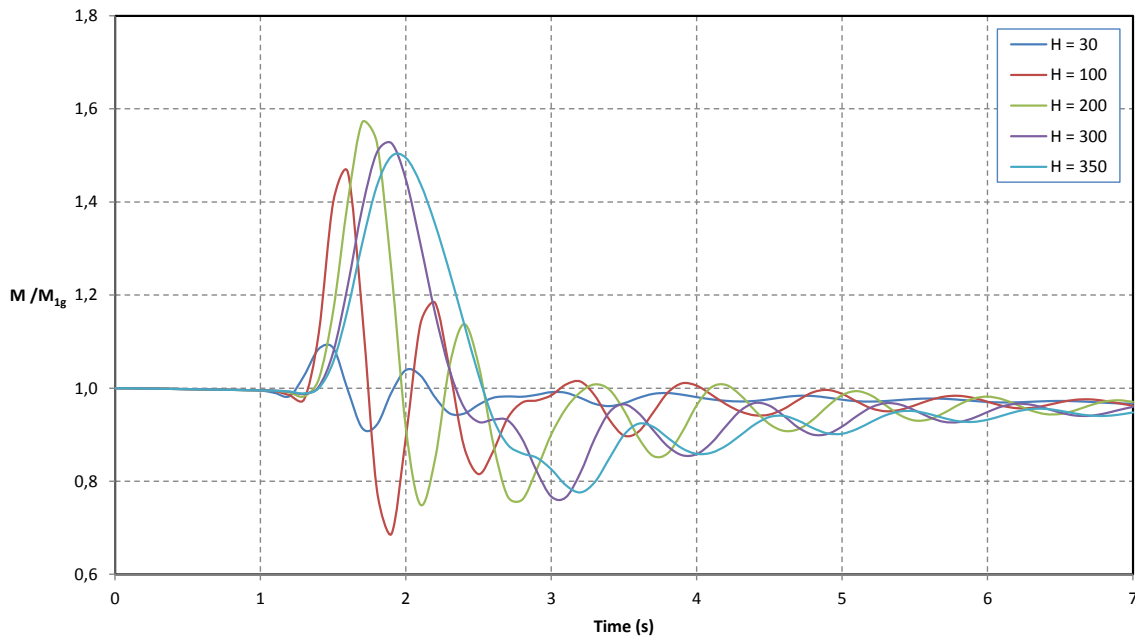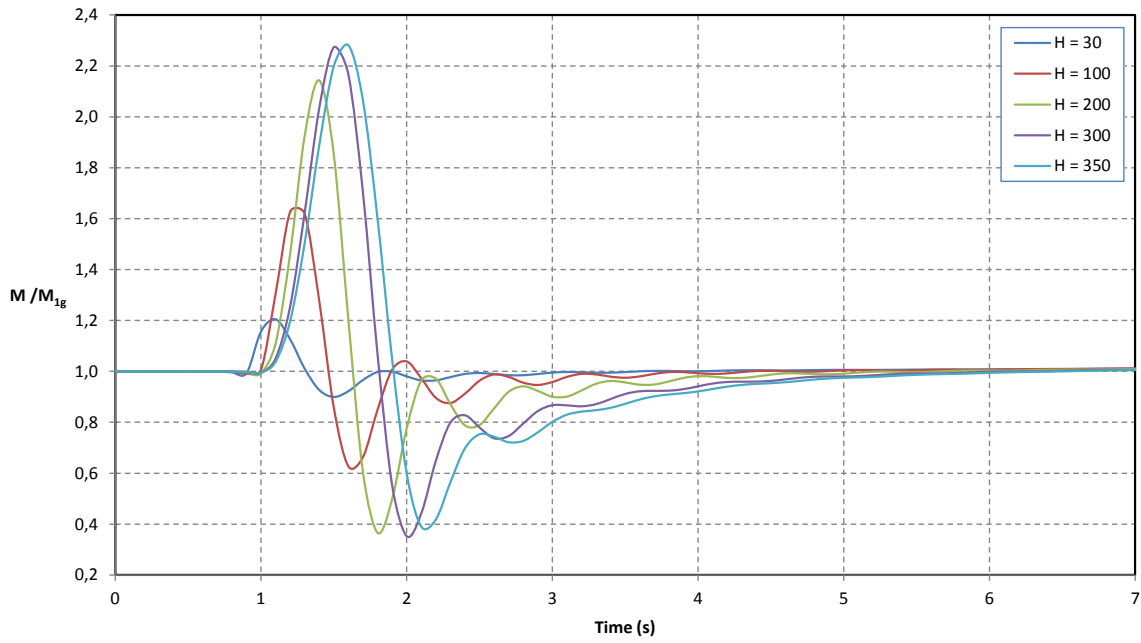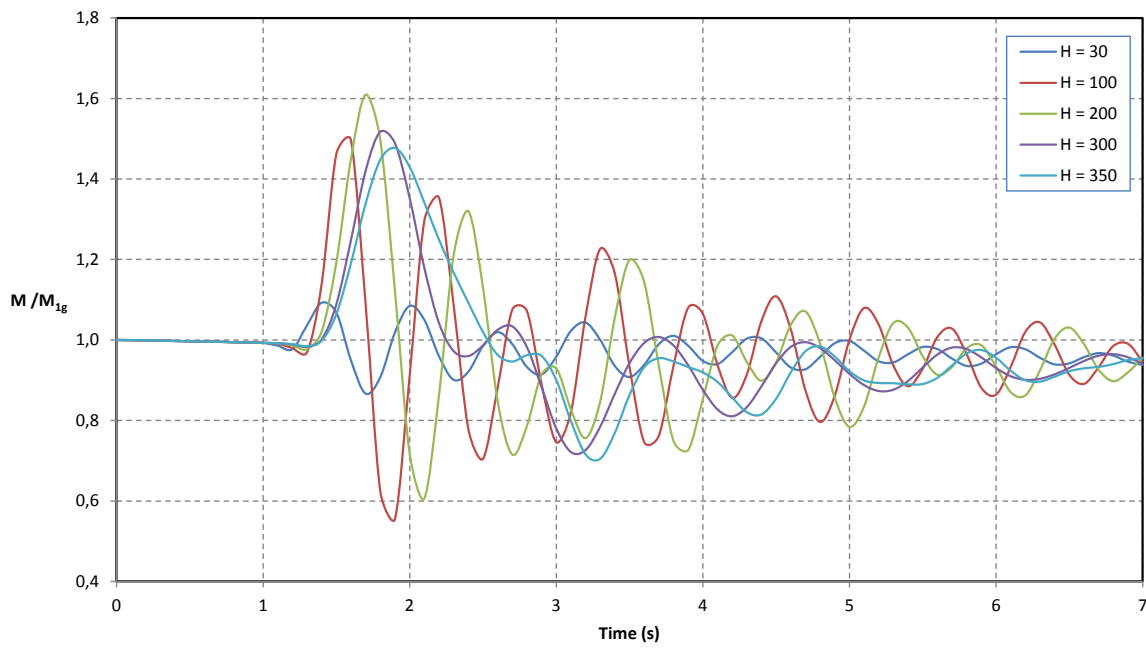
(a) Without Coupling

(b) With Coupling

Figure B-4: 737 Bending moment ratio for various gust lengths, $\theta = 15°$.
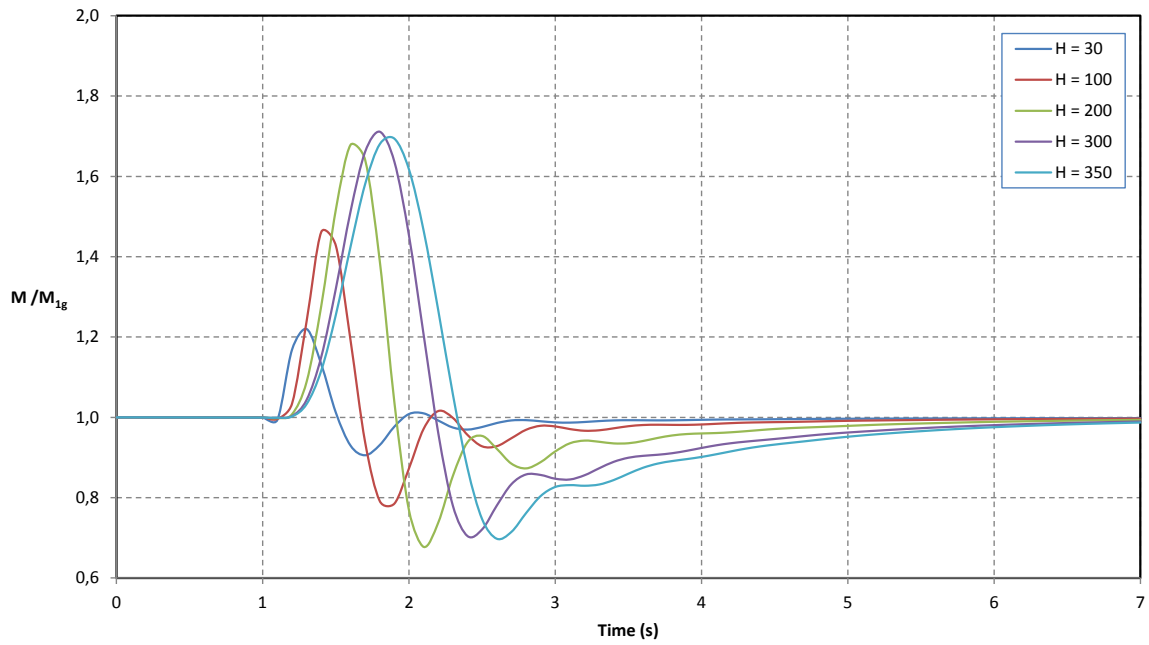
(a) Without Coupling
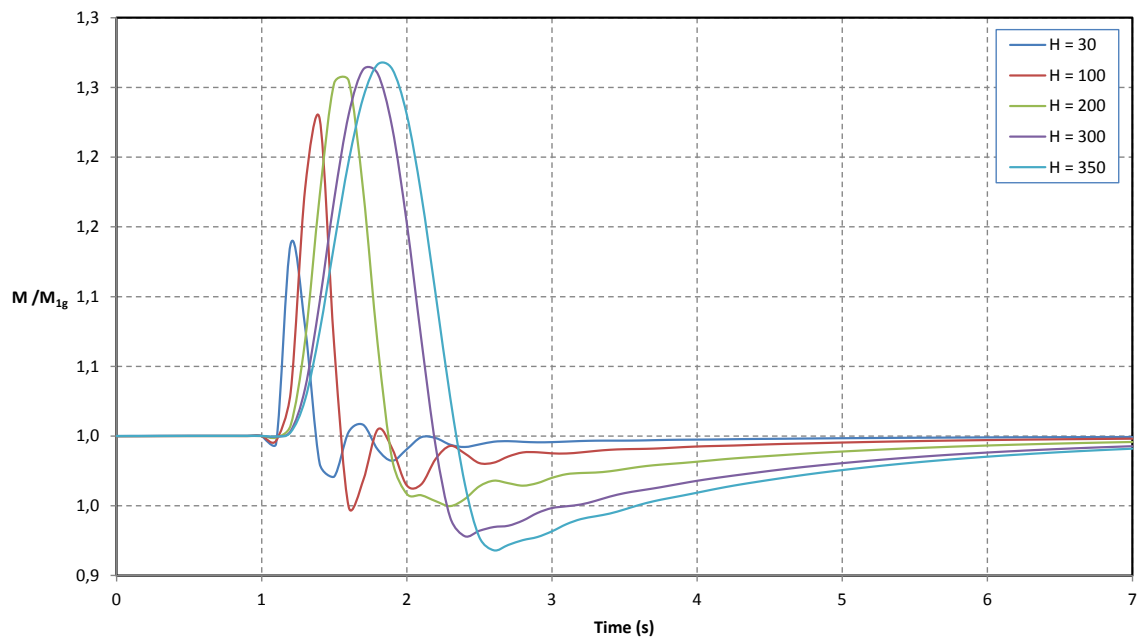
(b) With Coupling

Figure B-5: 737 Bending moment ratio for various gust lengths, $\theta = 20°$.

B.1.2 737 Static Versus Dynamic Critical Bending Moments for Various Layup Angles

Figures B-6 to B-10 compare the limit static load increase to the critical gust case for each 737 wing layup angle. On every graph, curves are plotted both for the coupled and uncoupled wings, except for the $\theta = 0°$ wing since it is impossible to generate coupling with that layup. Therefore, for each layup angle the critical load case between the static or dynamic case can be identified. Whichever case generates the highest bending moment is defined as the critical case for that particular wing layup angle. This critical case can then be used to properly size the wing.
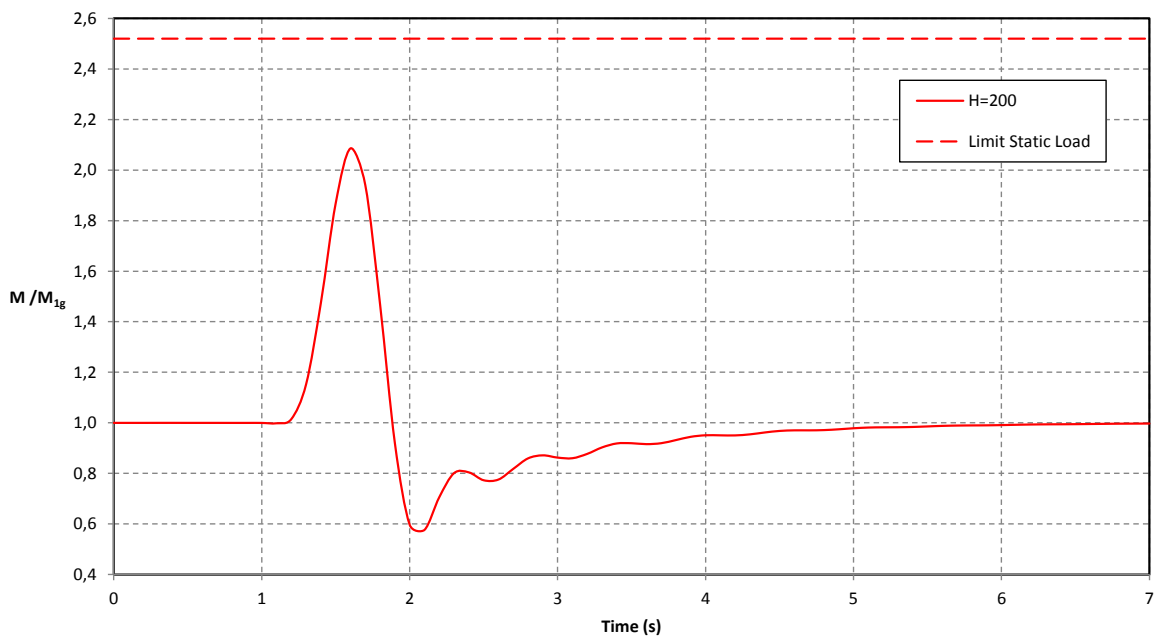
Figure B-6: 737 Bending moment ratio for the critical gust and static load cases, $\theta = 0°$.
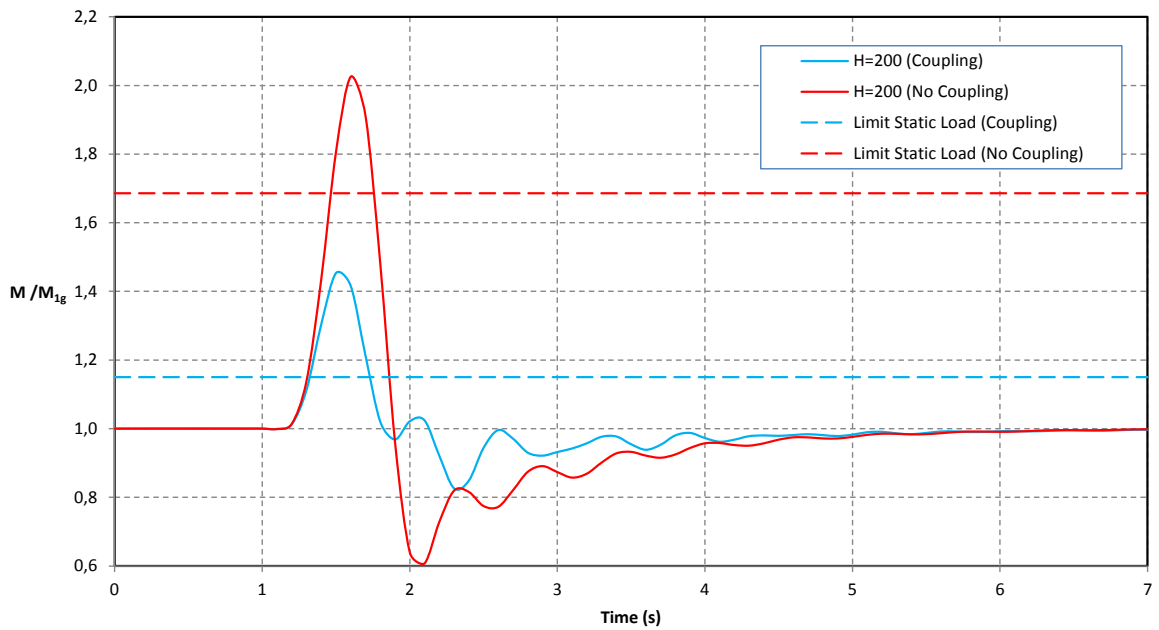
Figure B-7: 737 Bending moment ratio for the critical gust and static load cases, $\theta = 5°$.
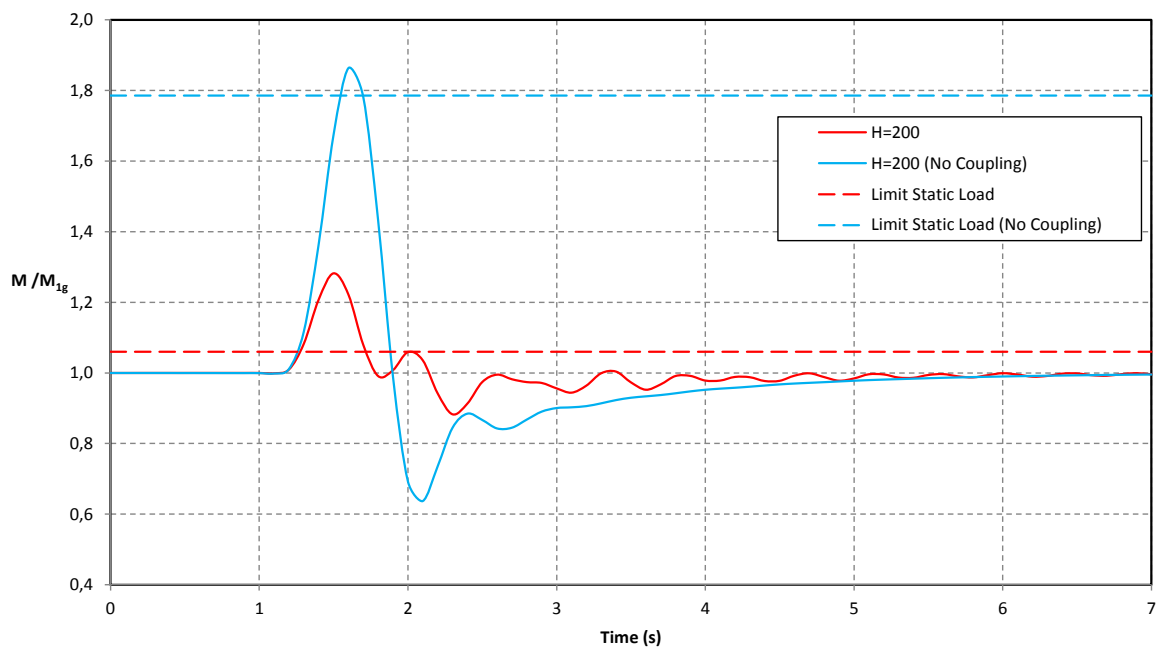
Figure B-8: 737 Bending moment ratio for the critical gust and static load cases, $\theta = 10°$.
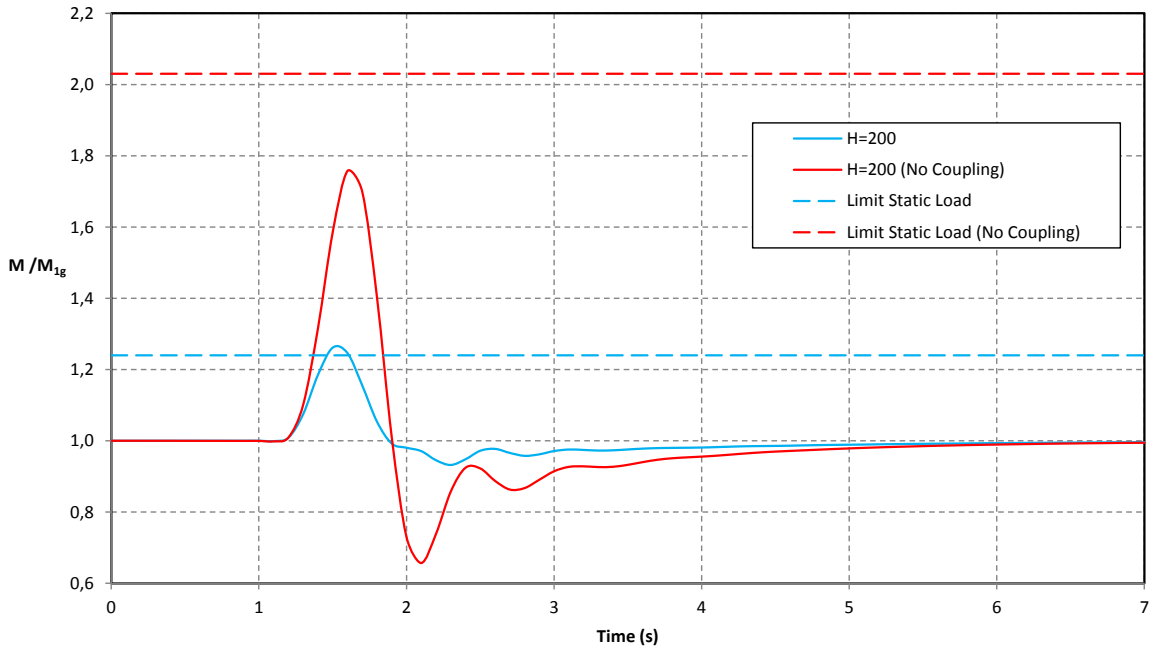
Figure B-9: 737 Bending moment ratio for the critical gust and static load cases, $\theta = 15°$.
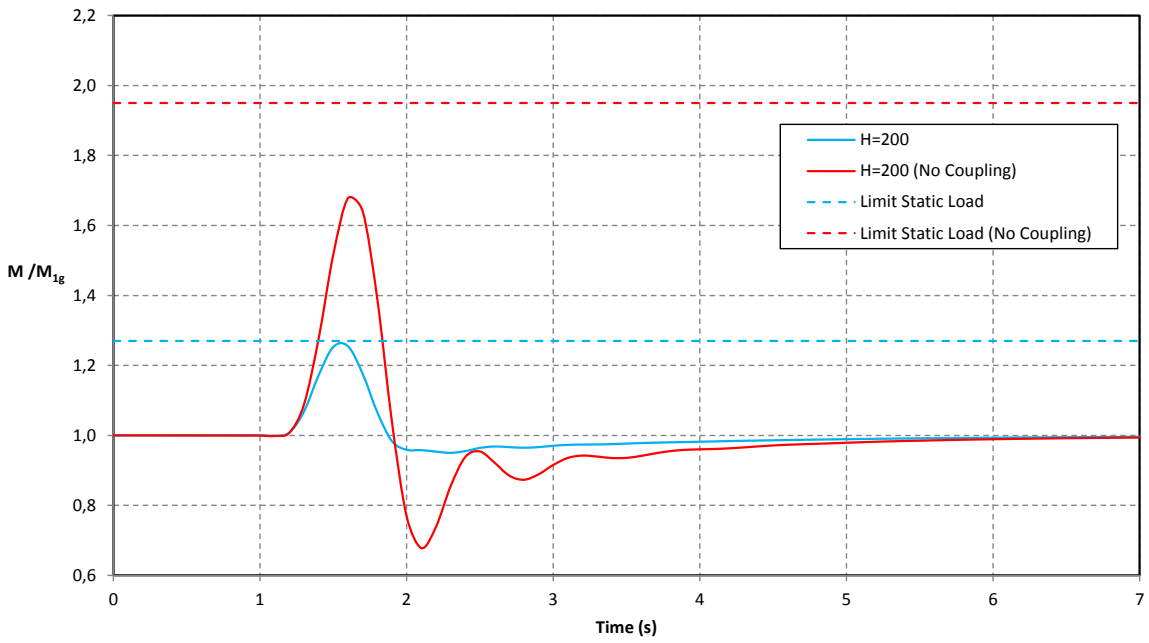
Figure B-10: 737 Bending moment ratio for the critical gust and static load cases, $\theta = 20°$.

B.2   777

The following plots were generated from the 777 ASWING model.

B.2.1   777 Critical Gust Cases for Various Layup Angles

Just like the 737, the 777's wing dynamic gust response also depends on the wing's overall stiffness. This effect can be seen on figures B-11 to B-15 by looking at the peak bending moment and its associated gust length as the wing's layup angle is changed.

Figure B-11: 777 Bending moment ratio for various gust lengths, $\theta = 0°$.

(a) Without Coupling

(b) With Coupling

Figure B-12: 777 Bending moment ratio for various gust lengths, $\theta = 5°$.

(a) Without Coupling

(b) With Coupling

Figure B-13: 777 Bending moment ratio for various gust lengths, $\theta = 10°$.

(a) Without Coupling

(b) With Coupling

Figure B-14: 777 Bending moment ratio for various gust lengths, $\theta = 15°$.
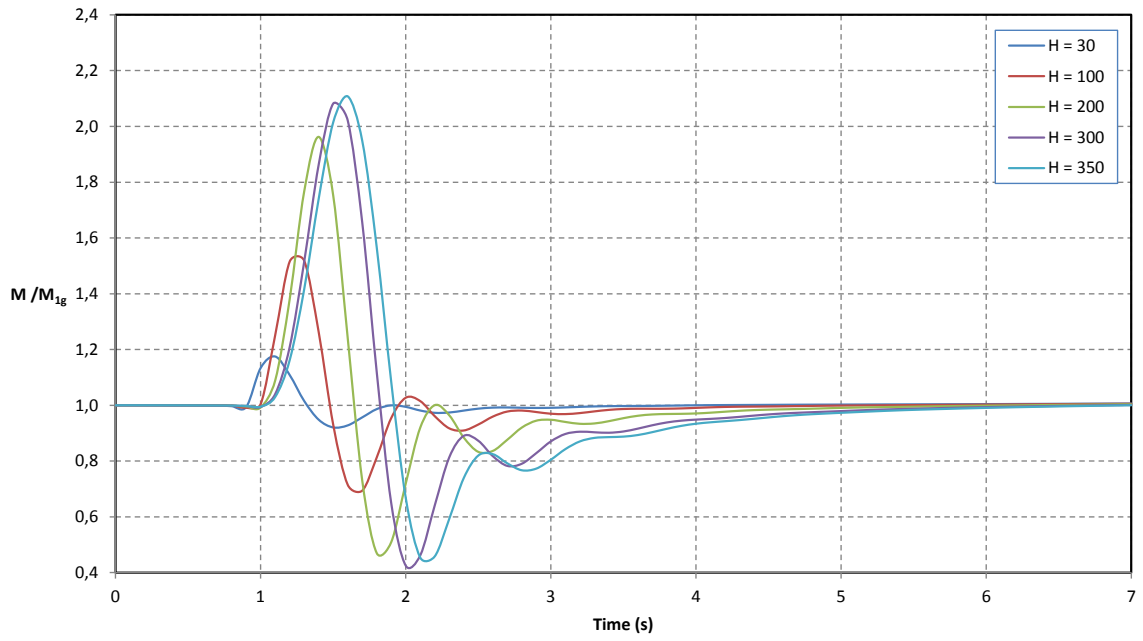
(a) Without Coupling
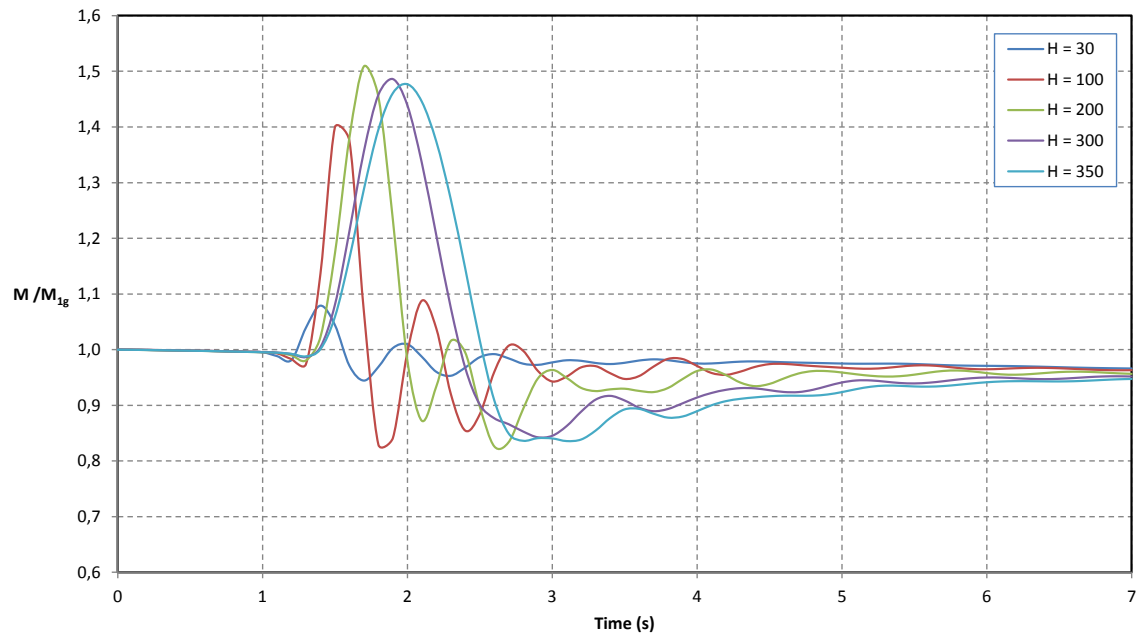
(b) With Coupling

Figure B-15: 777 Bending moment ratio for various gust lengths, $\theta = 20°$.

B.2.2 777 Static Versus Dynamic Critical Bending Moments for Various Layup Angles

Similarly to the 737, figures B-16 to B-20 provide a comparison between the static and dynamic bending moment of the 777 for each layup angle simulated. The impact of structural coupling is also provided by plotting curves with and without coupling. Ultimately, the critical load case can then be identified for every layup angle simulated by finding the peak bending moment on each chart. This critical case can then be used to properly size the wing.
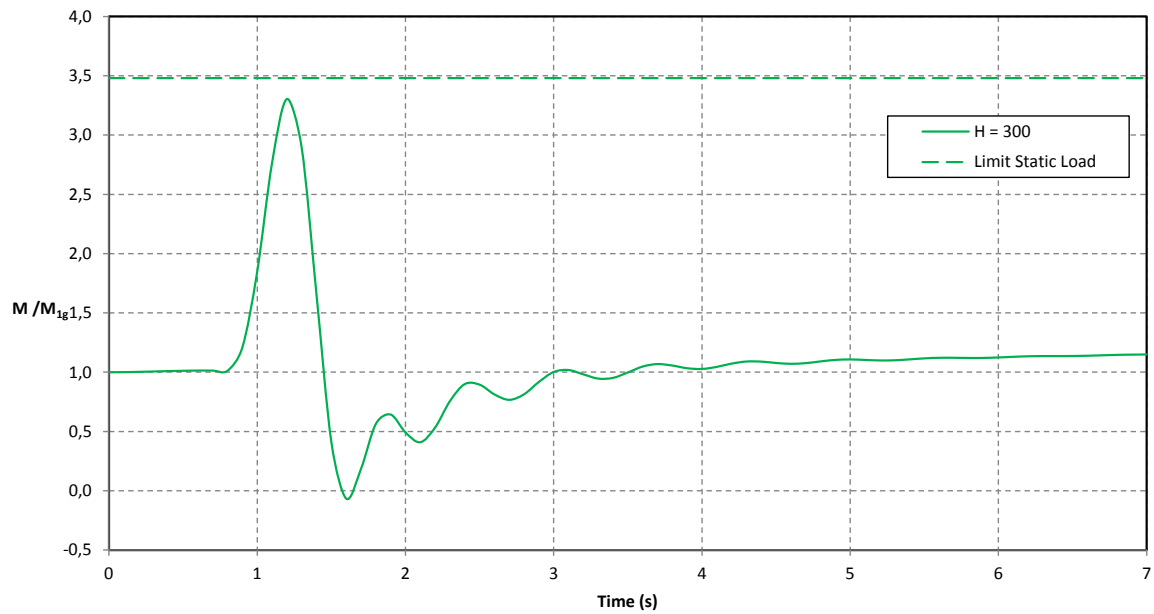
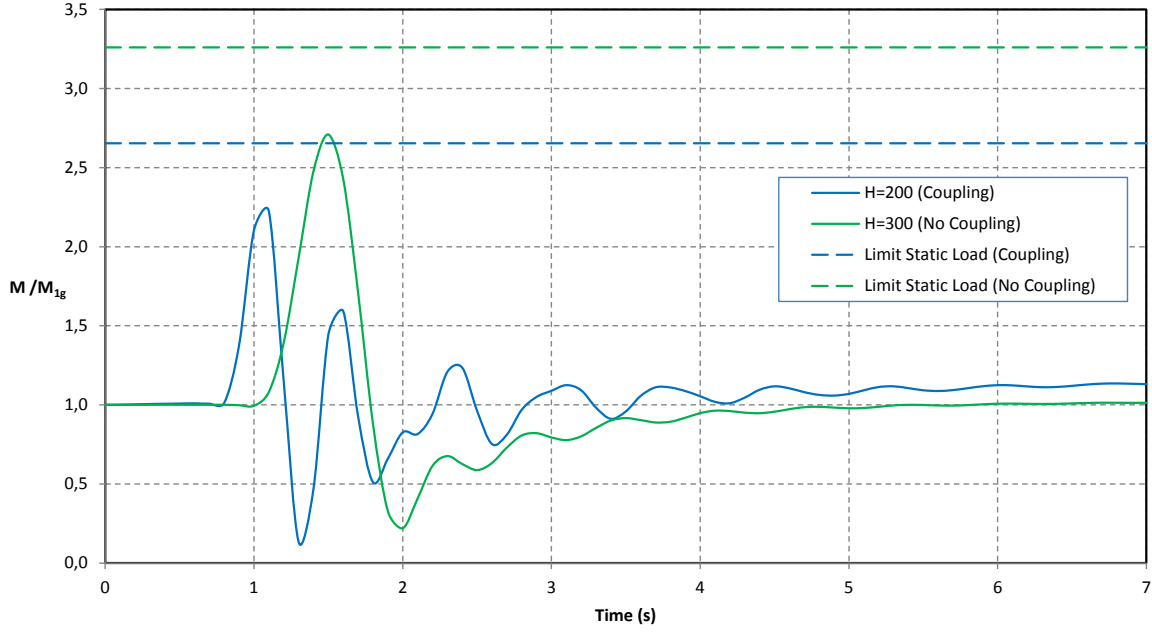Figure B-16: 777 Bending moment ratio for the critical gust and static load cases, $\theta = 0°$.

Figure B-17: 777 Bending moment ratio for the critical gust and static load cases, $\theta = 5°$.

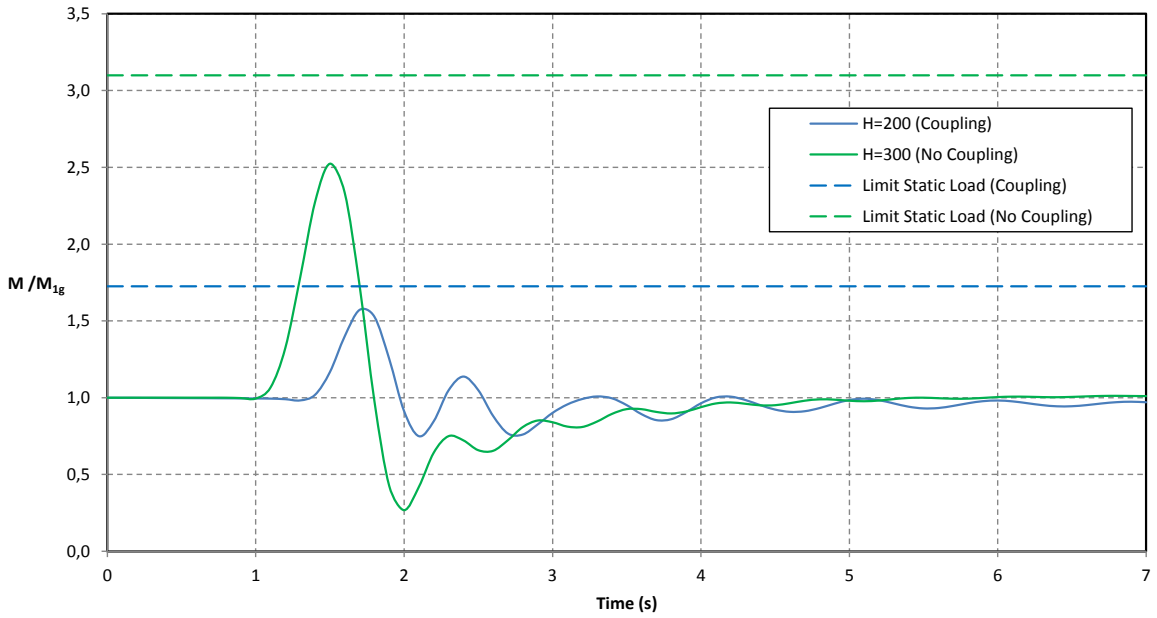
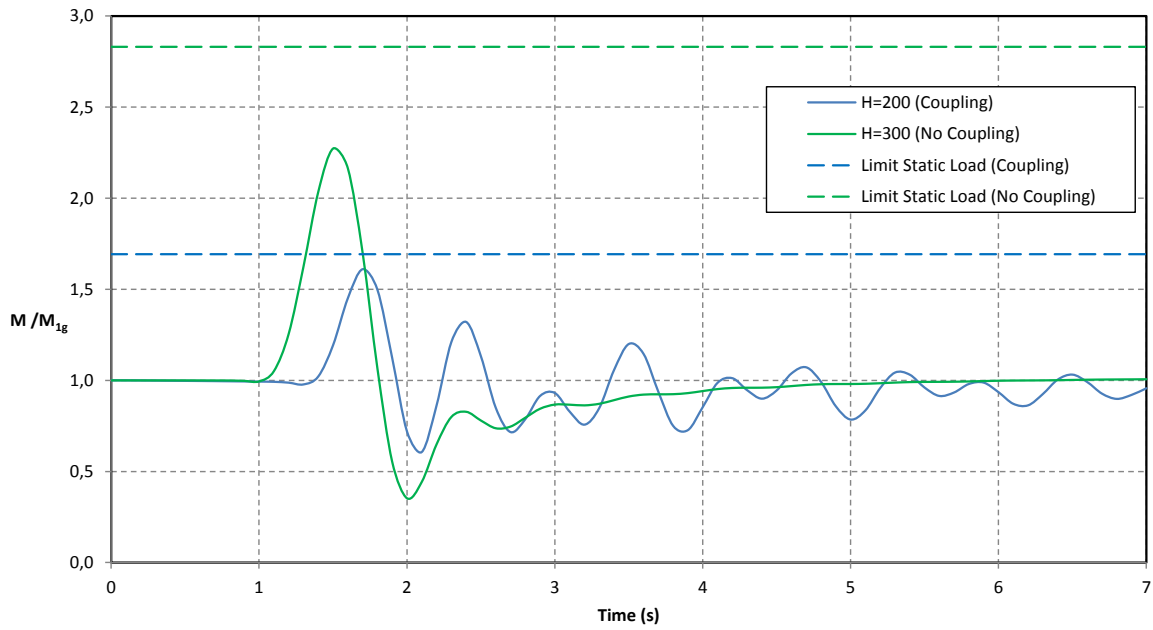Figure B-18: 777 Bending moment ratio for the critical gust and static load cases, $\theta = 10°$.

Figure B-19: 777 Bending moment ratio for the critical gust and static load cases, $\theta = 15°$.
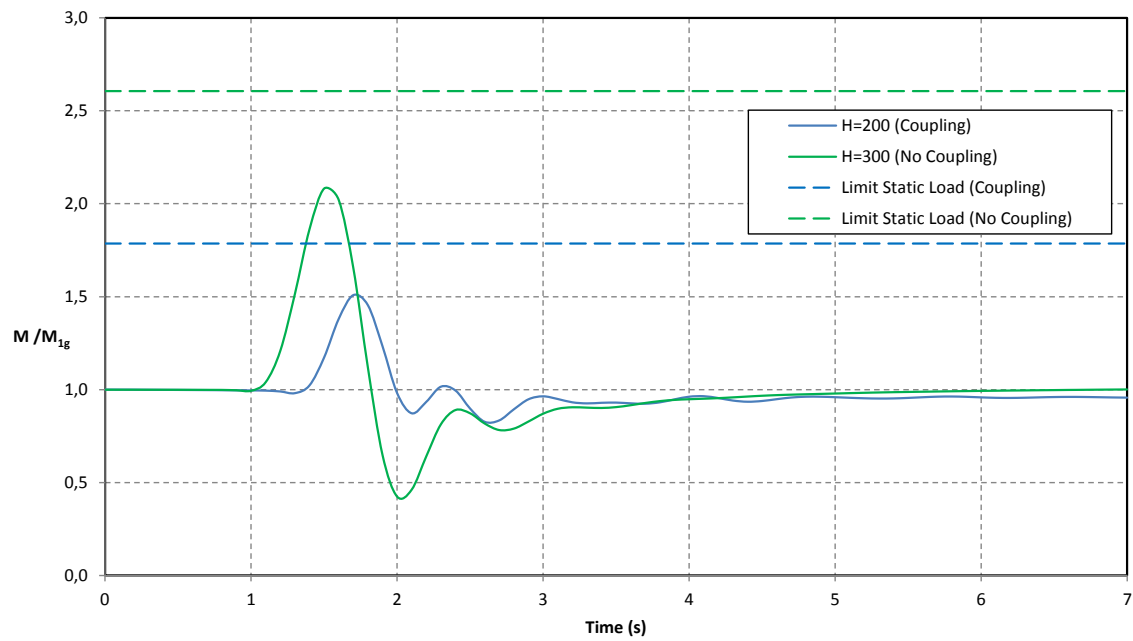

Figure B-20: 777 Bending moment ratio for the critical gust and static load cases, $\theta = 20°$.